พฤติกรรมการตกผลึกและการเปลี่ยนเฟสของไคอะลูมินาที่สังเคราะห์ด้วยปฏิกิริยาสลายตัวทางความร้อนของอะลูมินัมไอโซโพรพอกไซด์ในตัวทำละลายอินทรีย์เจือยสองชนิด

นาย โอกร เมฆาสุวรรณดำรง

วิทยานิพนธ์นี้เป็นส่วนหนึ่งของการศึกษาตามหลักสูตรปริญญาวิศวกรรมศาสตรดุษฎีบัณฑิต

สาขาวิชาวิศวกรรมเคมี ภาควิชาวิศวกรรมเคมี

คณะวิศวกรรมศาสตร์ จุฬาลงกรณ์มหาวิทยาลัย

ปีการศึกษา 2546

ISBN 974-17-3427-7

CRYSTALLIZATION AND PHASE TRANSFORMATION BEHAVIORS OF CHI-ALUMINA PREPARED BY THE THERMAL DECOMPOSITION OF ALUMINUM ISOPROPOXIDE IN TWO INERT ORGANIC SOLVENTS

Mr. Okorn Mekasuwandumrong

A Dissertation Submitted in Partial Fulfillment of the Requirements
for the Degree of Doctor of Engineering in Chemical Engineering
Department of Chemical Engineering
Faculty of Engineer
Chulalongkorn University
Academic year 2003

ISBN 974-17-3472-7

Thesis Title	CRYSTALLIZATION AND PHASE TRANSFORMATION BEHAVIORS OF χ-ALUMNA PREPARED BY THE THERMAL DECOMPOSITION OF ALUMINUM ISOPROPOXIDE IN TWO INERT ORGANIC SOLVENTS
By	Mr. Okorn Mekasuwandumrong
Field of Study	Chemical Engineering
Thesis Advisor	Professor Piyasan Praserthdam, Dr.Ing.
Thesis Co-advisor	Professor Masashi Inoue, D.Eng.

Accepted by the Faculty of Engineering, Chulalongkorn University in Partial Fulfillment of the Requirements for the Doctor's Degree

……Dean of Faculty of Engineering
(Professor Somsak Panyakeow, D.Eng.)

THESIS COMMITTEE

…….Chairman
(Professor Wiwut Tanthapanichakoon, Ph.D.)

……. Thesis Advisor
(Professor Piyasan Praserthdam, Dr.Ing.)

……. Thesis Co-advisor
(Professor Masashi Inoue, D.Eng.)

……. Member
(Varong Pavarajarn, Ph.D.)

……. Member
(Waraporn Tanakulrangsunk, D.Eng.)

……. Member
(Assistant Professor Siriporn Damrongsakkul, Ph.D.)

โอกร เมฆาสุวรรณดำรง : พฤติกรรมการตกผลึกและการเปลี่ยนเฟสของไคอะลูมินาที่สังเคราะห์ด้วยปฏิกิริยาสลายตัวทางความร้อนของอะลูมินัมไอโซโพรพอกไซด์ในตัวทำละลายอินทรีย์เฉื่อยสองชนิด (CRYSTALLIZATION AND PHASE TRANSFORMATION BEHAVIORS OF χ-ALUMINA PREPARED BY THE THERMAL DECOMPOSITION OF ALUMINUM ISOPROPOXIDE IN TWO INERT ORGANIC SOLVENTS). อ. ที่ปรึกษา : ศ.ดร.ปิยะสาร ประเสริฐธรรม, อ. ที่ปรึกษาร่วม : PROFESSOR MASASHI INOUE, 122 หน้า, ISBN 974-17-3472-7

ปฏิกิริยาสลายตัวโดยใช้ความร้อนของอะลูมินัมไอโซโพรพอกไซด์ในโทลูอีนที่ 315 องศาเซลเซียสเป็นเวลา 2 ชั่วโมง ให้ไคอะลูมินาที่มีเสถียรภาพทางความร้อนสูง ในขณะที่ผลิตภัณฑ์ที่มีโครงสร้างแบบอสัณฐานจะเตรียมได้ที่อุณหภูมิต่ำ ไคอะลูมินาที่ได้จะเปลี่ยนเฟสไปเป็นอัลฟาอะลูมินาโดยตรงที่อุณหภูมิประมาณ 1150 องศาเซลเซียส ผลิตภัณฑ์ที่มีโครงสร้างแบบอสัณฐานจะเปลี่ยนเฟสไปเป็นแกมมาอะลูมินาและซีต้าอะลูมินาหลังจากเผาที่อุณหภูมิสูง ไคอะลูมินาที่เตรียมที่อุณหภูมิ 315 องศาเซลเซียส และทำการเก็บผลิตภัณฑ์โดยทำการแยกตัวทำละลายออกที่ 315 องศาเซลเซียสมีเสถียรภาพทางความร้อนสูงที่สุด การเก็บผลิตภัณฑ์โดยใช้วิธีนี้จะให้อะลูมินาที่มีพื้นที่ผิวและปริมาณรูพรุนสูง ปฏิกิริยาสลายตัวโดยใช้ความร้อนของอะลูมินัมไอโซโพรพอกไซด์ในพาราฟินเหลวที่ 250-300 องศาเซลเซียสเป็นเวลา 2 ชั่วโมง ให้ไคอะลูมินาที่มีเสถียรภาพทางความร้อนสูง กลไกการเกิดไคอะลูมินาเกี่ยวข้องกับการเกิดสารประกอบที่มีโครงสร้างแบบอสัณฐานก่อนที่จะสลายตัวให้ไคอะลูมินา ไคอะลูมินาที่เตรียมได้จะเปลี่ยนเฟสไปเป็นอัลฟาอะลูมินาโดยตรงที่อุณหภูมิสูงกว่า 1100 องศาเซลเซียส เมื่ออุณหภูมิสูงขึ้นขนาดผลึกของไคอะลูมินาที่เตรียมได้ในตัวทำละลายทั้ง 2 ชนิด จะเพิ่มขึ้นจนถึงค่าวิกฤตที่ประมาณ 15 นาโนเมตรและเปลี่ยนเฟสไปเป็นอัลฟาอะลูมินาโดยอาศัยกระบวนการเกิดนิวเคลียสและการโตของผลึกโดยการแพร่

ภาควิชา.....วิศวกรรมเคมี.....ลายมือชื่อนิสิต.....

สาขาวิชา.....วิศวกรรมเคมี.....ลายมือชื่ออาจารย์ที่ปรึกษา.....

ปีการศึกษา.....2546.....ลายมือชื่ออาจารย์ที่ปรึกษาร่วม.....

4371823221 : MAJOR CHEMICAL ENGINEERING
KEY WORD : thermal decomposition/χ-alumina/solvent/phase transformation

OKORN MEKASUWANDUMRONG : CRYSTALLIZATION AND PHASE TRANSFORMATION BEHAVIORS OF χ-ALUMINA PREPARED BY THE THERMAL DECOMPOSITION OF ALUMINUM ISOPROPOXIDE IN TWO INERT ORGANIC SOLVENTS. THESIS ADVISOR: PROFESSOR PIYASAN PRASERTHDAM, Dr.Ing, THESIS COADVISOR: PROFESSOR MASASHI INOUE, D.Eng. 122 pp. ISBN 974-17-3472-7

Thermal decomposition of aluminum isopropoxide (AIP) in toluene at 315°C for 2 h gave χ-alumina product having the high thermal stability and while the reaction at lower temperature resulted in formation of an amorphous product. The thus-obtained χ-alumina transformed directly to α-alumina at approximately1150^{o}C, bypassing other transition alumina phases. The amorphous product transformed to γ-alumina then to θ-alumina, after calcination at high temperature. It was found that when χ-alumina synthesized at 315°C was recovered by the removal of the solvent at the reaction temperature, the product showed the highest thermal stability. This procedure is convenient avoiding bothersome work-up process yielding large surface area and large pore volume alumina. Thermal decomposition of AIP in mineral oil at 250-300°C over a 2 h duration results in χ-alumina powders having high thermal stability. The mechanism of the process involves the formation of amorphous complex before further decomposition takes place. Phase transformation of the obtained products was also investigated. It was found that χ-alumina synthesized by this method transformed directly to α-alumina at temperature higher than 1000°C. χ-alumina prepared in both organic solvents attains a critical crystallite size around 15 nm through accretion on calcination and then transforms directly to α-alumina through nucleation and growth process.

Department……Chemical Engineering……Student's signature…….
Field of study…….Chemical Engineering……Advisor's signature…….
Academic year……..2003…….Co-advisor's signature……

CONTENTS

PAGE

CONTENTS (CONT.)

PAGE

LIST OF TABLES

TABLE **PAGE**

LIST OF FIGURES

FIGURE **PAGE**

CHAPTER I

INTRODUCTION

Many industrial solid catalysts are made up by active centers anchored on supports having high porosity and surface area, preferably with good mechanical strength and thermal stability. Transition aluminas are most widely used in industry because varieties of aluminas with such properties are commercially available. Recently, much attention has been paid to improve the properties of catalysts at high temperatures, especially in prevention of catalyst due to transformation of alumina phases and sintering. The surface area of the catalyst or the catalyst support must be unchanged by high reaction temperature, in order to avoid loss of active centers.

Alumina is an important material in field of catalytic technology because of its good important properties. It has high surface area with the fine particle size, good adsorbent, catalytic activity, and high melting point (above 2000°C) which is also desirable for the support. Alumina can be used in three types: as catalyst, co-catalyst and support. For example, alumina is used as catalyst in the reaction of steam reforming and clause process at high temperature. Alumina is used as co-catalyst in the catalytic reforming of gasoline and as support in many cases, such as in catalytic converter, in membrane technology etc.

It is understood that commercial alumina powders produced by the conventional Bayer procedures does not possess the required characteristics for most applications. Therefore, other preparation methods are developed to prepare alumina powders that possess the required characteristics. Some of these non-conventional methods may be mentioned as sol-gel synthesis [1], hydrothermal synthesis [2], microwave synthesis [3], emulsion evaporation [4], precipitation from solution [5], and solvothermal synthesis [6-13]. In such methods, the required characteristics are obtained by controlling the crystal type, crystal size, particle shape, particle size distribution, agglomeration degree and porosity [14-17].

Sol-gel method exhibits many advantages on the material synthesis. One of the major advantages of the new processes appears to be much lower temperature required for obtaining products, than the conventional method. Furthermore, the obtained products are homogeneous. Sol-gel derived alumina offers a number of advantages such as well-defined nanostructure, large surface area, and superior mechanical properties [1]

In the method of precipitation from solution, the reactants may or may not be in the same phase before the precipitation takes place. If they are in the same phase, the precipitation is homogeneous, otherwise, it is heterogeneous. Most often the homogeneous precipitation is preferred because its behavior is more controllable [5]. Homogeneous precipitation of alumina precursors is carried out by heating the aqueous solution containing excess urea and aluminum salt approximately up to its boiling temperature [18-19]

Solvothermal synthesis is one of the interesting methods. It is improved from the hydrothermal synthesis by using organic solvent instead water at elevated temperature (200-300°C) under autogeneous pressure of organics during the preparation process. The advantages of this method are reproducibility, no requirement of any precaution and purification of starting materials. Inoue et al. [6-13] has found that the reactions of metal alkoxide in organic solvent give the product with good properties such as: surface area, crystallinity, and thermal stability.

The phase transformation of metastable alumina is one of the important properties. Normally it starts with aluminum hydroxide ($Al(OH)_3$ and AlOOH) and transforms to low-temperature phase (γ and χ) at temperature around 150-500°C, to high temperature-phase (δ, θ, κ) at temperature around 650-1000°C. Finally, the thermodynamically stable phase, α-alumina, is formed at temperature around 1100-1200°C. It is generally believed that the α-phase transformation occurs through the nucleation and growth mechanism of high-temperature phase. Tucker [20] has demonstrated that the transformation to α-phase tends to begin at the neck region of sintered particles. This is consistent with the fact that such neck region should contain abundant anion vacancies created by the removal of hydroxyl groups by dehydroxylation. Johnson [21] has also reported that the surface hydroxyl groups come into play in the particle growth of transition alumina. He has

proposed that the particle growth occurs by successive elimination of water from two hydroxyl groups residing on adjacent particles, close to an area of contact. This generates an Al-O-Al bond and brings more hydroxyls into adjacency. With the progress of dehydroxylation, there are necks forms between particles and, finally, small particles grow to larger ones accompanied by significant surface area loss.

In this work, we prepare the aluminas by the thermal decomposition of aluminum isopropoxide in various inert organic solvents.

In this research, the obtained aluminas have been used to investigate:

1. The crystallization mechanism of χ–alumina by thermal reaction of AIP in organic solvent.
2. The effect of product recovery method on the physical properties and thermal stability of χ-alumina product.
3. The formation of micro-spherical χ-alumina by the reaction of AIP in mineral oil..
4. The phase transformation behavior of χ-alumina.

This thesis is organized as follow:

Chapter II contains literature reviews of the structure of χ-alumina, preparation method, and the phase transformation behavior of transition alumina.

Chapter III composes of the theory about the precursors, the structure and the phase transformation sequence of transition alumina.

Description of experimental system, operation procedure and characterization are described in Chapter IV.

Chapter V reveals the experimental results and the discussions of the crystallization process of χ-alumina, the effect of product recovery on the properties, the phase transformation behavior of χ-alumina and the formation of micro spherical particle of χ-alumina prepared by thermal decomposition of AIP in mineral oil.

The overall conclusions are presented in chapter VI.

Finally, the sample of calculation of crystallite size and BET surface area are included in appendices at the end of this thesis.

CHAPTER II

LITERATUTRE REVIEWS

Alumina (Al_2O_3) exists in many metastable phases before transformation to the stable α-Al_2O_3 (corundum form). The metastable alumina can be divided into two groups: the face-centered cubic (fcc) and the hexagonal close packing (hcp) arrangement of oxygen anions. The distribution of aluminum cations depends on the structure of the polymorphs [22]. The Al_2O_3 structures based on fcc packing of oxygen include γ-, η- (cubic), θ- (monoclinic), and δ- (tetragonal or orthorhombic) phases, whereas the Al_2O_3 structures based on hcp packing of oxygen are the α (trigonal), κ (orthorhombic), and χ (hexagonal) phases.

Because of their fine particle size, high surface area, good catalytic activity, distinctive chemical, mechanical and thermal properties, the transition alumina finds many applications in industry i.e. as absorbents, catalyst, catalyst support, coatings, and soft abrasives [23]. The excellent stoichiometry and stability of Al_2O_3 make it an important constituent of many protective oxide scales formed on the surface of high-temperature metals and alloys. The dominant (and stable) phase in these scales is α-Al_2O_3, whose occurrence also dominates the adhesion and coherence of the scale. Thus, understanding of the metastable intermediate polymorphic structures and the transformation mechanisms that result in the formation of α-Al_2O_3 is important for heat treatments for promotion of stable scale formation. Understanding of the mechanisms of polymorphic phase transformations is also important for the sintering of nanosized Al_2O_3 powders, in which the starting materials are usually γ-Al_2O_3 and consequently transform to α-Al_2O_3 during sintering process. Both the sintering and the grain-growth behavior are related strongly to this phase transformation.

Boehmite is one of the polymorph of AlO(OH), and so-called pseudoboehmite is microcrystalline boehmite which has extra water content due to the surface hydroxyl groups. Pseudoboehmite, one of the most widely used precursors to produce alumina, is decomposed to form transition alumina, of which crystal phase of the product changes

with increasing temperatures, i.e. γ- to δ- to θ- and finally α-phase at high temperature. From the corresponding variation of surface area and surface properties, the thermal stability of alumina supports has been discussed with regard to the phase transformation. It is generally accepted that the phase transformation is the cause for the loss of surface area [24].

χ-alumina is a modification of transition alumina [22, 25-26]. It is characterized by the appearance of a diffraction peak at d = 0.212 nm, which cannot be explained by the spinel structure proposed for other transition aluminas, such as γ- and η- phases. χ-alumina is a crystallographic from of transition alumina, normally obtained by dehydration of gibbsite (<200 nm) [26-27]. Dollimore et al. [28] have reported that χ-alumina is formed by the thermal decomposition of aluminum oxalate and that aluminum oxalate has a crystal structure similar to that of gibbsite. Normally, χ-alumina transforms into κ-alumina at temperature around 650-750°C with a loss in surface area by phase transformation. There are three different unit cells suggested for χ-alumina structure: cubic and two forms of hexagonal close packing with different lattice parameters [29-30].

Recently, much attention has been denoted on the catalyst preparation. Currently, the chemical products are important for living. Therefore the catalyst with the good properties is significant in the chemical process. As year passed, preparation procedures have been improved. One of the interesting processes is the synthesis of inorganic material using organic solvents. Inoue et al. has developed new synthesis method for inorganic materials by using organic media at elevated temperature (200-300°C) under autogeneous pressure of organics for many years (1988-2002) [6-13]. It has been found that many oxides and mixed oxides can be crystallized in organic media at temperatures lower than that required by the hydrothermal reaction. In 1988, they have reported that the glycothermal treatment (the use of glycol instead of water for hydrothermal treatment) of gibbsite at 250°C yielded glycol derivative of boehmite [6]. In the latter reaction, the crystallite size of the glycol derivative of boehmite is affected by the carbon number of glycols and increases in the following order [7-8]: $HO(CH_2)_2OH$ < $HO(CH_2)_3OH$ < $HO(CH_2)_6OH$ < $HO(CH_2)_4OH$. This result can be explained by the heterolytic cleavage of the O-C bond of $AlO(CH_2)_nOH$ formed by the alkoxyl exchange between aluminum alkoxide and glycol. In 1992, they have found that the reaction of aluminum

isopropoxide (AIP) in toluene at 300°C results in χ-alumina [9]. Subsequently, they have prepared nanocrystalline tetragonal zirconia by the reaction of zirconium alkoxide in toluene and 1,4 butanediol [10-11]. In 1996 they have reported the formation of thermally stable porous silica-modified alumina via the glycothermal treatment of the mixture of AIP and tetraethyl orthosilicate (TEOS) in 1,4 butanediol [12]. Subsequently they have prepared the homogeneous mullite precursor, which decomposed to be high thermal stability mullite at 1000°C by the thermal decomposition of AIP and tetraethyl orthosilicate (TEOS) in toluene [13].

Kominami et al. have synthesized the nanocrystalline titanium (IV) oxide in the anatase form by thermal decomposition of titanium (IV) alkoxide in organic solvent [31]. The products have high surface area (>100m^2/g) even after calcination at 823K and show high activity in the photocatalytic mineralization of acetic acid in aerated aqueous solutions because of the high crystallinity and high surface area. Subsequently, they have synthesized the nanosized titanium (IV) oxide in the anatase form by hydrolysis of titanium (IV) alkoxide by adding small amount of water in the gap between a test tube and autoclave wall [32]. When the temperature rises, water evaporates and then dissolves in the organic solvent to hydrolyze the reactant. The rutile-transformation temperature of this titania is higher and the thermal stability is improved.

Highly porous solids can be prepared by the removal of solvent from a wet gel at a temperature above critical temperature of the solvent. Over the recent years, many researchers have built up strong technical background in such materials. Fanelli and Burlew have found a new polymerization catalyst system comprising an aluminum compound and a transition metal compound on an alumina-based aerogel support [33]. Armor and Carlson have prepared a catalyst composed of uniform dispersion of individual metallic palladium particles [34]. Armor and Carlson prepared high pore volume alumina by hydrolysis of aluminum isopropoxide with hypercritically removal of the fluid phase [35]. Aerogel had good properties such as high pore volume, high surface area and high thermal stability. These properties are results from this method that obviates the inherent shrinkage or structural collapse that occurs when precursor gels are conventionally dried to a solid form. Such shrinkage or compaction is the result from the surface tension of residual liquid trapped within the fragile gel structure. Praserthdam et

al. have prepared the high thermally stable porous silica-modified alumina by the reaction of AIP and TEOS in toluene combined with the supercritical drying of organic solvents [36].

Normally, transition aluminas start to lose their surface area even at temperature below 800°C due to the elimination of micro-pores. However, drastic loss occurs at temperature higher than 1000°C when the crystallization to the thermodynamically stable α-Al_2O_3 occurs [37]. It has been suggested that initial stage of sintering at temperature as low as 600°C starts with the elimination of water between hydroxyl groups of the particles in contact [38-39]. Continuation of the heating causes growth of the neck formed and the pore enlargement occurs by the coalescence of grains in contact.

The phase transformation of θ- to α-Al_2O_3 is believed to occur via a nucleation and growth process [40-41]. Investigations on the critical crystallite sizes of transformation have been reported previously [15, 42-47] although there is substantial discrepancy among them. Recent studies on the nanosized alumina powder have reported that the transformation process to α-Al_2O_3 requires critical size of θ-Al_2O_3 at the nucleation stage, which initiates the formation of the α-Al_2O_3 nucleus, and a primary size for α-Al_2O_3 at the growth stage, beyond which the transformation comes to a completion. During the transformation process the size of θ-crystallites increases to the critical size and remains as monodispersed crystallites before it transforms to α-Al_2O_3. The α-Al_2O_3 nuclei grow drastically before the polycrystalline α-Al_2O_3 particles are formed [48-49].

Several studies have been carried out on the direct phase transformation of alumina. The mechanism of phase transformation and the direct phase transformation from γ-alumina to α-alumina involving the conversion of the cubic close packing of oxygen ions into a stable hexagonal close packing which have been examined [50-51]. Others have reported on methods of enhancing the rate of phase transformation [52]. The effect of defects on the transformation behavior has been reported in many papers. Shek et. al. [53] reported that the γ-alumina produced by a relaxation process of amorphous nano alumina transform to stable α-alumina directly. This behavior was explained by the reduction of defect and lattice distortion in the relaxation process, releases a large amount of energy and thus promotes nucleation of α-Al_2O_3. Dynys and Halloran [37] reported

that lattice damage in γ-alumina by ball-milling process increased the density of nuclei and the transformation rate of α-alumina.

In this thesis, the solvothermal method is applied to prepare χ-alumina by the thermal decomposition of AIP in the inert organic solvents. This result has been reported by Inoue et al. [9], but many points are remaining to be clarified and need more explanation i.e. the mechanism of crystallization, the effect reaction conditions and product recovery method on the physical properties. These effects on thermal stability and phase transformation have not been investigated. They are investigated in this thesis and present in next chapters.

CHAPTER III

BACKGROUND

The basic knowledge of alumina including its precursors, the structure, and phase transformation sequences of transitions alumina is described in the first section of this chapter. Next, the explanation on the sol-gel method is provided. Then, concept of conventional hydrothermal method is described in the third section. Finally, phase transformation of crystalline material is described in the last section of this chapter.

3.1 Alumina (Al_2O_3)

Study of alumina has been subject of great interest for many decades. It is widely used as catalyst, catalyst support, wear-resistance material, ceramics, abrasives, medicinal material, and adsorbent [22-23], because of its distinctive chemical, mechanical and thermal properties. The details described in this part are based on review of Levin and Brandon [51] and text from Lippens and Steggerda [54]. The precursors of alumina are described in section 1). Alumina is prepared mostly by a thermal dehydration procedure. Because the properties of alumina are strongly related the structure and the morphology of precursors. These topics are dealt with in section 2). The structure and chemical properties of the alumina are summarized in section 3).

1) Precursors of Metastable Aluminas

Aluminum trihydroxide ($Al(OH)_3$) and aluminum monohydroxide (AlOOH) exhibit polymorphism and exist in many structure forms. The structure of all aluminum hydroxides consists of stacking of double oxygen layers with the aluminum cations located in octahedrally coordinated interstices. The packing of oxygen ions inside the layer can be either hexagonal or cubic, whereas the symmetry of the overall structure for each hydroxide is determined by the distribution of hydrogen. The relative distance between hydroxyl groups, both within and between the layers, has been suggested to control the mechanism of dehydration for the particular hydroxide. The structures of the most common alumina hydroxides are briefly summarized below.

1.1) Aluminum Trihydroxides

a) Gibbsite (hydrargillite) γ-$Al(OH)_3$

Gibbsite is the best known trihydroxide. Technically it is the most important because it is an intermediate for the production of aluminum metal from bauxite (Bayer process). The crystal structure of gibbsite is based on double layer AB of closely-packed hydroxyl ions with aluminum cations sandwiched in octahedrally coordinated interstices between the layers , with an occupancy of 2/3 [55]. There are two such double layers in the gibbsite unit cell, which contains eight $Al(OH)_3$ formula units. Each oxygen has one hydrogen atom attached to it forming hydroxyl ion. The number of O-O bonds in the gibbsite structure is less than the number of hydrogen atom to be accommodated. The resulting distribution of O-H bonds distorts the structure, resulting in monoclinic symmetry described by the space group $P2_1/n$. The lattice parameter are $a = 8.62$ Å, $b = 5.06$ Å, $c = 9.7$ Å, $\beta = 94^o$. The stacking of the O-H layers can be described as AB-BA. The double layers are kept together by the hydrogen bonds between OH-ions. The distance between two adjacent A-B layers is 2.81 Å, while the distance between A and B is 2.03 Å. The real structure of gibbsite can be obtained by deforming and stacking in such a way that the double layers are displaced relative to each other over the short distance in the direction of a-axis, thus

OH-ions of two different double layers come just above each other and give the monoclinic lattice.

b) Bayerite α-Al(OH)$_3$

Bayerite is rarely found in nature, but it can be synthesized in the laboratory by many processing route [22]. The oxygen coordination in the bayerite structure is similar to that in gibbsite, except the distribution of hydrogen atom, forming an AB-AB stacking sequence of the O-H layers. There is some controversy in the literature concerning the true symmetry of bayerite. Although both hexagonal and orthorhombic have been proposed for bayerite, base on XRD data [56], a later refinement of neutron powder diffraction spectra has resulted in an ambiguously monoclinic symmetry described by the space group of $P2_1/n$ [57].Three of six symmetrically independent hydrogen atoms in the unit cell are located within a single oxygen layer, and rest are bounded to adjacent layers.

1.2) Aluminum Monohydroxides

a) Boehmite γ-AlOOH

Boehmite is the major constituent of many bauxite minerals. It can also be synthesized in the laboratory, for instance, by neutralizing aluminum salts at temperature close to the boiling point of water by treating activated aluminum with boiling water or by hydrothermal reaction. The boehmite crystal structure consists of the cubic packed oxygen ions with the aluminum cations sandwiched between adjacent layers. The distribution of hydrogen atom results in an orthorhombic unit cell that has been described by the *Cmcm* space group. The lattice parameters of boehmite are a = 2.861 Å, b = 3.696 Å, and c = 12.233 Å [58].

In addition to the stoichiometric crystal structure described above, the name of boehmite has been used to describe the product of aging aluminum hydroxide gel, better referred as pseudoboehmite or gelatinous boehmite [22]. A pseudoboehmite typically contains 15% excess water comparing to the stoichiometric composition

AlOOH. Controversy continues concerning the exact location of the excess water in this structure. In boehmite, Al atoms are surrounded by a distorted octahedral group of O atoms, which are linked together to form a complex layer structure. Van Osterhout (1960) [59] reported an easy method to describe the structures of the corresponding iron compound which can be used for the aluminum compounds as well.

b) Diaspore α-AlOOH

Diaspore occurs in nature in type of clay and bauxite which is the interesting material for preparation of α-alumina. The structure consists of hexagonal layers of oxygen, which are significantly distorted. Aluminum cations are located in octahedral coordinated interstices between the adjacent oxygen layers. Diaspore possesses orthorhombic symmetry with the *Pbnm* space group and lattice parameters of a = 4.4 Å, b = 9.43 Å, c = 2.84 Å. The structure has four formula units per unit cell [55].

1.3) Tohdite $5Al_2O_3.H_2O$

The crystal structure of tohdite, determined by Yamaguchi et al., [60-61] consists of close-packed of oxygen layers with approximately ABACBAC stacking. The hexagonal unit cell of tohdite has lattice parameters of a = 5.567 Å, and c = 8.768 Å, and it contains ten aluminum cations, eight of which are in octahedrally coordinated and two in tetrahedrally coordinated interstices. The symmetry of this structure has been described by the hexagonal $P6_3mc$ space group. The refined positions of oxygen and aluminum for this structure are given in Ref. 61, but the exact distribution of hydrogen atoms in the toldhite structure remains uncertain.

1.4) Amorphous Anodic Al_2O_3 Films

Amorphous Al_2O_3 films can be formed by anodization of aluminum in acid solution. Nonporous Al_2O_3 films are formed in solutions that do not dissolved Al_2O_3, whereas Al_2O_3 films are developed in acid solutions, where partial solubility is possible [62]. The structure of Al_2O_3 films synthesized by anodization has been

studied by both X-ray adsorption fine structure (EXAFS) [63] and electron energy loss fine structure (EXELFS) techniques [64]. Amorphous Al_2O_3 films generally have been assumed to be a mixture of tetrahedrally and octahedrally coordinated aluminum. Results from both EXAFS and EXELFS have confirmed that dense Al_2O_3 films contain 80% aluminum cations in octahedral sites and 20% in tetrahedral sites. The aluminum cations in the porous Al_2O_3 films predominantly have tetrahedral or even lower coordination.

1.5) Alumina melt

The radial distribution function for an Al_2O_3 melt recently have been reported by Ansell et al. [65] in the temperature range of 2200-2700 K using X-ray synchrotron radiation. Al_2O_3 undergoes structural rearrangement on melting with a change of the aluminum cations coordination from octahedral, in α-Al_2O_3, to predominantly tetrahedral in the Al_2O_3 melt. These results contradict those reported earlier by Waseda et al. [66], who found octahedrally coordinated aluminum as the fundamental cluster configuration in the melt. No explanation that might account for this discrepancy has been given. However, quenching experiments do support the proposed tetrahedral coordination above the melting point, because high cooling rates ($>10^5$ K/s) from the melt result in crystallization of either γ-alumina or various types of transition alumina phases, all containing tetrahedrally coordinated aluminum.

2) The formation and the crystal structure active aluminas

Metastable alumina phases are commonly obtained by one of the processing routes summarized in Table 3.1. Differences in the phase transformation sequence are result from the difference in the precursor structure [56, 67]. The temperature ranges of stability given for the transition aluminas are only approximate and depend upon the degree of crystallinity, impurities in the starting materials, and the subsequent thermal history. All the phases of transition alumina are reproducible and stable at room temperature. However, the transformation sequence is irreversible. The phase transformation sequences, from metastable Al_2O_3 structures to the final stable α-alumina phase, reported in the literature on passing are also approximate.

Table 3.1: Common processing routes resulting in formation of different metastable Al_2O_3 structures and sequences of phase transformation toward the stable α-alumina

Approximate packing of oxygen for the metastable Al_2O_3 structures
hcp
$\alpha\text{-AlOOH (diaspore)} \xrightarrow{700°-800°C} \alpha\text{-}Al_2O_3$
$\gamma\text{-}Al(OH)_3\text{(gibbsite)} \xrightarrow{150°-300°C} \chi \xrightarrow{650°-750°C} \kappa \xrightarrow{1000°C} \alpha\text{-}Al_2O_3$
$5Al_2O_3\cdot H_2O\text{ (tohdite)} \xrightarrow{700°-800°C} \kappa' \xrightarrow{750°C} \kappa \xrightarrow{900°C} \alpha\text{-}Al_2O_3$
Vapor (CVD) $\rightarrow \kappa \rightarrow \alpha\text{-}Al_2O_3$
fcc
$\gamma\text{AlOOH (boehmite)} \xrightarrow{300°-500°C} \gamma \xrightarrow{700°-800°C} \delta \xrightarrow{900°-1000°C} \theta \xrightarrow{1000°-1100°C} \alpha\text{-}Al_2O_3$
$\alpha\text{-}Al(OH)_3\text{ (bayerite)} \xrightarrow{200°-300°C} \eta \xrightarrow{600°-800°C} \theta \xrightarrow{1000°-1100°C} \alpha\text{-}Al_2O_3$
Amorphous (anodic film) $\rightarrow \gamma \rightarrow \delta \rightarrow \theta \rightarrow \alpha\text{-}Al_2O_3$
Melt $\rightarrow \gamma \rightarrow \delta,\theta \rightarrow \alpha\text{-}Al_2O_3$

2.1) Dehydration Reactions

Aluminas are usually obtained by dehydration of various hydroxides. Much controversy exists about the dehydration of various sequences, even in recent work [22-23]. Apart from difficulties in characterization of the obtained forms, most of the confusion arises from insufficient information concerning the reaction conditions.

a) The dehydration of the trihydroxide

The dehydration of gibbsite in air and nitrogen give the sequence of products different from dehydration of bayerite and nordstrandite. Both crystallinity and particle size of gibbsite are much greater than those of bayerite and nordstrandite. Up to 25% of boehmite can be contaminated by the intergranular hydrothermal reactions in the dehydration product from gibbsite, whereas less than 5% is usually formed from bayerite and nordstrandite. However, very fine powders of bayerite [56] and gibbsite do not form any boehmite at all.

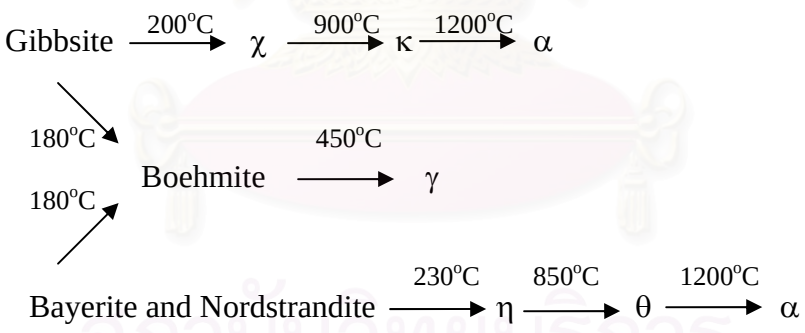

In the vacuum, three trihydroxide decompose at low temperatures into an almost completely amorphous product (ρ-alumina), which changes into γ- and η-alumina and further into θ-alumina at high temperature.

$$\begin{array}{l} \text{Gibbsite} \\ \text{Bayerite} \\ \text{Nonstrandite} \end{array} \xrightarrow{200^{o}C} \rho \longrightarrow \gamma \text{ or } \eta \xrightarrow{750^{o}C} \theta \xrightarrow{1200^{o}C} \alpha$$

$$\xrightarrow{180^{o}C} \text{boehmite}$$

b) The dehydration of oxide hydroxide

Diaspore is only aluminum hydroxide that transforms directly into α-alumina [19], which initially has high surface area before recrystallization.

The dehydration sequence of boehmite depends on its crystallinity. Well crystallized boehmite (crystal sizes > 1 μ) decomposes according to :

$$\text{Well crystallized boehmite} \xrightarrow{450^{o}C} \gamma \xrightarrow{700^{o}C} \delta \xrightarrow{1050^{o}C} \theta(+\alpha) \xrightarrow{1200^{o}} \alpha\text{–}Al_2O_3$$

The δ phase is strongly dependent on the impurities and crystallinity of the boehmite. A small amount of Na favors the formation of θ-alumina, whereas Li and Mg stabilize δ-alumina and can prevent the formation of θ-alumina. If boehmite has low crystallinity, the formation of δ-alumina is retarded.

Gelatinous boehmite (pseudoboehmite) decomposes at temperature around 300°C into alumina. Due to the poor crystallinity of the pseudoboehmite, formation of δ-alumina is hardly observed. Thus the dehydration scheme is:

$$\text{Gelatinous boehmite} \xrightarrow{300^{o}C} \gamma \xrightarrow{900^{o}C} \delta \xrightarrow{1000^{o}C} \theta+\alpha \xrightarrow{1200^{o}} \alpha\text{–}Al_2O_3$$

3.) The Structure of Aluminas

3.1) Structure of Al_2O_3 polymorphs based on face-centered cubic packing of oxygen anions

Al_2O_3 polymorphs based on fcc packing of oxygen are represented by eight X-ray powder diffraction files, which are based on the experiments performed 30-40 years ago. These files described structures denoted γ-, η-, δ-, and θ-phase with a few additional files in which the same phase notation is used for similar but not identical profiles.

a) Cubic, spinel-type aluminas: γ- and η-Al_2O_3

γ- and η-Al_2O_3 have been described as defect spinel structure [22]. The ideal spinel structure AB_2O_4 is represented by 2×2×2 array of an fcc closet packing, with A and B cations occupying the 8*a* (of the 64 available) tetrahedrally and the 16*d* (of 32) octahedrally coordinated interstitial sites (Fig 3.1). The symmetry of the spinel structure is described by the $Fd\bar{3}m$ space group [68]. The packing of the {111} oxygen layers forms an ABCABC sequence, whereas the packing of aluminum cations can be described by two type of alternating layers: either (i) layer containing only octahedrally coordinated cations or (ii) “mixed” layer containing both octahedrally and tetrahedrally coordinated cations. There are two types of tetrahedral coordinated sites: upward and downward.

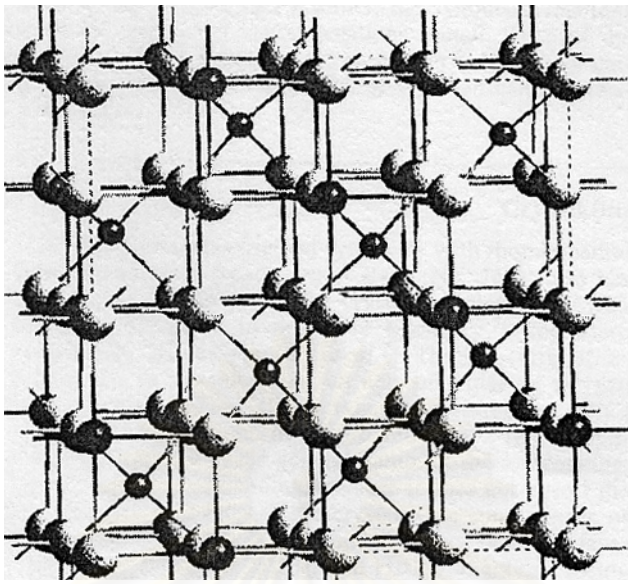

Figure 3.1: Three dimensional view of the spinel structure: White balls represent oxygen ions located at 32*e* Wyckoff positions. Large dark balls represent oxygen ions located at 16*d*, the smaller one represent 8*a*.

The commonly accepted structural model of γ-Al_2O_3 is related to that of ideal spinel and it is assumed to contain oxygen ions in 32*e* Wyckoff positions, which are approximately close packed, while 64/3 aluminum cations (to satisfy Al_2O_3 stoichiometry) are distributed over 16*d* octahedral and 8*a* tetrahedral sites [68]. In γ-Al_2O_3, 8/3 aluminum vacancies have been assumed random distribution over the tetrahedral sites [67]. Therefore the cation sublattice is partially disordered, comparing with the ideal spinel. Despite this disorder, the symmetry relations between the equivalent cation positions remain $Fd\bar{3}m$.

Shirasuka et al. [69] proposed that 62% of aluminum ions occupy 16-fold (16*c* and 16*d*) octahedral sites and assumed that the remaining aluminum ions distributed equally over the eightfold and the 48-fold tetrahedral sites. These results were confirmed by John et al. [70], who deduced that 62% of aluminum ions were in octahedral sites in η-Al_2O_3 according to the results from solid-state nuclear magnetic resonance (NMR). Recently, Zhou and Snyder [71] have applied Rietveld analysis of neutron diffraction profiles for the structure refinement of both γ- and η- structures. They have suggested that the presence of aluminum on abnormally coordinated 32*e*

sites in the surface layers of the both phases, but with no aluminum cations on the eight fold, tetrahedrally coordinated sites in η-Al_2O_3, in contradiction to the result by Shirasuka et al. However, the Zhou and Snyder interpretation seems reasonable, because it is consistent with molecule dynamic simulations of γ-Al_2O_3 surface [72]. However, it is not clear how these results which are associated with the influence of surface ions are related to the bulk structure.

γ-Al_2O_3 obtained from thermal oxidation of aluminum containing alloys, by annealing of amorphous anodic Al_2O_3 films, or by plasma spraying shows preferred orientation (crystalline texture), with both $<100>_\gamma$ and $<110>_\gamma$ direction preferentially oriented parallel to the surface normal [73-74]. Recent molecular dynamic simulations of the surface structure of γ-Al_2O_3, which have included the non-integer number of cations in the unit cell, result in the following relation between the surface energies: $\gamma_{\{001\}} < \gamma_{\{111\}} < \gamma_{\{110\}}$ [72]. These results are consistent with a {100} preferential orientation. These calculations indicate that the surface energies of γ-Al_2O_3 are much lower than those for α-Al_2O_3, which is consistent with high specific surface area of γ-Al_2O_3.

γ-Al_2O_3 developed by crystallization of anodic Al_2O_3 films or by thermal oxidation of aluminum and NiAl, contains a high density of {111} growth twins. These twins have been related to the platelike morphology of oxide scales [75-76] developed on the surface of NiAl during transient stages of thermal oxidation.

b) Al_2O_3 structures with tetragonal-orthorhombic symmetry: δ-Al_2O_3

δ-Al_2O_3 has been described as a superlattice of the spinel structure with ordered cation vacancies [54]. The δ supercell has been confirmed to be a tripled unit cell of spinel with 160 ions per cell. Two possible unit cells have been suggested based on X-ray and SAD: either tetragonal with $a_\delta = b_\delta = a_\gamma$, and $c_\delta = 3a_\gamma$ [15−16] or orthorhombic with $a_\delta = a_\gamma$, $b_\delta = 1.5a_\gamma$, and $c_\delta = 2a_\gamma$ [77-79].

In all reports of the tetragonal δ unit cell, the structure has been derived from boehmite, whereas the orthorhombic δ unit cell has been observed for precursors

obtained by quenching the melt or by thermal oxidation. It is not clear whether either structures exist or the tetragonal structure is a misinterpretation of the experimental data. The SAD results available on the orthorhombic δ-Al_2O_3 structure provide convincing evidence for the existence of this polymorph [80], whereas X-ray data ascribed the tetragonal unit cell also could have been derived from orthorhombic unit cell [81].

Jayaram and Levi [80] have studied orthorhombic δ-Al_2O_3 by TEM. Convergent-beam electron diffraction (CBED) has been used to determine the space group and $P2_12_12_1$ has been suggested.

c) Al_2O_3 structures with monoclinic symmetry: θ, θ'', λ, and θ' Al_2O_3

The most studied Al_2O_3 polymorph with monoclinic symmetry is θ-Al_2O_3. This structure has the space group *C2/m* and contains 20 ions, with the aluminum cations equally distributed over octahedral and tetrahedral sites. In many reports, θ-Al_2O_3 has been reported to be multiple twined, preliminary on the (001) plane [81]. Although the true symmetry of θ-Al_2O_3 has been determined to be monoclinic, this phase may also appear as orthorhombic due to polysynthetic twinning.

The existence of three additional monoclinic Al_2O_3 structure has been reported [82]. λ-Al_2O_3 has been observed in both plasma sprayed Al_2O_3 and thermally oxidized aluminum. θ'-Al_2O_3 has been found in annealed anodic Al_2O_3 films, and θ''-Al_2O_3 has been found in the plasma-sprayed Al_2O_3. Based on these results, all four monoclinic phase (θ-, θ''-, λ-, and θ'-Al_2O_3) are assumed to evolve from γ-Al_2O_3 by cation ordering on the interstitial sites of the oxygen subcell, which remains approximately undisturbed by these transformations. The lattice parameters and space groups of these four monoclinic Al_2O_3 phases, respected on γ-Al_2O_3 are summarized in Table 3.2.

Table 3.2: Metastable Al_2O_3 structures based on fcc packing oxygen anions

Phase	Lattice parameters	Space group	Cations/ unitcell	Orientation relationship with respect to γ-Al_2O_3
γ-Al_2O_3, η-Al_2O_3	$a_\gamma \approx 7.9$ Å	$Fd3m$	64/3	
θ-Al_2O_3	$a \approx 1.5a_\gamma$	$C2/m$	8	$(100)_\theta \parallel (001)_\gamma$
	$b = a_\gamma \sqrt{2}/4$			$[010]_\theta \parallel [110]_\gamma$
	$c = a_\gamma \sqrt{2}/2$			
	$\beta = 104^o$			
θ''-Al_2O_3	$a \approx 1.5a_\gamma$	$A12/n1^t$	64	$(100)_{\theta''} \parallel (001)_\gamma$
	$b = a_\gamma \sqrt{2}$			$[010]_{\theta''} \parallel [110]_\gamma$
	$c = a_\gamma \sqrt{2}$			
	$\beta = 104^o$			
θ'-Al_2O_3	$a \approx a_\gamma \sqrt{3}/2$	$C2/m$	16	$(010)_{\theta'} \parallel (110)_\gamma$
	$b \approx a_\gamma \sqrt{2}$			$[100]_{\theta'} \parallel [112]_\gamma$
	$c \approx a_\gamma \sqrt{2}$			
	$\beta \approx 94^o$			
λ-Al_2O_3	$a \approx 3\sqrt{2}a_\gamma/2$	$P2_1/c$	64	$[010]_\lambda \parallel [100]_\gamma$
	$b \approx 2a_\gamma$			$(100)_\lambda \parallel (013)_\gamma$
	$c \approx 1.5a_\gamma$			
	$\beta = 115^o$			
δ-Al_2O_3	$a \approx a_\gamma$	$P2_12_12_1$	64	$[100]_\delta \parallel [001]_\gamma$
	$b \approx 2a_\gamma$			$(100)_\delta \parallel (100)_\gamma$
	$c \approx 1.5a_\gamma$			
δ'-Al_2O_3	$a \approx a_\gamma$	$P4_1$	64	$[001]_{\delta'} \parallel [001]_\gamma$
	$c \approx 3a_\gamma$			$(100)_{\delta'} \parallel (100)_\gamma$

3.2) Structure of Al_2O_3 polymorphs based on hexagonal close packing of oxygen anions.

The common metastable Al_2O_3 crystal structures based on hcp close packing of the oxygen atom are κ- and χ-Al_2O_3. The existence of κ'-Al_2O_3 from the dehydration of tohdite has also been reported.

The partial transformation of gibbsite into boehmite, which gives its own dehydration products upon further heating, greatly complicates the interpretation of X-ray measurements for the structure of κ- and χ-Al_2O_3. Three different unit cells have been proposed. Stumpth et al. [29] suggest that χ-alumina has a cubic (not spinel) unit cell of lattice parameter 7.95 Å, whereas other researchers [30] propose hexagonal unit cells with either a = 5.56 Å and c = 13.44 Å or a = 5.57 Å and c = 8.64 Å. Hexagonal χ-alumina seems to possess a layer structure, the arrangement of anions being inherited from gibbsite, whereas the aluminum cations occupy octahedral sites with in the hexagonal oxygen layers. The stacking of the layers have strongly disordered in the *c*-direction. It is not yet clear whether all three of the above structures exist, or whether the differences among them are merely a matter of interpretation.

κ'-Al_2O_3 has been described in terms of the hcp packing of oxygen anions (inherited from tohdite), with the random distribution of cations over both tetrahedrally and octahedrally coordinated positions [83]. This polymorph is considered to be a transient phase in the transformation of tohdite to κ-Al_2O_3.

The structure of κ-Al_2O_3, which is considered important in the chemical vapor deposition (CVD) technology, had been believed for many years to be hexagonal [30, 83]. However, a recent lattice image studied by Liu and Skogsmo [84] combined with CBED, shows that the true symmetry for this structure is orthorhombic. The pseudohexagonal symmetry then results from the coexistence of three twin-related orthorhombic variants rotated by 120° with respect to one another. The space group of κ-Al_2O_3 is $Pna2_1$, and the lattice parameters are a = 4.69 Å, b = 8.18 Å and c = 8.87

Å. The proposed unit cell composes of 16 cations that are ordered on both tetrahedrally and octahedrally coordinated sites.

3.3) Structure of α-Al_2O_3

α-Al_2O_3 posses trigonal symmetry with rhombohedral Bravis centering (space group $R\text{-}\bar{3}c$) and has 10 atoms in the unit cell. The crystallography of α-Al_2O_3 has been discussed in detail by Kronberg [85] and Bilde-Sorensen et al. [86]. The structure of α-Al_2O_3 can be considered as an hcp sublattice of oxygen anions, with 2/3 of the octahedral interstices filled with aluminum cations in an ordered array. This simplified model describes the nature of the ion packing but is somewhat misleading, because it does not reflect true trigonal symmetry of the crystal. One consequence of the trigonal symmetry is the nonequivalence of cation layer translation along the $[10\bar{1}0]$ and $[\bar{1}010]$ directions (using hexagonal indices), which has important implications for both basal slip and basal twinning in α-Al_2O_3, as discussed by Kaplan et al. [87] and Pirouz et a1. [88]. (In some cases this nonequivalence has been attributed incorrectly to the lack of an inversion center in α-Al_2O_3, which would be inconsistent with a $-\bar{3}$ centrosymmetric point group.)

The oxygen anions in α-$A1_20_3$ occupy 18*c* Wyckoff positions (in the hexagonal description) with coordinates x,0,l/4 (x = 0.306), whereas the aluminum cations are located at 12c positions with coordinates 0,0,z (z = 0.347). Both x and z values deviate from the ideal value of 1/3, which would correspond to the atomic positions in the ideal close-packed structure. The aluminum cations are displaced along the [0001] direction toward the neighboring empty octahedral sites, resulting in a “puckering” of the cation layers. The cation displacements are accompanied by distortion of the oxygen sublattice. The hexagonal parameters for α-$A1_20_3$, are c = 1.297 nm and a = 0.475 nm, with c/a = 2.73 nm and corresponds to six oxygen layers along the c-axis of the unit cell. For the oxygen sublattice alone (three oxygen layers), c/a = 1.58, slightly smaller than the ideal value of 1.63 associated with a hard-sphere model.

3.2 Surface Area Measurement [38, 89]

Surface area and pore size distribution are important properties of catalyst and catalyst support. These attributes are measured by the use of nitrogen adsorption/desorption isotherms at liquid nitrogen temperature and relative pressures (P/Po) ranging from 0.05-1.0.

1) Total Surface Area

The total to determine the method used to determine surface area, Table 1, showed that six of the respondents used a single point surface area of a catalyst can be measured by either a multipoint or single point technique. Results of a survey method, the remaining five respondents used a multipoint method. Most respondents used data points in the range of 0.05-.30 P/P_o, only one used a P/P_o below 0.05. In either the single point or multipoint method, the isotherm points are transformed with the BET equation:

$$\frac{1}{W\,[(P_o\ /\ P)-1]} = \frac{1}{W_m C} + \frac{(C-1)}{W_m C}\frac{P}{P_o}$$

where W is the weight of nitrogen adsorbed at a given P/P_o, and W_m the weight of gas to give monolayer coverage and C, a constant that is related to the heat of adsorption. A linear relationship between $1/W[(P_o/P)-1]$ and P/P_o is required to obtain the quantity of nitrogen adsorbed. This linear portion of the curve is restricted to a limited portion of the isotherm, generally between 0.05-0.30. The slope and intercept are used to determine the quantity of nitrogen adsorbed in the monolayer and used to calculate the surface area. For a single point method, the intercept is taken as zero or a small positive value, and the slope from the BET plot used to calculate the surface area. The surface area reported will depend upon the method used, as well as the partial pressures at which the data are collected.

2) V_a-t plot

Various methods have been devised for comparing experimental isotherms with standard isotherm obtained on a suitable non-porous reference solid. The most convenient of these empirical methods is probably *t* method of Lippens and de Bore [89]. The *t* plot is a direct method for analyzing physical physical adsorption isotherms of gases and vapors. It is the plot of statistical thickness of the adsorbed film versus P/P_o for nonporous adsorbents.

The statistical thickness is defined as the thickness of adsorbed nitrogen, calculated by assigning the same density of adsorbed layer as a capillary condensed liquid. This value obtained by dividing the volume of adsorbed nitrogen at a given relative pressure P/P_o by the specific surface area:

$$t = \frac{X \times 10^4}{S} = (M \times V_{sp} / 22.4).(V_a / S) \times 10^4 \text{ Å}$$

where:

t is the statistical thickness of adsorbed layer;

X, the adsorbed volume in ml of liquid adsorbate;

S, the specific surface area in m^2/g;

M, the molecular weight of adsorbate;

V_{sp}, the specific volume of the adsorbate in ml/g; and

V_a, the specific volume of the adsorbate in ml gas STP/g of adsorbent.

For nitrogen we obtained

$$t = 15.47 V_a / S$$

For S in this equation, we can estimate this value by BET surface area calculated from the volume of monolayer adsorbed V_m.

$$S_{BET} = 4.37V_m \ \ \mathrm{m^2/g}$$

Introducing to the equation of t we obtain:

$$t = 3.54(V_a / V_m)\ \text{Å}$$

.

3.3 Hydrothermal method [90]

The method involves heating the reactants in water/steam at high pressure and high temperature. Water performs two roles, i.e. as a pressure-transmitting medium and as solvent, in which the solubility of the reactants is pressure and temperature dependent. In addition, some or all of the reactant are soluble in the water under pressure. This enables reaction to take place in, or with the aid of, liquid and/or vapor phases. Under these conditions, reactions that would occur only at much high temperatures in the absence of water may occur. The method is therefore particularly suited for the synthesis of phases that are unstable at higher temperatures. It is also a useful technique for growing single crystals. By arranging suitable temperature gradient in the reaction vessel, dissolution of the starting material may occur at the hot zone and reprecipitation at the cooler zone of the vessel.

Hydrothermal equipment is basically a tube, usually of steel, closed at one end. The other end has a screw cap with a gasket of soft copper to provide a seal. Alternatively, the “bomb” may be connected directly to and independent pressure source, such as a hydraulic ram; this is known as the “cold seal” method. The reaction mixture and an appropriate amount of water are placed inside the bomb, which is then sealed and placed inside an oven at the required temperature, usually at a temperature in the range of 100-500°C. Pressure is controlled either externally or by the degree of filling in a sealed bomb. According to the P/T phase diagram, Figure 3.2, curve AB is saturation curve which separates liquid water (above) from steam (below). At temperatures above 374°C, (point B), the water is in the supercritical condition and there is no distinction between liquid and vapor states.

The applications of the hydrothermal method are:

1) Synthesis of new phases: calcium silicate hydrate.

Hydrothermal methods have been used successfully for the synthesis of many kinds of material. A good example is the family of calcium silicate hydrates, many of which are important components of set cement and concrete. Typically, lime (CaO) and quartz (SiO_2) are heated with water at temperatures in the range of 150 to 500°C

and pressure of 0.1 to 2 kbar. The synthesis of different from of calcium silicate hydrate requires different reaction conditions composition of starting mixture, temperature, pressure and time. For example, xonolite, $Ca_6Si_6O_{17}(OH)_2$, may be prepared by heating equimolar mixtures of CaO and SiO_2 at saturated stream pressures and temperature in the range of l50 to 350°C.

2) Growth of single crystals.

For the growth of single crystals by hydrothermal methods, it is often necessary to add a mineralizer. A mineralizer is a compound added to the aqueous solution that speeds up the crystallization. It usually operates by increasing the solubility of the solute through the formation of soluble species that would not usually be in the water. For instance, the solubility of quartz in water at 400°C and 2 kbar is too small to permit the recrystallization of quartz, in a temperature gradient, within a reasonable time. With an addition of NaOH as a mineralizer, however, large quartz crystals can be readily grown. Using the following conditions, crystals of kilogram size have been grown: quartz and 1.0 M NaOH solution being held at 1.7 kbar and 400°C where some of the quartz dissolves. Temperature gradient is arranged in the reaction vessel. At 360°C the solution is supersaturated with respect to quartz, which precipitates onto a seed crystal. Therefore, quartz dissolves in the hottest part of the reaction vessel and is transported throughout the vessel via convection currents. Finally, it precipitates in cooler part of the vessel where its solubility in water is lower. Quartz single crystals are used in many devices such as radar and sonar, piezoelectric transducers and as monochromators in X-ray diffraction. World production of quartz single crystals, using hydrothermal and other methods, is currently a staggering at 600 tons annually.

Using similar method, many substances have been prepared as high quality single crystals, e.g. corundum ($A1_2O_3$) and ruby ($A1_2O_3$ doped with Cr^{3+}).

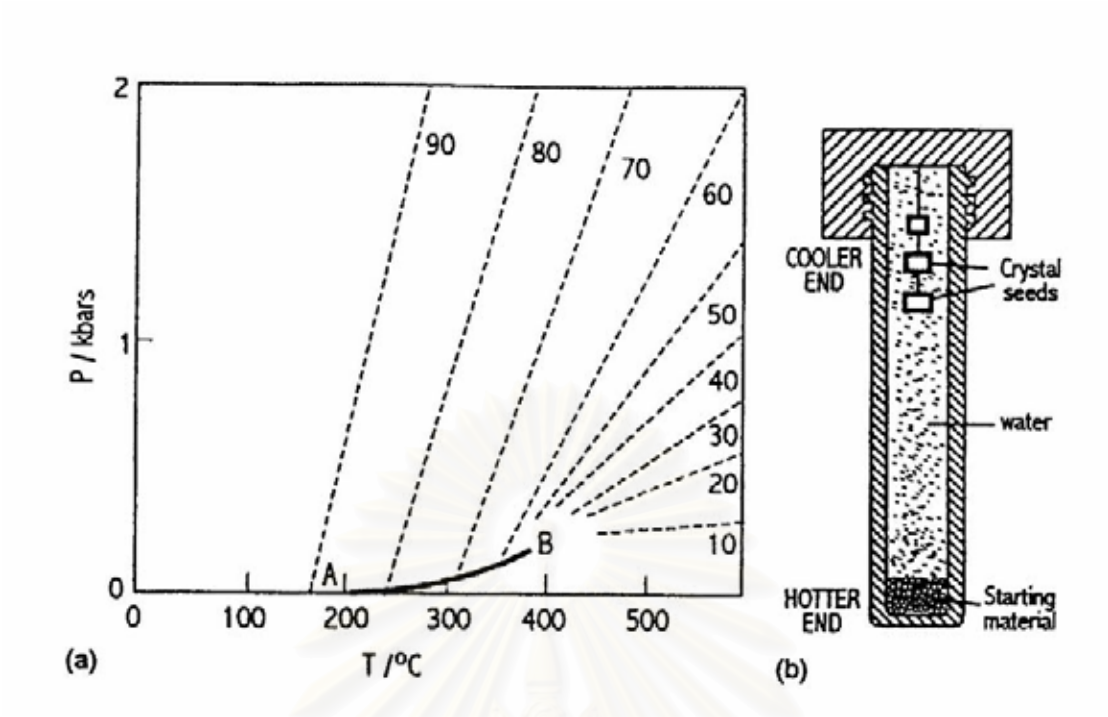

Figure 3.2: (a) Pressure-temperature relations for water at constant volume, dashed curves represent pressures developed inside a close vessel by water at ordinary P, T. (b) Schematic hydrothermal bomb used for crystal growth. [90]

3.4 Sintering of crystalline materials

Sintering is a process of densification driven by interfacial energy. Material moves by viscous flow or diffusion in such a way to eliminate porosity and thereby reduce the solid/vapor interfacial area. There are many excellent reviews on this subject, including the text by Kingery et al. [91]. Coble and Burke [92] described the physical principles of sintering, including early theoretical and experimental work. Theoretical and practical aspects of microstructural control sintering are discussed by Yan [93]

As for viscous sintering, the driving force for densification of crystalline materials is surface energy. The surface energy is often higher than for glasses, typical values being ~1000-1200 ergs/cm^2 [91] but are equally weakly dependent on temperature and composition. Material tends to move from regions of positive (convex) curvature to regions of negative (concave) curvature. This leads to the filling of necks between particles. One important aspect, in which crystalline and amorphous materials are different, is that the plane of contact between crystals, called the grain boundary, has a specific interfacial energy, γ_{gb}. This energy reflects the fact that the crystal planes in the respective particles do not match perfectly at the boundary. The existence of the grain boundary energy means that the energy gained by eliminating porosity is partially offset by the energy invested in creating necks between the grains. It also means that grains have a tendency to grow to reduce their energy by decreasing their surface-to-volume ratio. The grain boundary energy dictates the shape of pores. Balance of forces requires that the surfaces of the grains meet at the grain boundary at the dihedral angle, ψ, where

$$\psi = 2\cos^{-1}(\gamma_{gb}/\gamma_{sv})$$

The pore will shrink if the surface of the grains is concave toward the pore. The tension created by curvature produces higher concentration of vacancies, so that atoms tend to diffuse from the grain boundary to the surface of pore. When many grains surround a pore, the requirement of preserving ψ at the grain boundary forces the grains to have positive curvature i.e. the center of curvature is within the solid

phase. This reduces the vacancy concentration at the surface of the pore, inducing diffusion away from the pore, causing it to grow. Whether a pore will shrink or grow thus depends on the value of ψ and the number of grains surrounding the pore [94] (the fewer neighbors, the more likely it is to shrink). Neither stable nor growing pores are thermodynamically favorable in amorphous systems. This is account in part for the relative ease of glasses sintering.

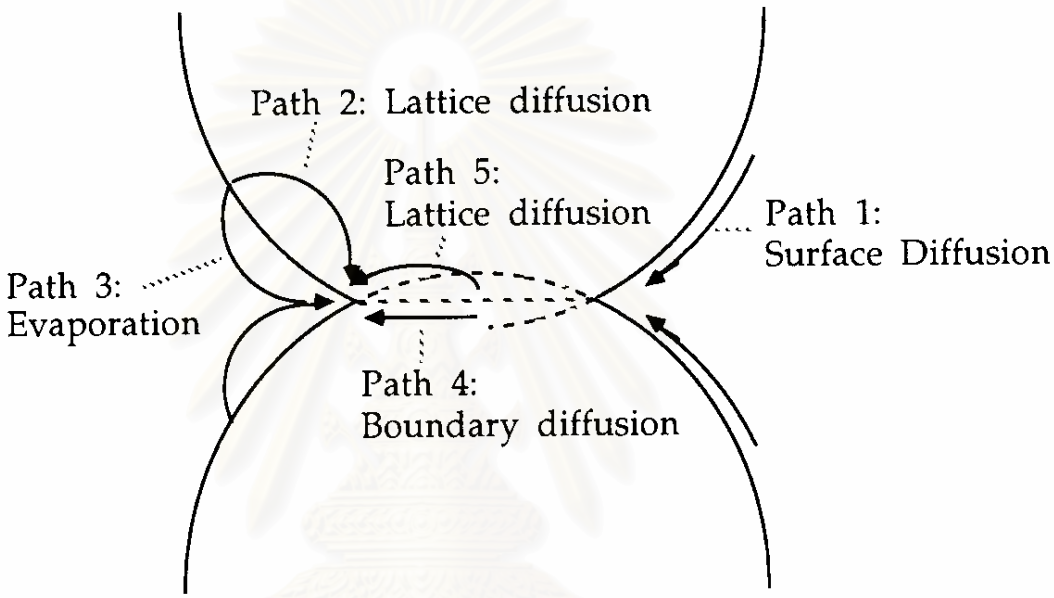

Figure 3.3: Paths for material transport in sintering of crystalline materials [89]

Several mechanisms and paths by which material can be transported are illustrated in Figure 3.3. The easiest paths are (1) along the surface of the particle and (3) through the vapor phase. Both surface diffusion and evaporation/condensation carry material to the neck and thereby reduce the energy of the system, but neither mechanism produces densification. The same is true for path (2), which brings material from the convex surface to the neck by diffusion through the crystal lattice. Such processes coarsen the body by making the necks and possibly the pores, larger (see Figure 3.4). Shrinkage can only occur if material is removed from the point of contact (i.e., from the grain boundary), so that the centers of the particles can move toward one another. Paths (4) and (5) carry material from the grain boundary to the perimeter of the neck, resulting in shrinkage. The mobility of the atoms is high within the grain boundary, but the flux of atoms is small because the grain boundary is very

thin (~l nm). Diffusion through the lattice is much slower, but the flux can pass through a much larger area. Thus, the net rate of transport by lattice diffusion may by greater. The size of the particles influences whether grain boundary diffusion or lattice diffusion (also called volume diffusion) is more important: the smaller the grain, the larger the volume fraction occupied by the grain boundary. In addition, the activation energy for grain boundary and surface diffusion are lower than the activation energy for lattice diffusion, so the latter tends to dominate at higher temperatures. The kinetics of sintering depend on which of these paths and transport mechanisms is dominant. The importance of grain boundaries in sintering of crystalline materials can hardly be overestimated. A pore that is not intersected by a grain boundary is, for all practical purposes, trapped. That is, a pore inside a grain cannot shrink without diffusion of atoms through the grain from some distance boundary.

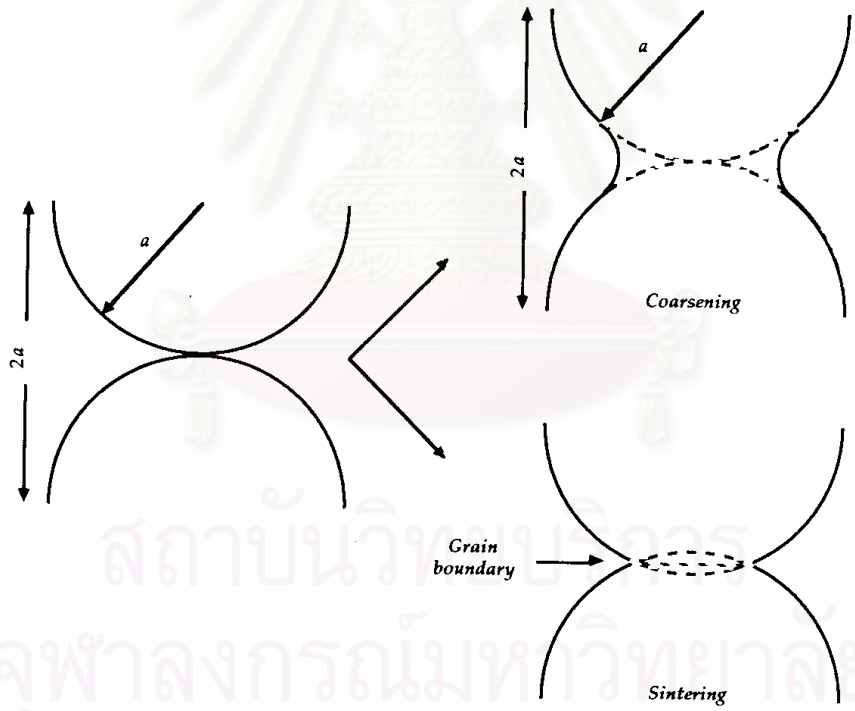

Figure 3.4 Coarsening is a growth in the neck between particles without any decrease in the distance between their centers. Densification requires removal of material from the grain boundary between particles. [89]

CHAPTER IV

EXPERIMENTAL

The experimental system and the procedures for preparation of alumina are presented in this chapter. There are two different types of equipments explained in this chapter depend on the experiment done at Inoue laboratory Kyoto Japan (IL) or Catalysis laboratory Thailand (CL). The chemicals and the experimental equipment are shown in sections 1 and 2, respectively. The preparation and characterization of products are explained in section 3 and 4, respectively.

4.1 Chemicals

The list of chemicals using in the experiment are shown in the following:

1. Aluminum isopropoxide (98%+) (AIP, $((CH_3)_2CHO)_3Al$) available from Aldrich Chemical Company, USA.
2. Toluene (99%) $C_6H_5CH_3$ available from Merck Co., Ltd., Germany.
3. Mineral oil available from Merck Co., Ltd., Germany.
4. Ultra high purity nitrogen gas (99.99%vol.) with oxygen and moisture content less than 3 ppm available from Thai Industrial Gas Co., Ltd., Thailand.

4.2 Equipment

All equipments using for the catalyst preparation consisted of:

4.2.1) Autoclave reactor

- Made from stainless steel
- Volume of 1000 cm^3 (IL) 200 cm^3 (CL)
- Maximum temperature of 350^oC
- Pressure gauge in the range of 0-140 bar (IL) and 0-300 bar (CL)
- Relief valve used to prevent the runaway reaction (CL)
- Iron jacket was used to reduce the volume of autoclave to be 300 cm^3 (CL)
- Test tube was used to contain the reagent and solvent
- Cooling line was used to condense the solvent vaporizing from the autoclave

The autoclave reactor is shown in Figure 4.1

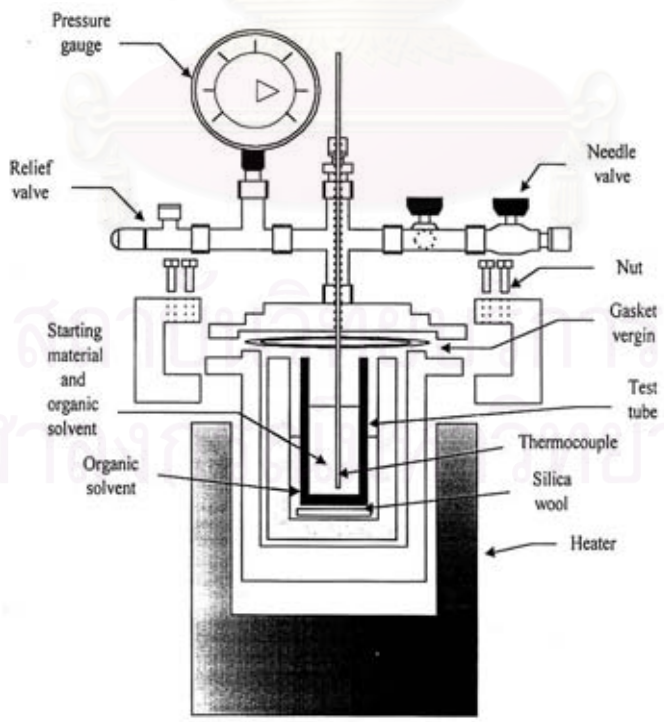

Figure 4.1: Autoclave reactor

4.2.2) Temperature program controller

A temperature program controller was connected to a thermocouple attached to the reagent in the autoclave.

4.2.3) Electrical furnace (Heater)

Electrical furnace supplied the required heat to the autoclave for the reaction.

2.4) Gas controlling system

Nitrogen was set with a pressure regulator (0-150 bar) and needle valves are used to release gas from autoclave.

The diagram of the reaction equipment is shown in Figure 4.2.

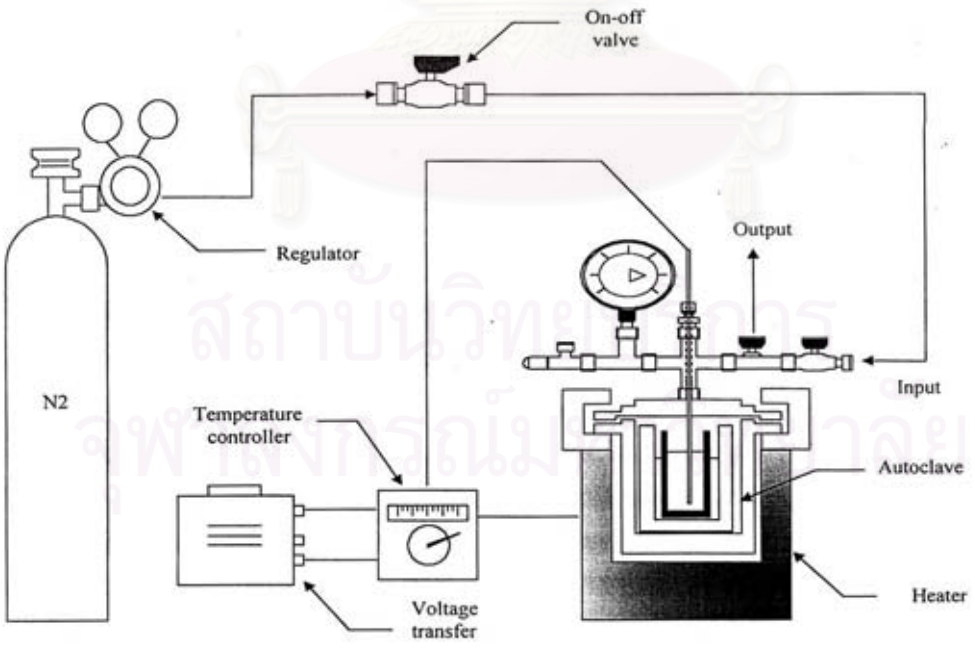

Figure 4.2: Diagram of the reaction equipment for the catalyst preparation

4.3 Synthesis of alumina

Appropriate amount of aluminum isopropoxide (AIP) was dissolved on 100 ml of inert organic solvent (toluene or mineral oil) in a test tube, which was then placed in the autoclave. The gap between the test tube and the autoclave wall was filled with 30 ml of the same solvent. The autoclave was purged completely by nitrogen and heated up to the desired temperature at a rate of 2.5^{o}C/min, and held at that temperature for a desired reaction time. After the mixture was cooled down, the resulting product was repeatedly washed with acetone and then dried in air.

For the experiment in Japan the same procedure was followed but only 60 ml of toluene was added in the beaker.

For some experiments in toluene, a different drying process was applied as follows. After the reaction for 2 h, the valve of the autoclave was slightly opened to release the organic solvent from the autoclave by flash evaporation while keeping at the reaction temperature. The valve was opened until the pressure inside the autoclave was decreased to atmospheric level. The dry products were obtained directly after the assembly was cooled down without the step of washing by methanol and centrifugation.

The calcination of the thus-obtained product was carried out in a box furnace. The product was heated at a rate of 10°C/min to a desired temperature and held at that temperature for 1 h.

4.4 Characterization

4.4.1) X-ray diffraction (XRD)

In Thailand, the powder X-ray diffraction (XRD) was performed on a X-ray diffractometer SIEMENS D5000. The experiment was carried out by using Ni-filtered CuKα radiation, whereas a powder X-ray diffractometer (Shimadzu XD-D1, Kyoto, Japan) was operated using CuKα radiation and a carbon monochromator in Japan. Scans were performed over the 2θ ranges from 10° to 70°. The crystallite size was calculated from the Scherrer equation. The value of shape factor, K, was taken to be 0.9 and α-alumina was used as an external standard.

4.4.2) Scanning electron microscopy (SEM)

The morphology and the size of secondary particle of the samples were observed on a JSM-5410LV scanning electron microscope at the Scientific and Technological Research Equipment Center, Chulalongkorn University (STREC).

4.4.3) Transmission electron microscope

The morphology and the size of primary particles of the samples were observed on a JEOL TEM-200cx transmission electron microscope, operated at 100 kV at the Scientific and Technological Research Equipment Center, Chulalongkorn University (STREC).

4.4.4) Thermogravimetric analysis and Differential thermal analysis (TG&DTA)

The weight loss and thermal behavior of the samples were performed on a Shimadzu TG-50 thermal analyzer at a heating rate of 10°C min^{-1} in a 40 ml min^{-1} flow of dried air.

4.4.5) Infrared Spectroscopy

The functional group in the samples was determined by using an Infrared spectrometer Nicolet Impact 400 at Petrochemical Engineering Laboratory, Chulalongkorn University. Before measurement, the sample was mixed with KBr and then was formed into a thin wafer.

4.4.6) Surface area measurement

Nitrogen adsorption isotherms were determined on a gas sorption system (Quantachrome, Autosorb-1, Yuasa-Ionics, Tokyo, Japan). The pore size distribution was calculated by BJH method using desorption branch of the isotherm.

Specific surface area of the product was calculated using the BET single point method on the basis of nitrogen uptake measurement at 77 K.

CHAPTER V

RESULTS AND DISCUSSIONS

In this chapter, the experimental results and discussions are presented and divided into 4 sections. Effects of reaction conditions on the formation of χ-alumina prepared by the thermal reaction of AIP in toluene, which is important in the study of the crystallization mechanism of χ-alumina, is discussed in section 5.1. Section 5.2 is devoted to the effects of stirring and product recovery method on the properties of χ-alumina, i.e., phase transformation behavior, pore size distribution, and pore volume. Thermal decomposition of AIP in mineral oil is presented in section 5.3. Finally, the phase transformation behavior of χ-alumina prepared in both solvent is proposed in section 5.4.

5.1 Effect of reaction conditions on the formation of χ-alumina

The XRD patterns of products obtained by the thermal decomposition of AIP in toluene under various conditions are shown in Figure 5.1. The product obtained by the reaction at 300°C for 2 h (Al300C2h) was essentially amorphous, although weak peaks due to pseudoboehmite were apparently observed. On the other hand, the XRD pattern of Al315C2h clearly showed a peak at $2\theta = 42.5^{o}$. This peak corresponds to the prohibited 321 diffraction of the spinel structure and clearly indicates the formation of χ-alumina [24, 26, 51]. An amorphous product was obtained when the reaction was quenched just after the autoclave temperature reached 315°C (Al315C0h). This result suggests that crystallization of χ-alumina took place by a solid-state transformation mechanism from the amorphous product deposited from the solution.

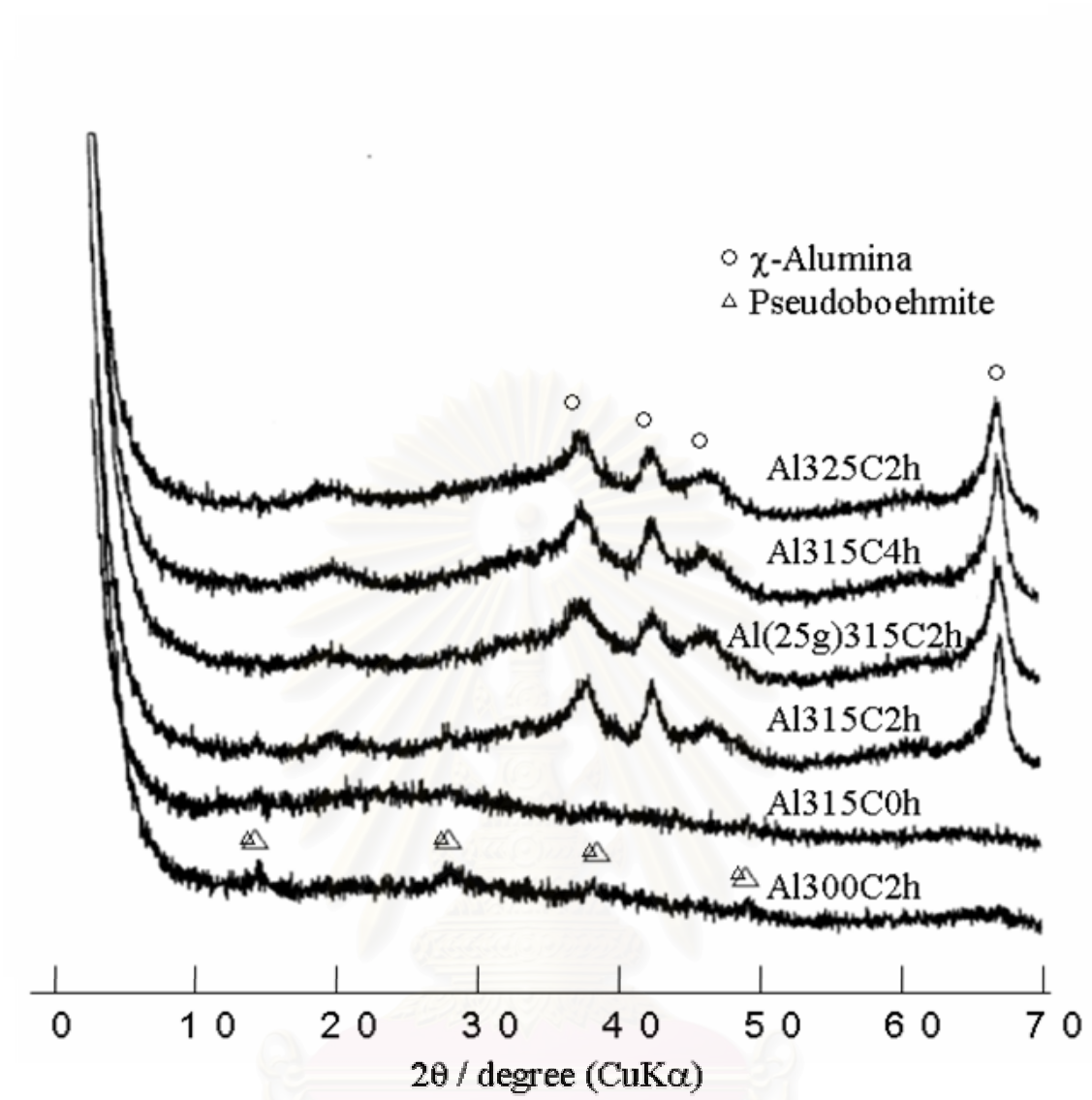

Figure 5.1: XRD patterns of the product obtained by thermal decomposition of AIP in toluene under various conditions

To examine the stoichiometry of the reaction, the recovered solvent was analyzed by gas chromatography. Only toluene was detected, but 2-prpanol was not found, indicating that the organic moiety of AIP decomposed into propene. Therefore, overall reaction can be written as follows:

$$Al(OCH(CH_3)_2)_3 \xrightarrow{\text{toluene}} 1/2Al_2O_3 + 3C_3H_6 + 3/2H_2O$$

When a large amount of water (5-10 ml) was added in the gap between the autoclave wall and the test tube, pseudoboehmite was formed by the hydrothermal

reaction of AIP. However, a small amount of water (0.7 ml) did not affect the formation of χ-alumina, indicating that the presence of toluene in the reaction retarded the hydrothermal conversion into pseudoboehmite. Note that this procedure avoids direct hydrolysis of AIP because water was not added to the reaction vessel. However, water dissolved in the reaction medium from the gas phase at high temperatures facilitates hydrothermal crystallization of the products. This method was originally applied for the synthesis of large surface area zirconia from zirconium alkoxide [11].

Physical properties of the as-synthesized products are summarized in Table 5.1. Amorphous products (Al300C2h and Al315C0h) had higher surface areas and lower bulk densities and exhibited larger weight losses when compared with the χ-alumina products. Surface areas and crystallite sizes of the latter products fell within a relatively narrow range irrespective of the reaction conditions.

Table 5.1: The physical properties of products obtained by the thermal decomposition of AIP in toluene with the different of reaction temperature and holding time

Sample name	BET surface area (m^2/g)	Crystallite size (nm)	Bulk density (g/cm^3)	%Weight loss
Al300C2h	292	-	0.34	28
Al315C0h	291	-	0.35	36
Al315C2h	201	10.3	0.6	12
Al325C2h	211	10.7	0.64	18
Al315C4h	213	10.8	0.67	11
25Al315C2h	244	9.9	0.6	16

Al300C2h means the product prepared by the reaction of AIP in toluene at 300°C for 2 h.
Al315C0h means the product prepared by the reaction of AIP in toluene at 315°C for 0 h.
Al315C2h means the product prepared by the reaction of AIP in toluene at 315°C for 2 h.
Al325C2h means the product prepared by the reaction of AIP in toluene at 325°C for 2 h.
Al315C4h means the product prepared by the reaction of AIP in toluene at 315°C for 4 h.
25Al315C2h means the product prepared by the reaction of 25 g of AIP in toluene at 315°C for 2 h.

If one assumes that the primary particle of χ-alumina is a sphere having a diameter identical to the crystallite size (10 nm), and that the true density of χ-alumina is 3.0, the specific surface area of the sphere is calculated to be 200 m^2/g. This value is in good agreement with the observed surface areas of the products, indicating that each primary particle (crystallite) of the product exposes its entire surface to the adsorbate molecules (nitrogen).

It must be noted that χ-alumina (Al(25g)315C2h) was also obtained when a large amount of AIP (25 g) was charged to the reaction. This is important for a large-scale production of χ-alumina. As shown in Table 5.1, the increase in the charged amount of AIP slightly decreased the crystallite size and increased the BET surface area of the product. This result can be explained by the increase in the nucleation population in the homogeneous solution.

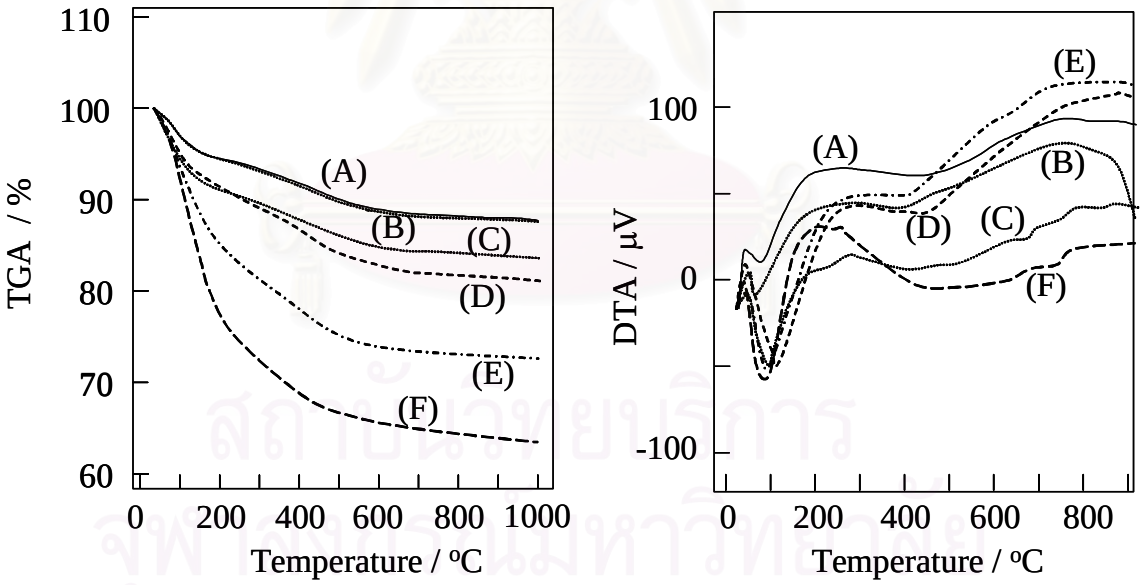

.

Figure 5.2: TG and DTA data of the products: (A) Al315C4h, (B) Al315C2h, (C) 25Al315C2h, (D) Al325C2h, (E) Al315C0h, (F) Al300C2h

Results for thermal analysis of the products are shown in Figure 5.2. Two weight-decrease processes were detected, both of which were accompanied by endothermic peaks in DTA. The first was observed below 160°C and is due to the desorption of physisorbed water. The second weight decrease occurred at 300-600°C and may be attributed to the dehydration of surface hydroxyl groups. However, if one assumes that the whole surface (200 m^2/g) of the product is covered with surface hydroxyl groups, each of which occupies 7.8 x 10^{-2} nm^2 (calculated from the cell dimension of gibbsite), the weight decrease due to the dehydration of the surface hydroxyl groups yielding surface anion vacancies and surface oxide ions is calculated to be 3.83%. The observed weight decrease at 300-600°C was 4.2-5.6% and exceeds the calculate value. Therefore, the products seem to contain structural hydroxyl groups or strongly bound chemisorbed water.

IR spectra of the products are shown in Figure 5.3. Peaks characteristic of organic moieties such as isopropyl groups and aromatic rings were not observed, indicating that the organic moiety of AIP decomposed completely during the reaction and only hydroxyl groups was presented on the surface of products. All the products exhibited weak bands due to boehmite [12]. Since the transition alumina had a broad, featureless band in the structural vibration region, presence of a small amount of boehmite can be detected by the IR spectra even though XRD patterns did not exhibit the peaks due to boehmite.

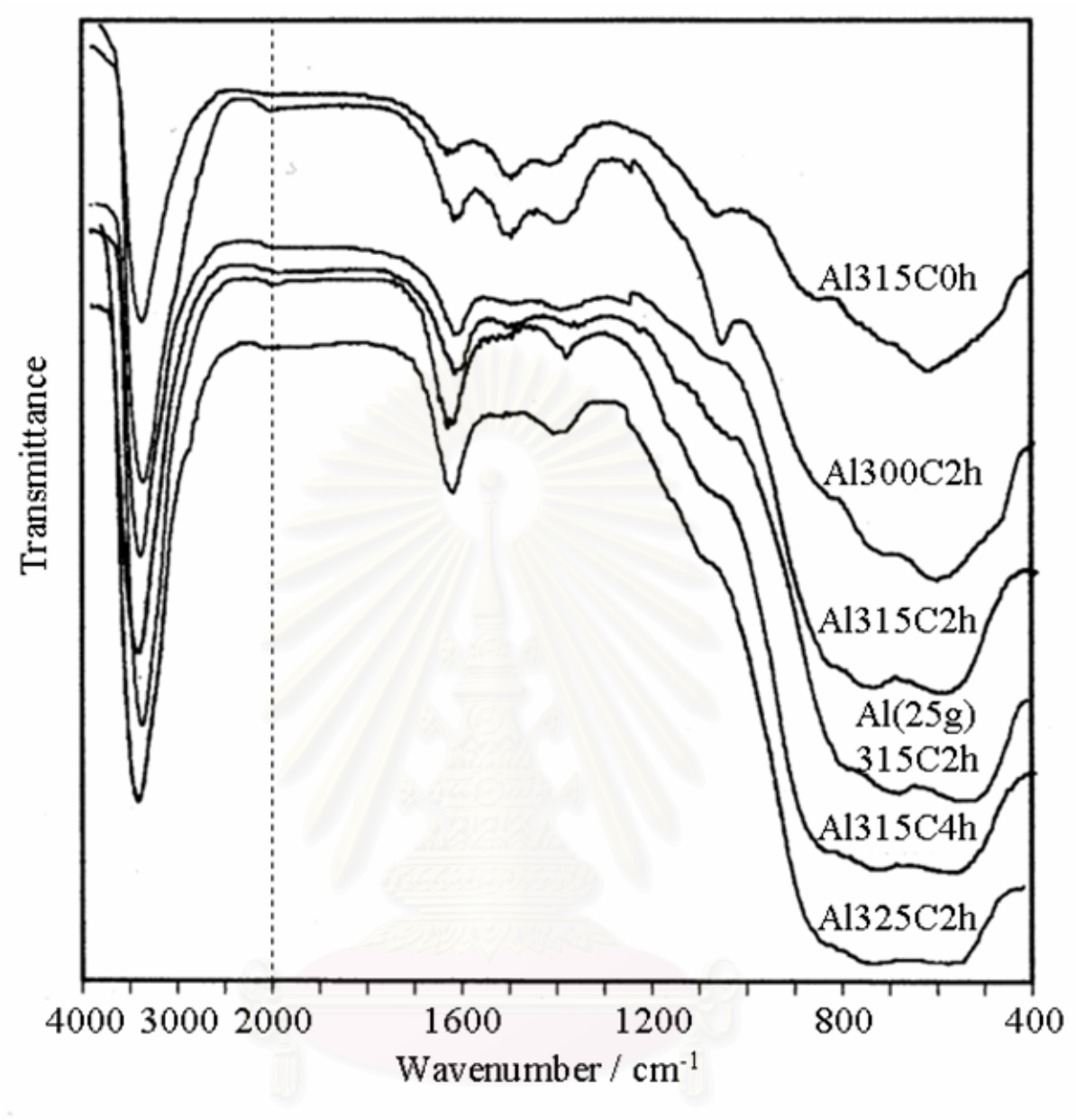

Figure 5.3: The IR spectra of as-synthesized products

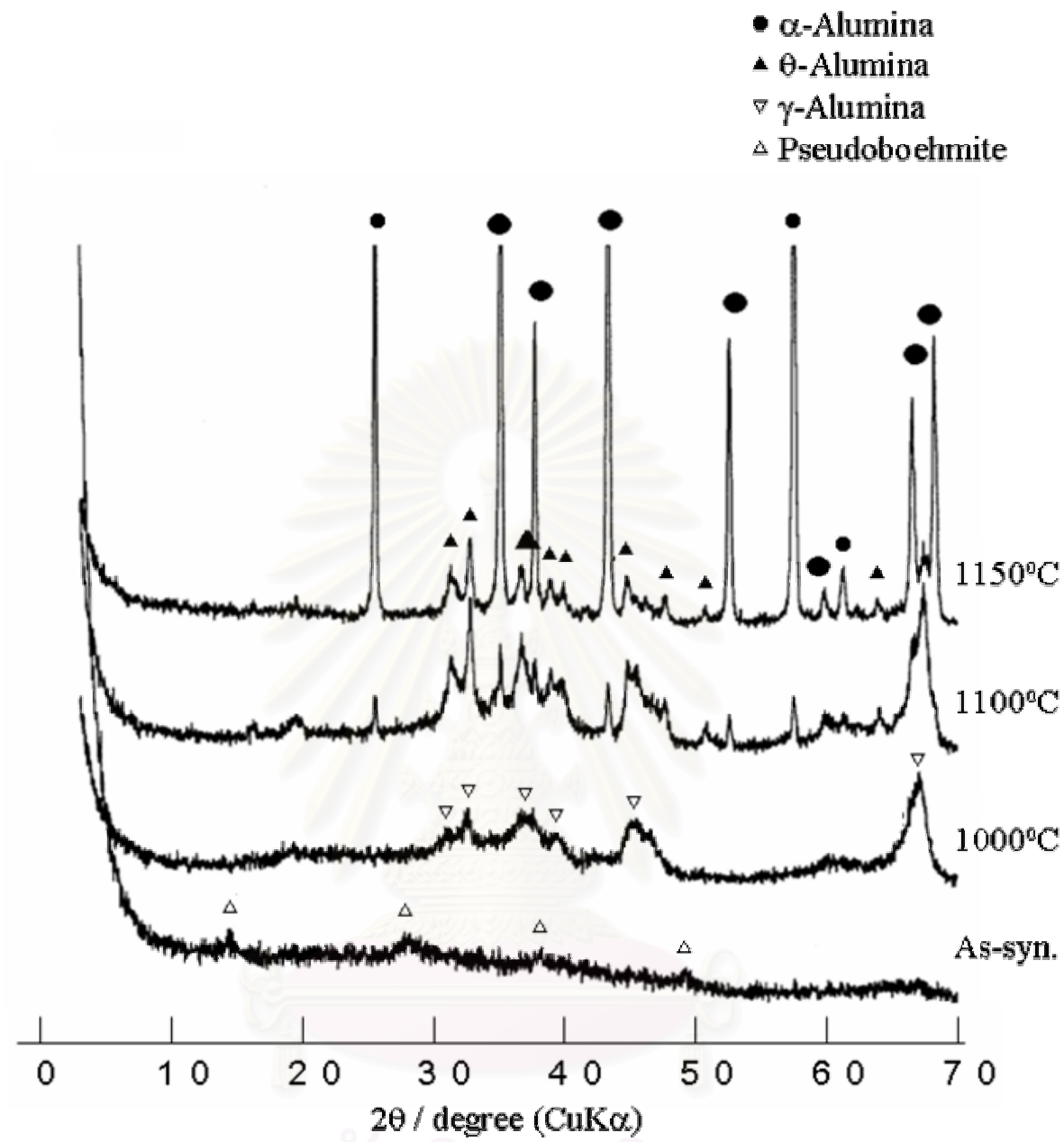

Figure 5.4: The XRD patterns of the product obtained by the thermal decomposition of AIP in toluene at 300°C for 2 h and calcined product thereof at various temperatures.

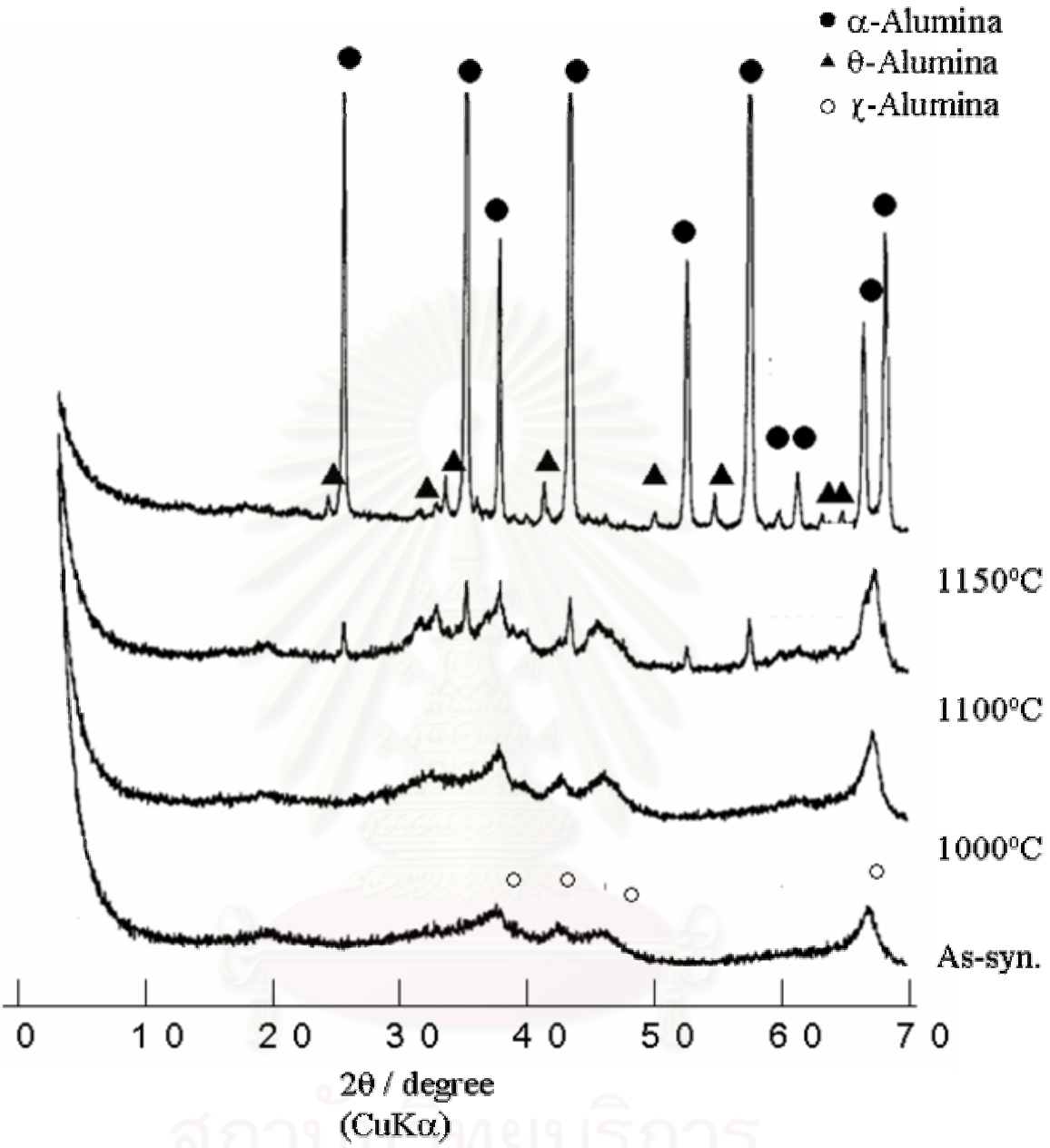

Figure 5.5: The XRD patterns of the product obtained by the thermal decomposition of AIP in toluene at 315°C for 2 h and calcined product thereof at various temperatures.

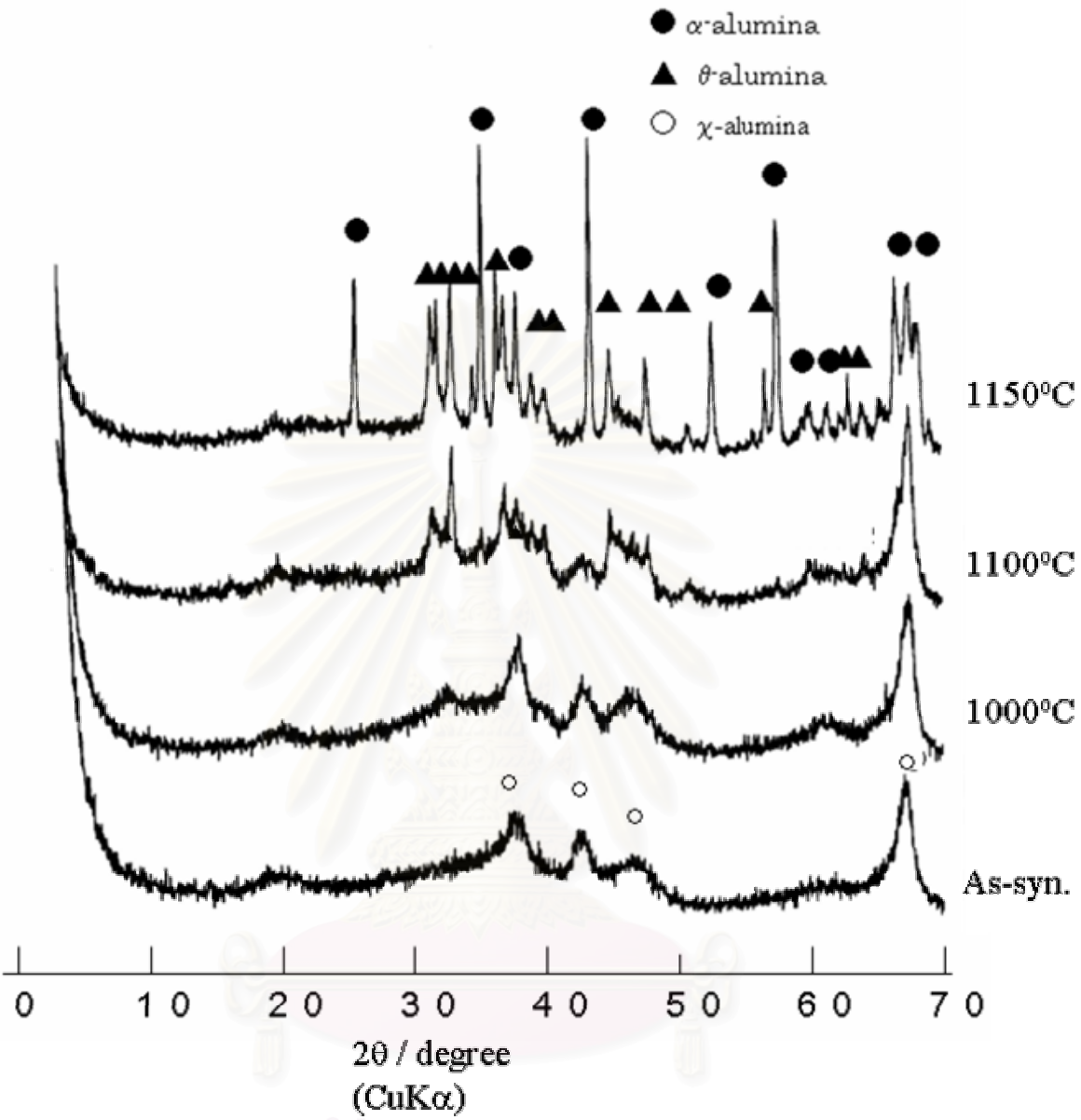

Figure 5.6: The XRD patterns of the product obtained by the thermal decomposition of AIP in toluene at 325°C for 2 h and calcined product thereof at various temperatures.

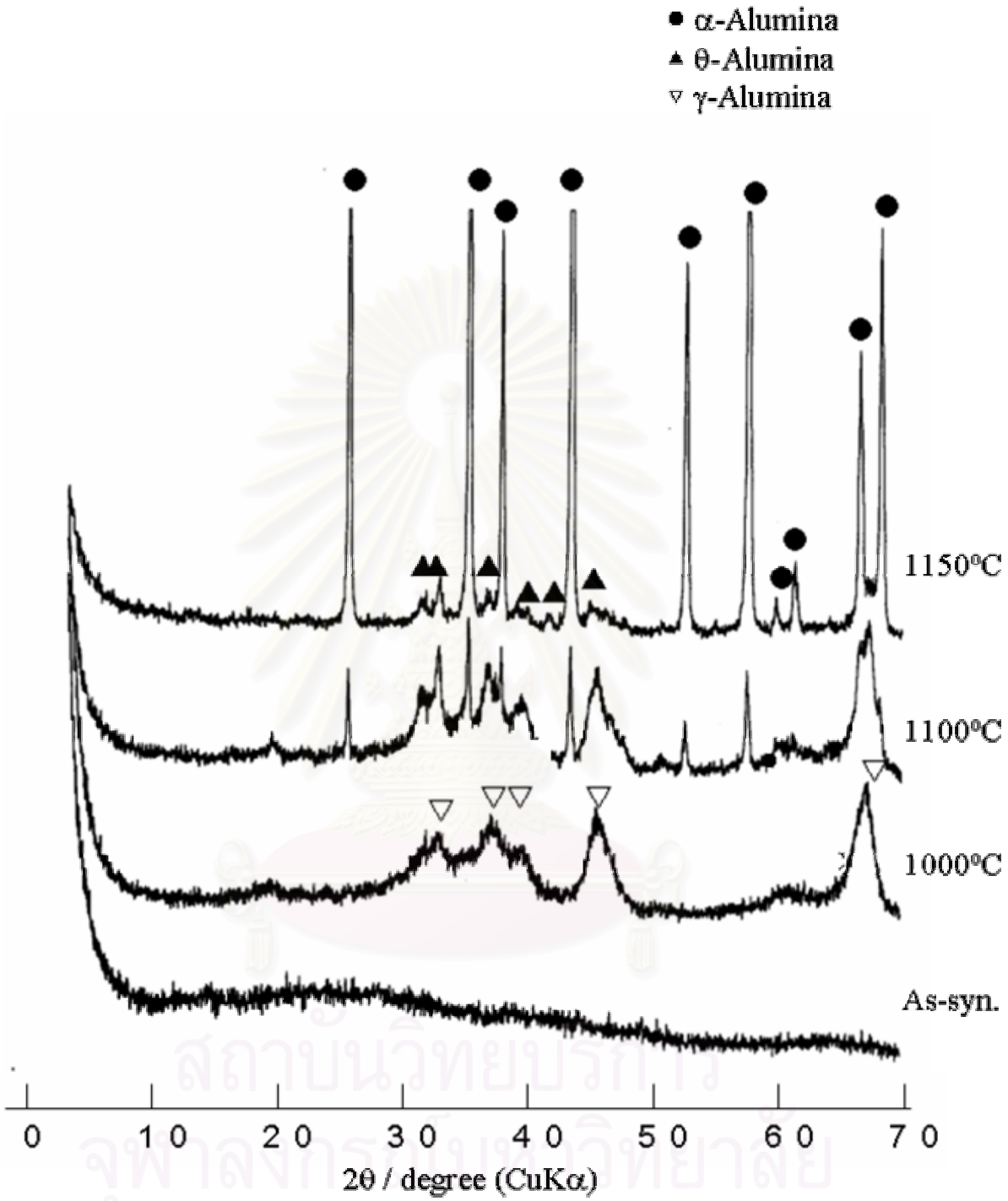

Figure 5.7: The XRD patterns of products obtained by the thermal decomposition of AIP in toluene at 315°C without holding time calcined at various temperatures.

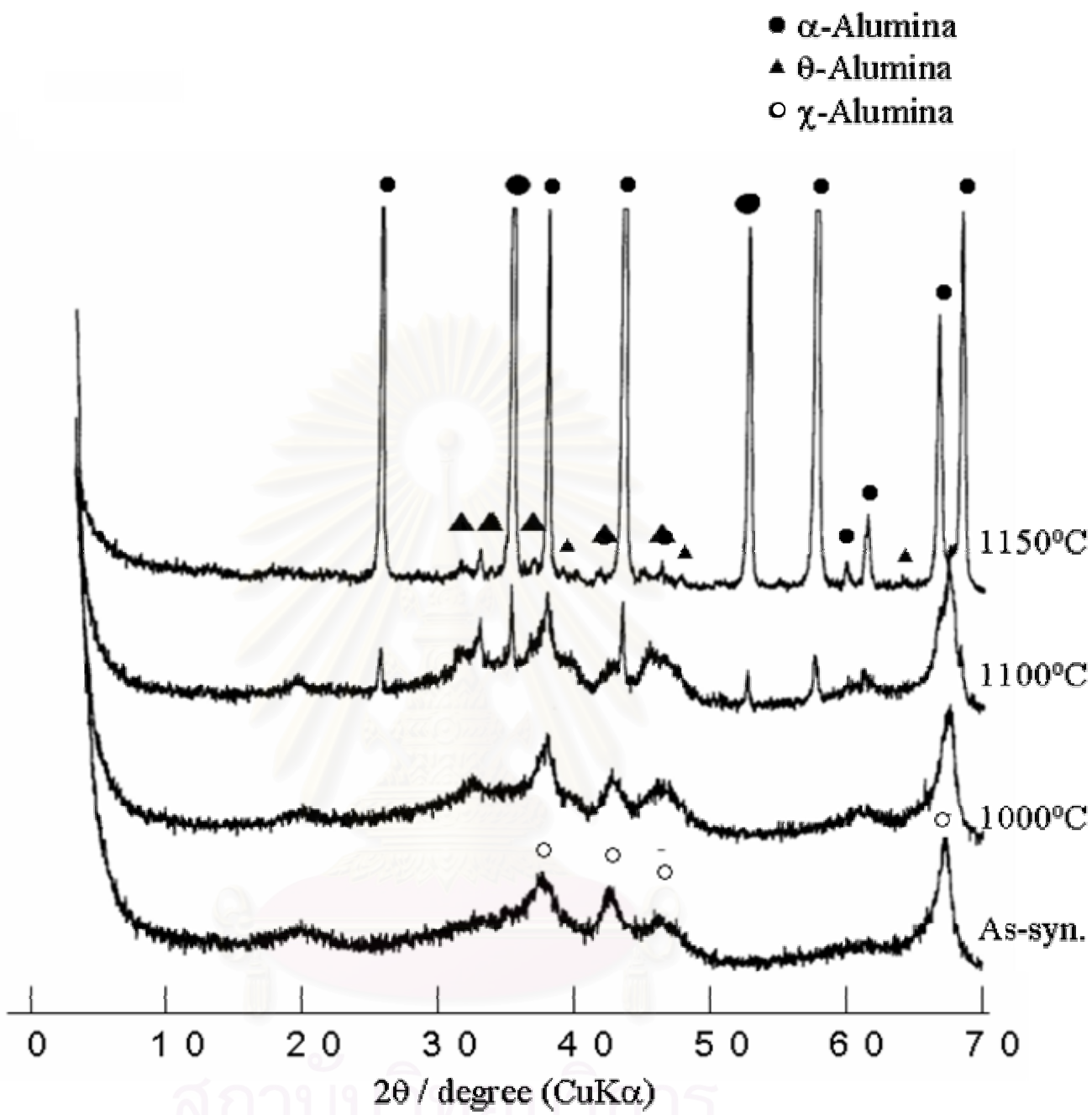

Figure 5.8: The XRD patterns of the product obtained by the thermal decomposition of AIP in toluene at 315°C for 4 h calcined at various temperatures.

The XRD patterns of Al300C2h calcined at various temperatures are shown in Figure 5.4. From the amorphous product, γ-alumina crystallized at lower temperatures. The XRD peaks due to θ-alumina were observed for the sample calcined at 1100°C, and crystallization of α-alumina started at around this temperature. Note that the peak at 42.5^{o} 2θ was not observed during the thermal transformation of the amorphous products. Since χ-alumina was not formed by thermal treatment of the amorphous phase, crystallization in the inert organic solvent seems to be essential for the formation of χ-alumina.

Figure 5.5 shows the XRD patterns of the product obtained by the reaction of AIP in toluene at 315°C for 2 h (Al315C2h) and subsequently calcined at various temperatures. The direct phase transformation of χ-alumina to α-alumina started at calcination temperature around 1100°C and almost completely transformed at 1150°C. The XRD patterns of the products obtained by the thermal decomposition of AIP in toluene at 325°C for 2 h (Al325C2h) calcined at various temperatures are shown in Figure 5.6. It is clearly observed that the α phase transformation was not complete at 1150°C.

The XRD patterns of the calcined product obtained by the thermal decomposition of AIP in toluene at 315°C without holding time (Al315C0h) are shown in Figure 5.7. Phase transformation behavior of Al315C0h, as this product was amorphous, was similar to that of Al300C2h, although the amount of θ-alumina remaining after calcinations at 1150°C was smaller than that for Al300C2h.These results indicate that χ-alumina is not formed by thermal treatment of the amorphous phase. Instead, crystallization in inert organic solvent is essential for the formation of χ-alumina. The α phase transformation still occurred at around 1100°C and complete at 1150°C.

Figure 5.8 shows the XRD patterns of Al315C4h calcined at various temperatures. Direct phase transformation of χ-alumina to α-alumina started at around 1100°C and essentially completed at 1150°C. A small amount of θ-alumina was detected for the sample calcined at 1150°C, and this phase seems to be formed from contaminated pseudoboehmite detected by the IR spectrum. Al315C2h

exhibited phase transformation behavior similar to that of Al315C4h.

In general, χ-alumina obtained by the dehydration of gibbsite (<200 nm) transforms into α-alumina through κ-alumina [22, 24, 25, 26, 29]:

gibbsite → χ-alumina → κ-alumina → α-alumina

However, χ-alumina obtained by the thermal decomposition of AIP in toluene transformed to stable α-alumina directly, bypassing the formation of the high temperature transition alumina, i.e., κ-alumina.

In the literature, direct transformation of low temperature transition aluminas (i.e., γ-, η- and χ-aluminas) into α-alumina without formation of high temperature transition aluminas (i.e., δ-, θ- and κ-phases) has been reported. For example, Chou and Nieh synthesized nanocrystalline alumina thin films by radio-frequency reactive sputtering deposition, and reported that the nucleation of α-alumina occurred along {220} crystallographic plane of γ-alumina [95]. Johnston et al. reported that γ-alumina prepared by laser ablation of an aluminum target in an oxygen atmosphere directly transformed into α-alumina at 1200°C, and they suggested that this result was due to the lack of water in the as-synthesized powders [96]. Shek et al. reported that amorphous powders prepared by oxidation of pure aluminum metal crystallized to γ-alumina, which directly transformed to α-alumina at 1370 K. They attributed this result to facilitation of nucleation of α-alumina by the strain relaxation of the transition alumina lattice [53]. However, relaxation of the γ-alumina structure should decrease the energy level of γ-alumina and disturb the nucleation of more stable phases. Simpson et al. reported that samples prepared via electron-beam evaporation of alumina onto a sappier substrate held at room temperature crystallized into γ-alumina, which transformed into α-alumina without formation of the other intermediate phases [50]. They attributed this result to the epitaxial growth of α-alumina on the sapphire substrate. Ogihara et al. prepared monodispersed, spherical alumina by the controlled hydrolysis of aluminum alkoxide in a dilute solution containing octanol and acetonitrile [97]. They found that the amorphous product

crystallized to γ-alumina at 1000°C which converted to α-alumina at 1150°C without intermediate phases [97]; however they did not give any explanation to this result. It is also reported that γ-alumina formed by thermal decomposition of aluminum sulfate transforms into α-alumina directly [98-100].

Although we cannot draw common feature for the aluminas that directly transform into α-alumina, the following two points are addressed:

1) Except those formed from aluminum sulfate, the transition aluminas that exhibited direct transformation into α-alumina were prepared from aluminum metal or alkoxide and therefore free from foreign ions.

2) γ-Alumina crystallized at high temperatures has tendency to transform to α-alumina without formation of high temperature transition aluminas.

The first point would stabilize the low temperature transition alumina structure and disturb the crystallization of high temperature transition alumina, thereby facilitating direct crystallization of α-alumina. For the second point, γ-alumina crystallized at high temperature would contain a lesser number of crystal defects than that crystallized at lower temperatures, since sufficient thermal energy is supplied at the crystallization stage. This also lower the energy level of the transition alumina and prohibits the formation of high temperature transition aluminas.

Gibbsite is usually contaminated with a small amount of Na^{+} ions [22, 24], and thermal dehydration of gibbsite yielding χ-alumina cannot eliminate the Na^{+} ions from the matrix. Therefore, it exhibits very broad peaks in the XRD pattern due to the low crystallinity and many defects in the structure. It is possible that these defects in the χ-alumina structure promote the formation of κ-alumina. On the other hands, χ-alumina obtained by the thermal decomposition of AIP in toluene is not contaminated with Na^{+} ions. Moreover, the presence of a small amount of water in the solvothermal reaction possibly increases the crystallinity of the product. These situations stabilize the χ-alumina structure and disturb the formation of κ-alumina, facilitating direct transformation into α-alumina.

The BET surface areas of the calcined products are summarized in Table 5.2. Although the BET surface areas of the amorphous products (Al300C2h and Al315C0h) were higher than those of the χ-alumina products, they rapidly decreased, and ~50 m^2/g of the surface area remained when the products were calcined at 1100^oC. On the other hand, Al325C2h exhibited higher thermal stability, and maintained a BET surface area of 85 m^2/g after calcination at the same temperature.

It is generally believed that the α-transformation occurs by the nucleation and growth mechanism [20, 37, 101]. Although phase transformation of an oriented γ-alumina film was reported to proceed by a topotactic process [95], this result should be considered to be rather special case [51, 102], because topotactic transformation of transition aluminas in powder or pellet form has never been reported. Since formation α-alumina from transition alumina requires rearrangement of cubic oxygen-sublattice into hexagonal one, large activation energy is required. Nucleation of α-alumina is the rate-determining step and explosive crystal growth follows [20, 37, 101]. Because of the rapid crystal growth accompanied by α-alumina transformation, surface area of the product calacined at 1150^oC abruptly decreased as shown in Table 5.2.

Imamura et al. compared the catalytic activities of χ-alumina prepared by the present method and γ-alumina obtained by the hydrolysis of AIP, and found that these two catalysts had essentially identical activities for the isomerization of 1-butene, although the latter material had a higher surface area (261 m^2/g) [103]. Moreover, they also reported that calcinations at 1000^oC of the χ-alumina maintained 56% of the surface area of the as-synthesized product, while that of the γ-alumina decreased to 37% [103]. This result is reasonable because the former compound did not suffer from the phase transformation, while the latter transformed into high temperature transition aluminas.

Table 5.2: BET surface area of the product products obtained by the thermal decomposition of AIP in toluene with the different of reaction temperature and holding time calcined at various temperatures

Sample name	BET surface area (m^2/g)			
	As-syn	1000°C	1100°C	1150°C
Al300C2h	292	117	47	25
Al315C0h	291	107	55	10
Al315C2h	201	137	85	11
Al325C2h	211	105	75	43
Al315C4h	213	100	80	15

5.2 Effect of product recovery and stirring

Figure 5.9 shows the XRD patterns of the products obtained by the reaction of AIP in toluene at 315°C with stirring (SAl315C2h) and/or with the removal of the solvent at the reaction temperature (SPAl315C2h and SAl315C2h) showed that all the products were χ-alumina. The physical properties of the products are summarized in Table 5.3. By the removal of the solvent at the reaction temperature, BET surface area slightly increased and total pore volume significantly enlarged, while bulk density of the product decreased. These results can be attributed to the fact that this procedure avoided coagulation of the particles caused by surface tension of the liquid remaining among the particles [34], which takes place during the drying stage of the ordinary procedure.

Table 5.3. Effect of stirring and product recovery procedure on the physical properties of the as-synthesized product obtained by the thermal decomposition of AIP in toluene

Sample	BET surface area (m^2/g)	Crystallite Size (nm)	$S_t^{\dagger}$ (m^2/g)	Bulk density (g/cm^3)	Total pore volume[‡] (cc/g)	Average pore diameter[¶] (nm)	Mode pore diameter* (nm)
Al315C2h	201	10.3	203	0.6	0.709	14.1	13.2
SAl315C2h	285	12.4	283	0.57	0.626	8.8	7.4
PAl315C2h	255	8.3	243	0.1	1.899	23.5	-
SPAl315C2h	281	9.3	281	0.12	2.321	33.1	-

Al315C2h means product prepared by the reaction of AIP in toluene at 315°C for 2 h.
SAl325C2h means product prepared by the reaction of AIP in toluene at 315°C for 2 h with stirring.
PAl325C2h means product prepared by the reaction of AIP in toluene at 315°C for 2 h and recovered by super critical drying method.
SAl325C2h means product prepared by the reaction of AIP in toluene at 315°C for 2 h with stirring and recovered by super critical drying method.
[†]Calculated from the initial slope of the *t*-plot. [‡]Total nitrogen uptake at relative pressure of 0.98. [¶]Calculated from total pore volume and BET surface area assuming that the pore is tubular. *Calculated from the desorption branch of the isotherm using the BJH method.

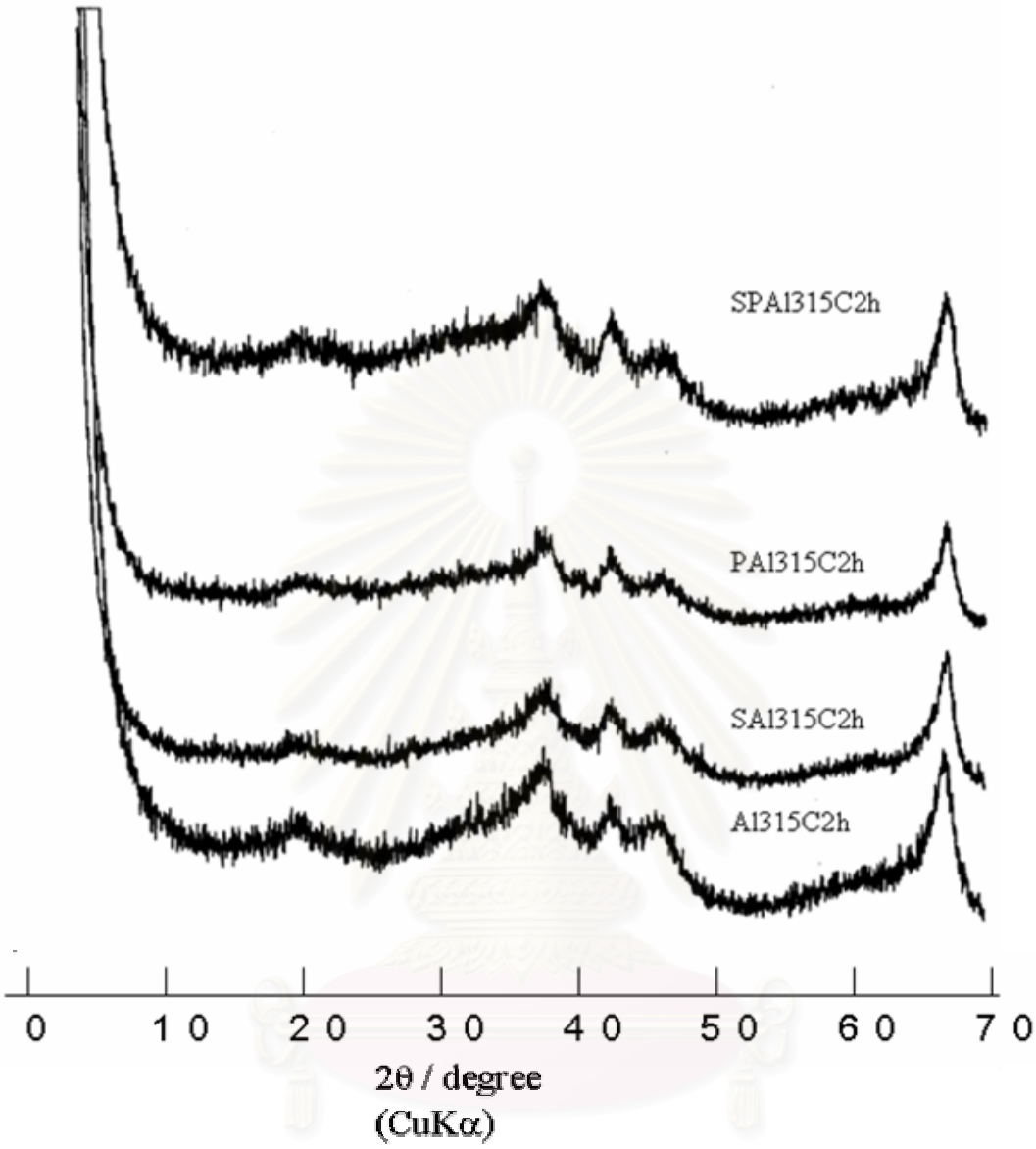

Figure 5.9: The XRD patterns of the products obtained by the reaction of AIP in toluene at 315°C by different reaction and product recovery conditions

Although the reaction temperature (315°C) was slightly lower than the critical point of toluene (318 ^{o}C), the fluid near the critical point has a nature similar to that of the supercritical fluid, and therefore this product recovery procedure can be considered as the supercritical drying method [34, 35]. By using this procedure we can conduct both the solvothermal reaction and supercritical drying in one pot, avoiding bothersome work up processes and coagulation of the products [36].

The XRD patterns of SAl315C2h calcined at various temperatures are shown in Figure 5.10. The phase transformation started at around 1100°C and completed at 1150°C. θ-Alumina was not detected during the phase transformation. This result suggests that SAl315C2h is more homogeneous than Al315C2h. Since water content in the gas phase is much higher than that in the reaction medium, particles formed near the surface of the medium can be affected by water in the gas phase. Stirring during the reaction can avoid this effect, and therefore, more homogeneous product was obtained.

BET surface areas of the calcined products are summarized in Table 5.4. It must be noted that the stirring during the reaction had a minor effect on the physical properties of the calcined products, although SAl315C2h had a larger surface area than Al315C2h. As discussed above, the reaction proceeds by initial formation of an amorphous phase through the deposition from a homogeneous solution followed by transformation into χ-alumina with the aid of adsorbed water. The surface area of the χ-alumina products seems to be determined by the particle size of the amorphous phase, which was, in turn, determined by supersaturation degree of the system. Therefore, stirring scarcely affected the surface areas of the calcined products.

Figures 5.11 and 5.12 show the XRD patterns of the products obtained by the reaction of AIP in toluene and the fluid phase was separated by the supercritical drying method with (SPAl315C2h) and without stirring (PAl315C2h) respectively. The phase transformation started at around 1150°C and almost completed at around 1200°C. PAl315C2h showed essentially the same phase transformation behavior as SPA315C2h. Note that the transformation temperatures of the products obtained by supercritical drying were more than 50°C higher than those recovered by the ordinary

method. This point will be discussed later.

As is shown in Table IV, SPAl315C2h and PA315C2h maintained high surface areas of ~75 m^2/g even after calcinations at 1150°C. This result can be attributed to the fact that these products transformed into α-alumina at higher temperatures.

Table 5.4: The BET surface areas of products calcined at various temperatures

Sample name	BET surface area (m^2/g)				
	As-syn	1000°C	1100°C	1150°C	1200°C
Al315C2h	201	137	85	11	7
SAl315C2h	285	132	85	13	8
PAl315C2h	255	142	108	73	10
SPAl315C2h	281	148	115	77	14

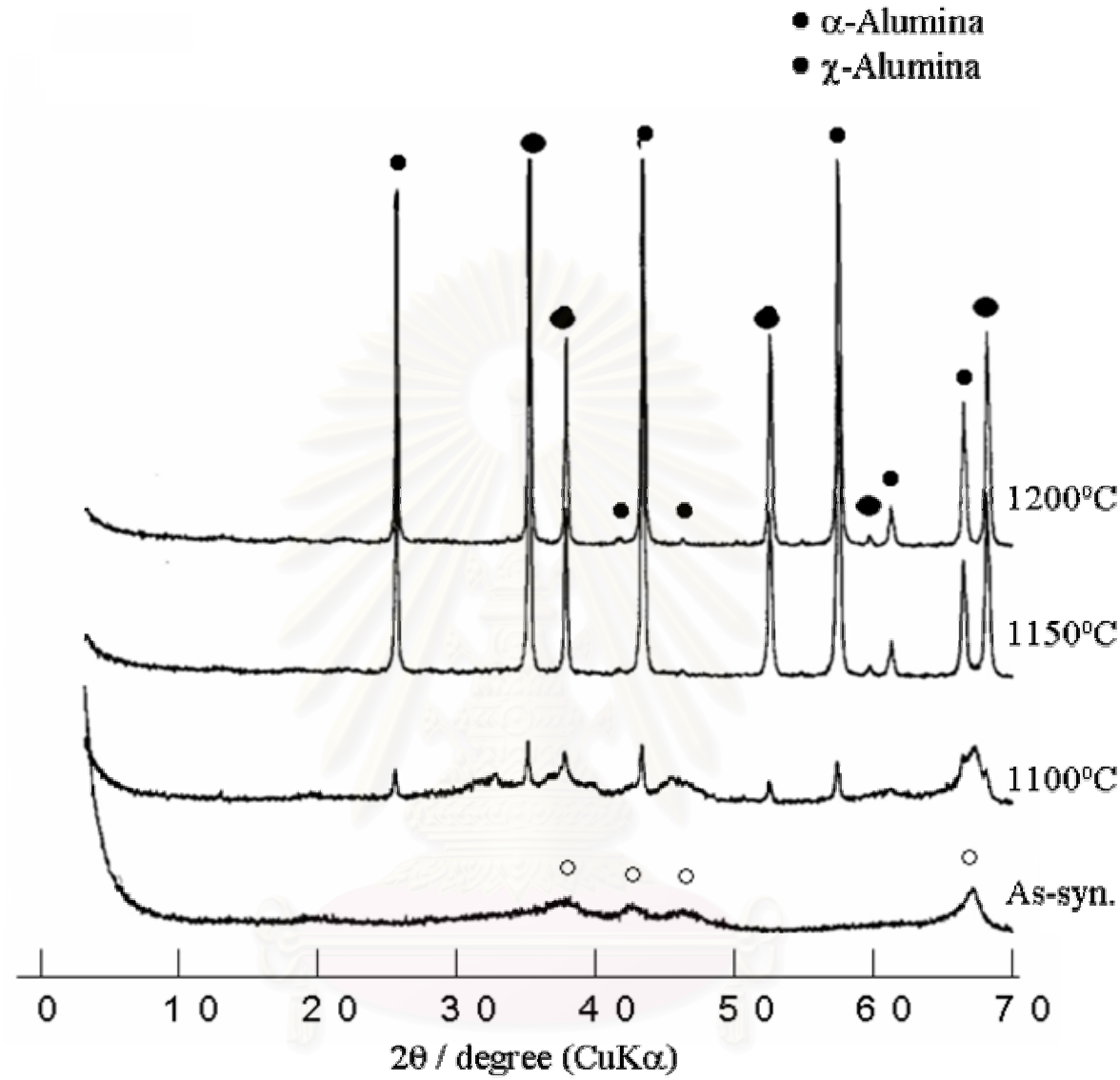

Figure 5.10: The XRD patterns of the product obtained by the reaction of AIP in toluene with stirring (SAl315C2h) and subsequently calcined at various temperatures.

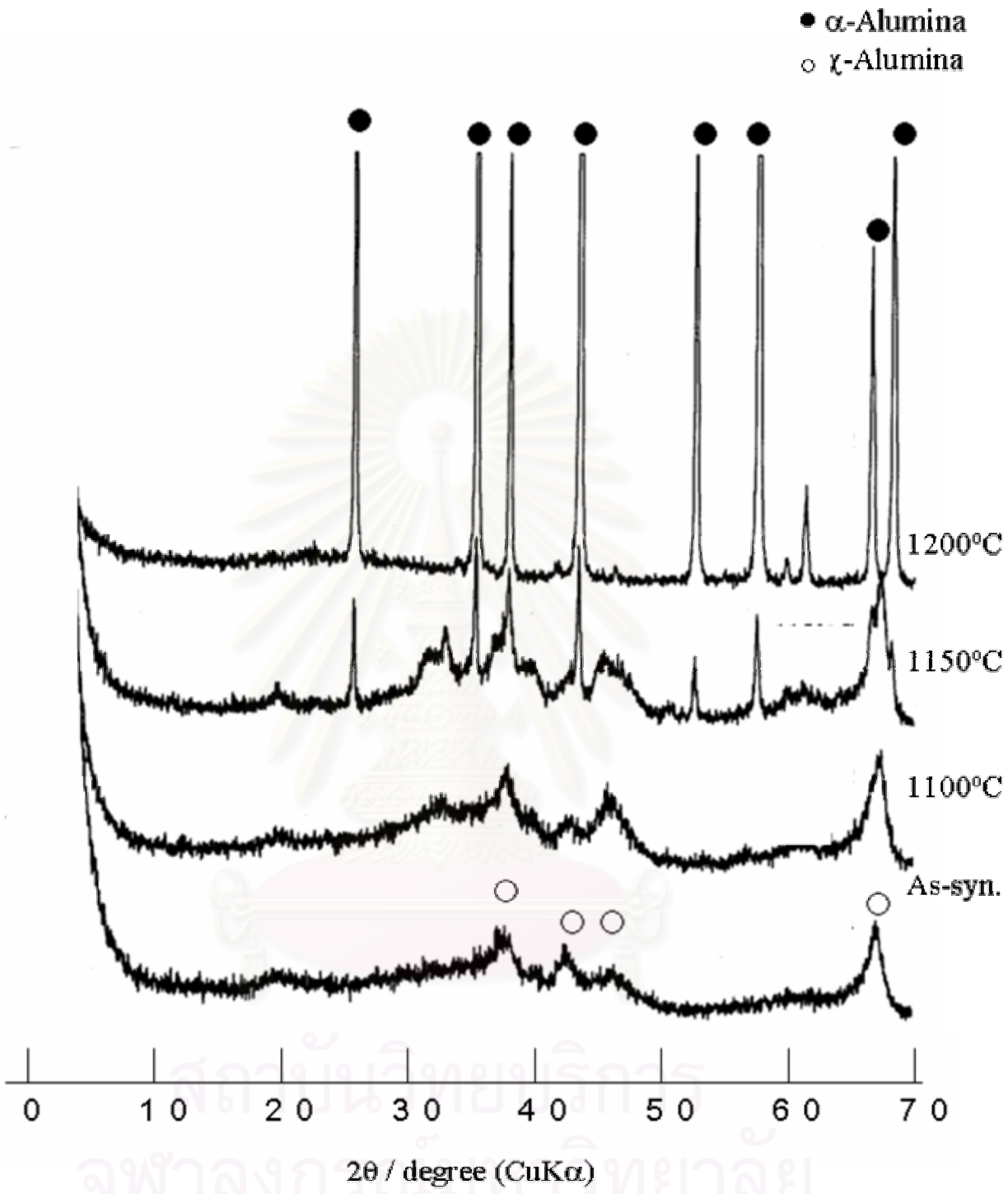

Figure 5.11: The XRD patterns of the product obtained by the reaction of AIP in toluene and the fluid phase was separated by the supercritical drying method (PAl315C2h) and subsequently calcined at various temperatures.

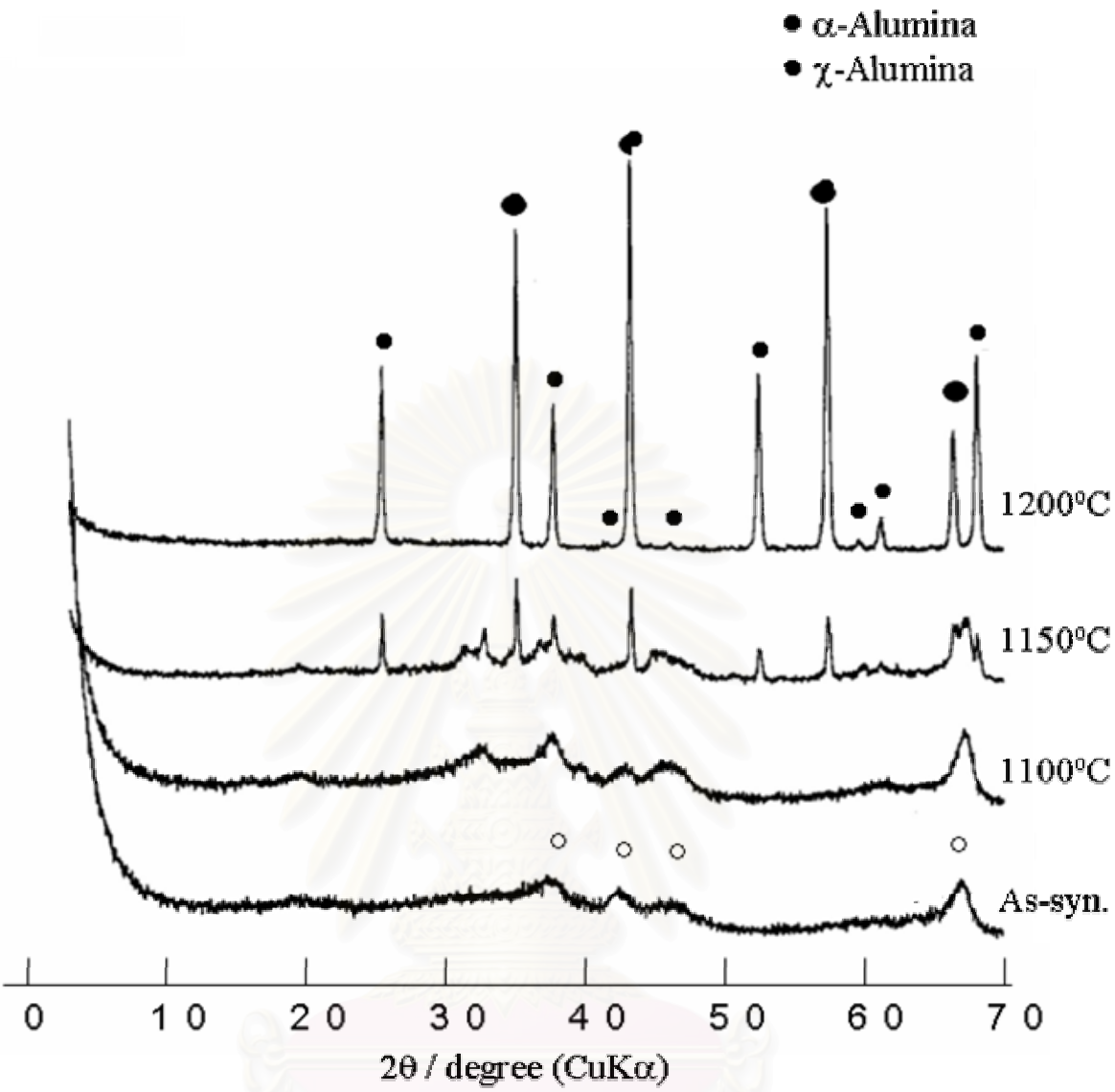

Figure 5.12: The XRD patterns of the product obtained by the reaction of AIP in toluene and the fluid was separated by the supercritical drying method with stirring (SPAl315C2h) calcined at various temperatures.

The nitrogen adsorption isotherms of the as-synthesized products are shown in Figure 5.13. The products recovered by the ordinary method (Al315C2h and SAl315C2h) exhibited a hysteresis loop characteristic of type E as classified by de Boer [104], which is explained by the presence of tabular or ink-bottle pores of varying radius [104]. Since this type of the hysteresis loop is commonly observed for shperoidal cavities or voids between close-packed spherical particles, the observed hysteresis loop seems to be due to the capillary condensation into the voids between the primary particles of χ-alumina.

The *t* plots [105-106] derived from the isotherm are presented in Fig. 5.14. In all the cases, the first part of the plot was a straight line going through the origin, and from the slope of the line, total surface area, S_t, can be calculated. When a sample has a micropore system, an abrupt decrease in the slope is detected [105-106]. The present products did not show any sign of the decrease in the slope in *t* plots indicating the absence of the micropore system. Good agreement between S_{BET} and S_t (Table 5.3) also supports this argument. At higher relative pressures (higher *t* values), the deviation from the straight line occurred because of the capillary condensation in the mesopore system formed between the primary particles of χ-alumina. The pore size distributions are shown in Fig. 5.15. Al315C2h and SAl315C2h had mode pore diameters in the mesopore range.

When the supercritical drying was performed for the product recovery, the type E hysteresis loop disappeared, which is ascribed to enlargement of pore sizes. The mode pore diameters of PAl315C2h and SPAl315C2h (Fig. 5.15) were much larger than those observed for Al315C2h or SAl315C2h, indicating that the primary particles were packed quite loosely. The supercritical drying method prevented the coagulation of the primary particles, and therefore PAl315C2h and SPAl315C2h had a macropore system formed between the loosely packed primary particles.

From the XRD and BET data, it is apparent that the products prepared by the one-pot synthesis (PAl315C2h and SPAl315C2h) had higher thermal stabilities. This can be explained by the increase in the pore size and the total pore volume (Table 5.3). Transformation from transition alumina into α-alumina takes place by mean of the nucleation-and-growth mechanism [20, 37, 101] and it is generally believed that nucleation occurs at the contact point between the particles [53]. Since the product obtained by the supercritical drying had a lesser number of contact points, the transformation into α-alumina requires higher temperature. Moreover, long distance mass transfer paths are required for the sintering of these products, which also contributes to their thermal stabilities [107].

Although sintering of the particles inevitably occurred, thermal treatment of the present products caused relatively small decrease in the surface area, because they did not suffer from the phase transformation to high temperature transition aluminas. Therefore, the present products have a potential use as catalyst materials for the use at relatively high temperatures.

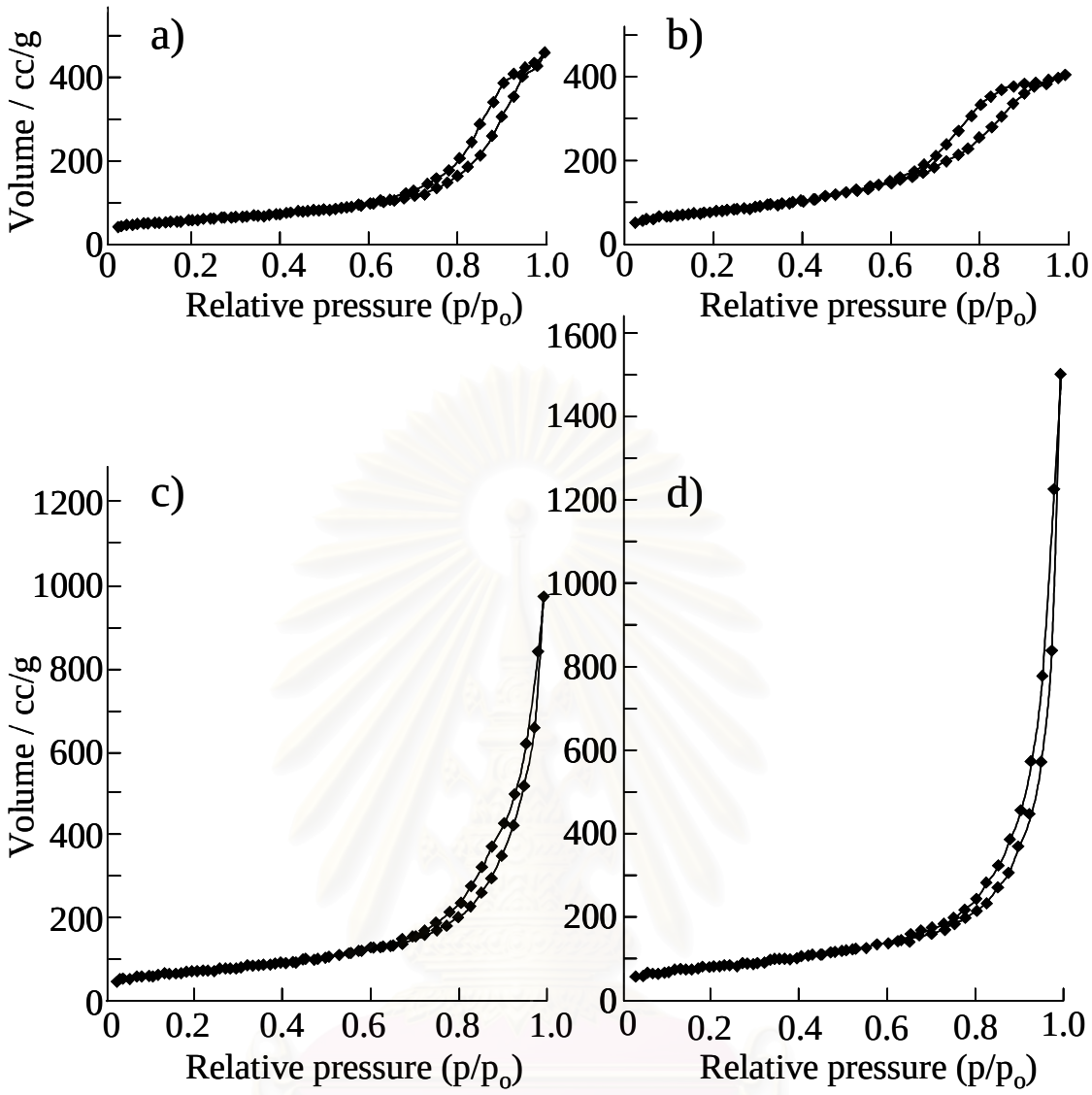

Figure 5.13: The nitrogen adsorption isotherms of as-synthesized product : (A) Al315C2h, (B) SAl315C2h, (C) PAl315C2h, (D) SPAl315C2h

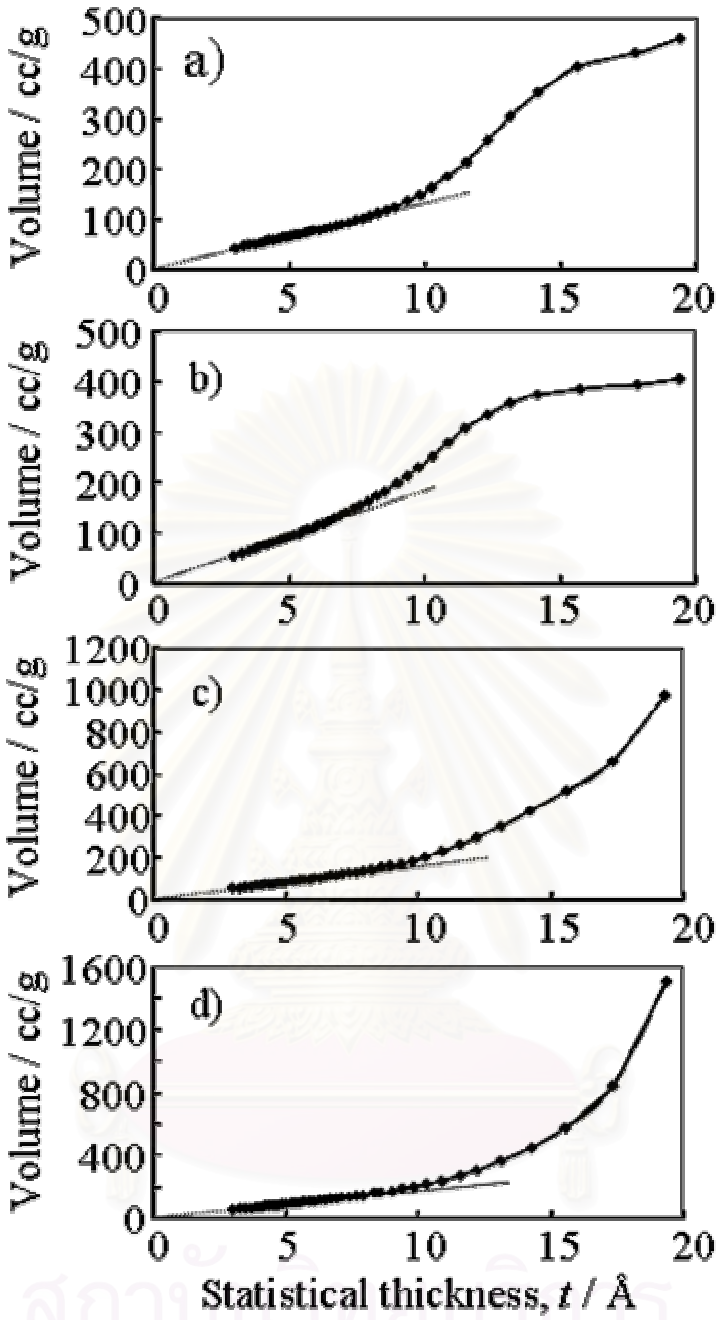

Figure 5.14: The V-t plot of as-synthesized product: (A) Al315C2h, (B) SAl315C2h, (C) PAl315C2h, (D) SPAl315C2h

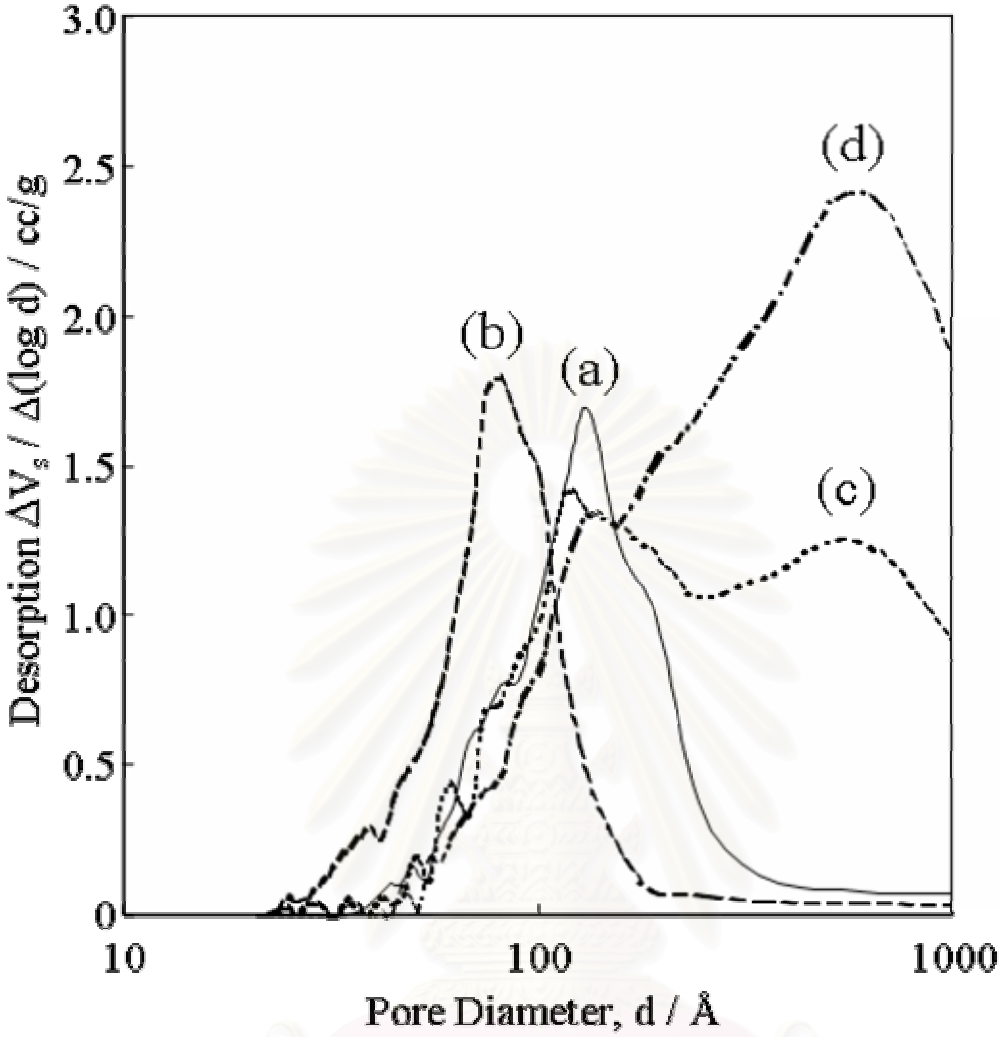

Figure 5.15: Pore size distribution of as-synthesized product

5.3 Thermal decomposition of AIP in mineral oil

The XRD patterns of as-synthesized powder are shown in Figure 5.16. The products obtained by the thermal reaction of AIP in mineral oil at 250 and 300°C with a holding time of 2 h and 6 h exhibited the typical pattern for χ-alumina. On the other hand, the product obtained by quenching the reaction just after the reaction temperature reached 250°C and product of the reaction at 250 ^{o}C for 1 h exhibited the typical pattern for an amorphous product. The crystallite sizes of all the crystalline products calculated from Scherrer equation are summarized in Table 5.5.

Table 5.5: The crystallite size of the as-synthesized and calcined products calculated by the Scherrer equation

Reaction Temperature (^{o}C)	Holding time (h)	Crystallite size of alumina (nm)				
		As-syn	1000	1100	1150	1200
250	0	-	6.2$^{\gamma}$	16.5$^{\gamma}$, 31.1$^{\alpha}$	33.7$^{\alpha}$	-
	2	9$^{\chi}$	9.2$^{\chi}$	9.6$^{\chi}$	12.3$^{\chi}$, 36.4$^{\alpha}$	68$^{\alpha}$
270	2	10.2$^{\chi}$	9.4$^{\chi}$	10.3 $^{\chi}$	15.6$^{\chi}$, 33.5$^{\alpha}$	97.5$^{\alpha}$
300	2	9.4$^{\chi}$	10.8$^{\chi}$	14.2$^{\chi}$, 39.5$^{\alpha}$	14.6$^{\chi}$, 41.3$^{\alpha}$	44.7$^{\alpha}$

$^{\chi}$ means χ-alumina, $^{\gamma}$ means γ-alumina and $^{\alpha}$ means α-alumina

The IR spectra of the products are shown in Figure 5.17. The as-synthesized powder shows two absorption bands attributed to adsorbed water: 3500-3200 cm^{-1} (υ(OH)) and 1640 cm^{-1} (δ(OH)) [108]. The amorphous powder obtained by quenching after reaction temperature reached 250°C shows strong absorption bands due to the iso-propyl groups [108]. With increasing in holding time and reaction temperature, intensity of the absorption band due to the organic group decreased and eventually disappeared. The characteristic peaks of boehmite were observed at 773 and 615 cm^{-1} [14] in the products obtained by the reaction at 250 and 300°C with holding time for 2 h. This observation can be explained by the presence of water in the reaction system.

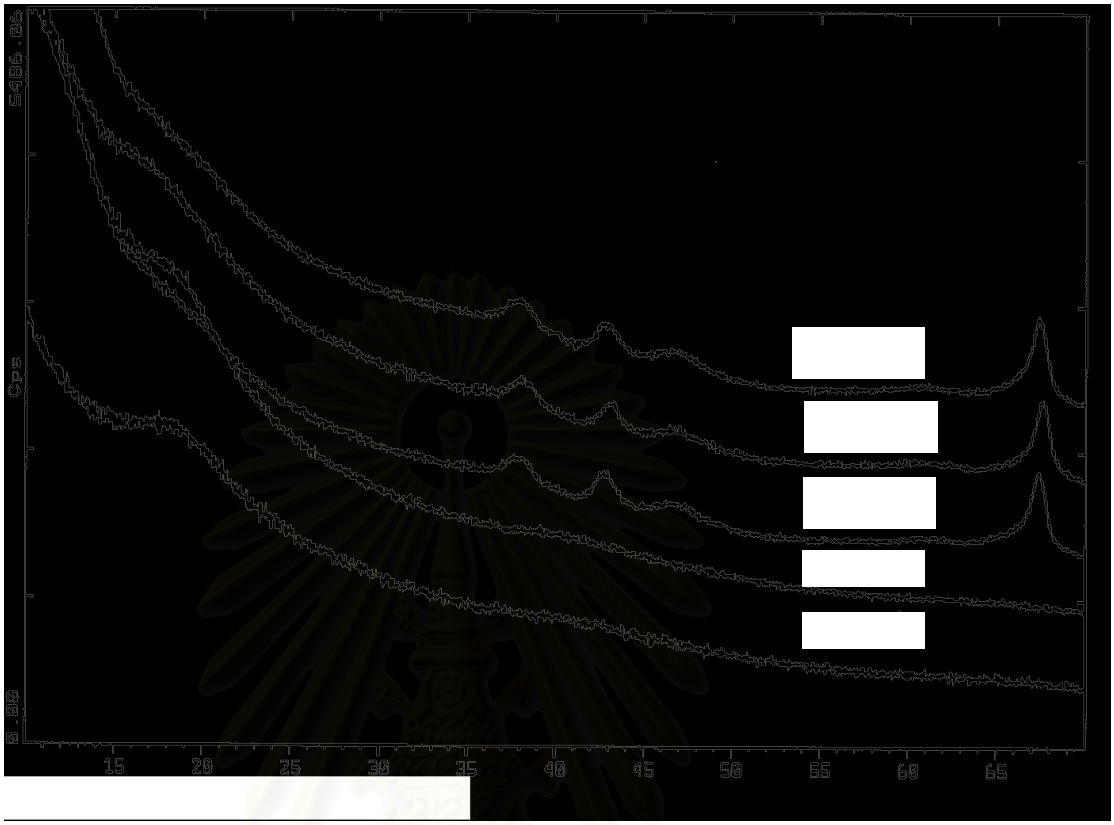

Figure 5.16: The XRD patterns of the powders synthesized by the reaction of AIP in mineral oil under various reaction conditions.

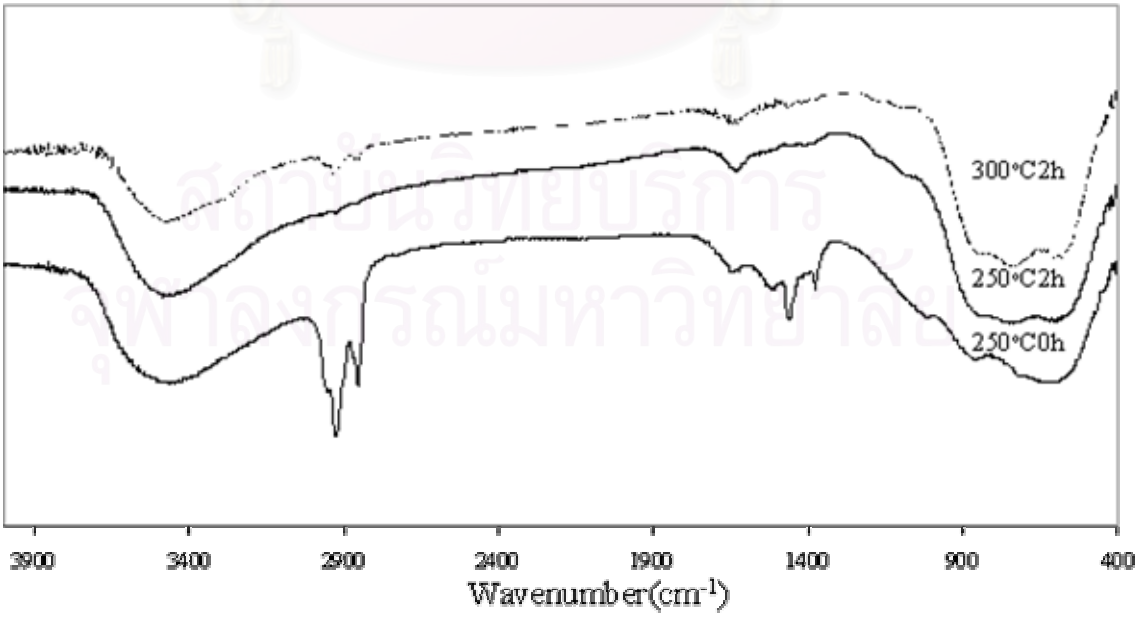

Figure 5.17: IR spectra of aluminas prepared in mineral under various conditions.

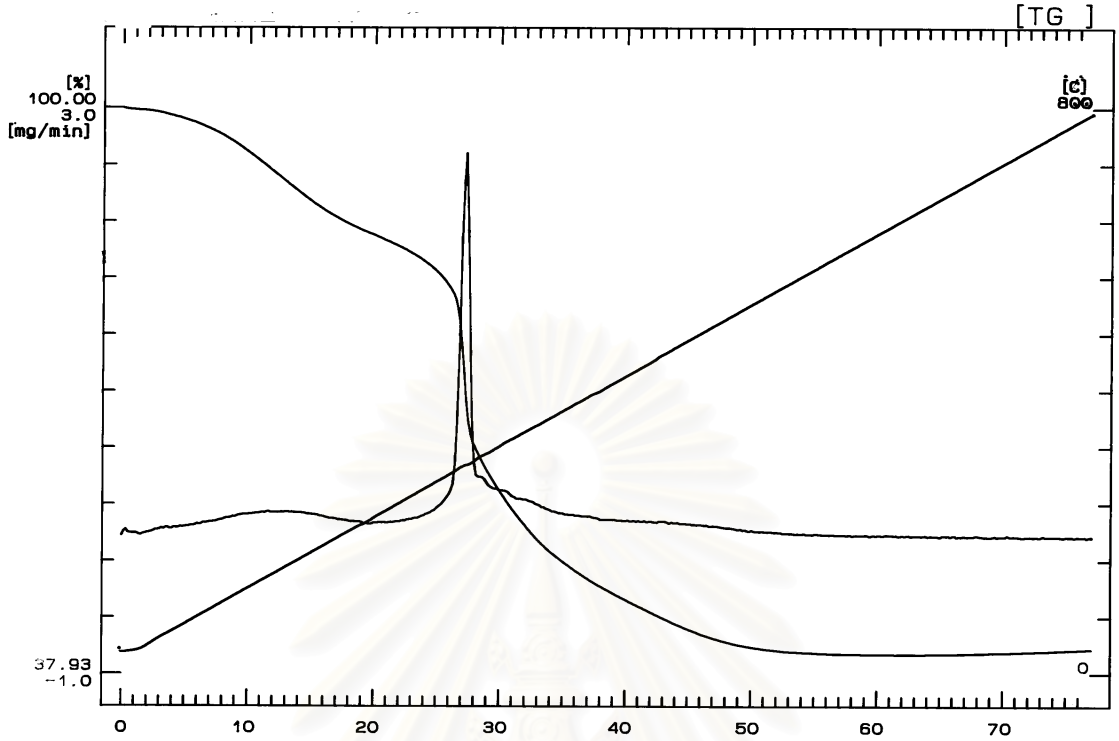

Figure 5.18: TG and DTA data of the as-synthesized products prepared by quenching reaction at 250°C.

TGA and DTG profile of the powder prepared by quenching the reaction in mineral oil after temperature reached 250°C is shown in Figure 5.18. Two weight decrease processes were detected. The first step at around 80-200°C is attributed to the desorption of physisorbed water. The second step with a sharp DTG peak at around 300°C is attributed to the combustion of organic moiety. The weight loss of this sample was around 45%, which was lower than theoretical loss for AIP decomposition (75%). This result indicates that the organic moieties remained in the product after partial decomposition of AIP.

The nitrogen adsorption isotherms of as-synthesized products are shown in Figure 5.19. All the crystalline samples exhibited the hysteresis loop characteristic of type A, which assigned for the presence of two-ended tabular pore structure. On the other hand, the amorphous product have the hysteresis loop characteristic of type E, which is the indication for the presence of tabular, through short pores with winded parts of various widths. These pores are formed among the primary particles of χ-alumina. Moreover, amount of N_2 adsorbed on the amorphous product was much smaller than that adsorbed on the crystalline products.

The V-t plots derived from the isotherm are presented in Figure 5.20. Total surface area of all sample are calculated by slope of a straight line at the first part of curves. If the sample consists of a micropore system, an abrupt decrease in the slope will be detected. The present products clearly show the indication of the decrease in the slope. It indicates the formation of micropore system in the products. At higher relative pressure (higher t values), the deviation from the straight line occurs because of the capillary condensation pressure in pore system. The pore size distributions are shown in Figure 5.21. All products exhibited the typical characteristic of mesopore system with the narrow size distribution.

Particle properties of the as-synthesized products are summarized in Table 5.6. Amorphous product prepared by quenching reaction when temperature reached 250°C (MAl250C0h) had the lowest BET surface area and pore volume. On the other hand, χ-alumina obtained by the reaction at 250°C for 2 h (MAl250C2h) had the highest BET surface area and pore volume. With increasing reaction temperature and holding time, BET surface area and pore volume decreased by the coagulation of primary particles by thermal effect.

Table 5.6: Particle properties of as-synthesized products prepared in mineral oil calculated by BET calculation, V_a-t plot and pore size distribution

Sample name	S_{BET} (m^2/g)	S_t (m^2/g)	Pore volume (cc/g)	Mode pore diameter (nm)
MAl250C0h	7	7	0.03	11.8
MAl250C2h	192	186	0.64	13.3
MAl250C6h	149	189	0.43	11.5
MAl270C2h	180	210	0.52	11.5
MAl300C2h	124	138	0.45	14.2

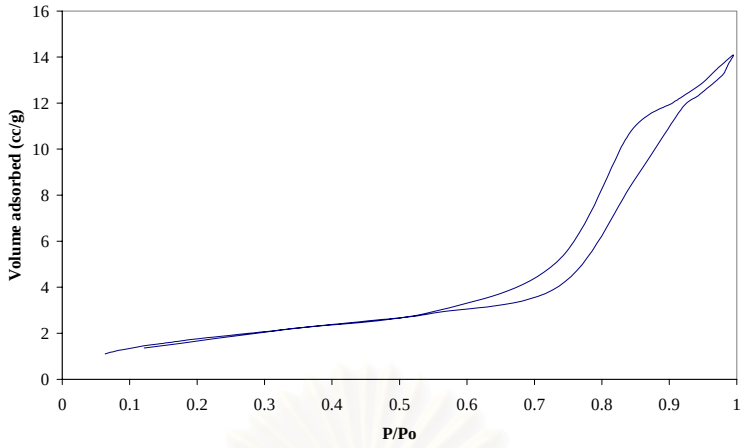
Volume adsorbed (cc/g)
P/Po
0
2
4
6
8
10
12
14
16
0
0.1
0.2
0.3
0.4
0.5
0.6
0.7
0.8
0.9
1

(a)

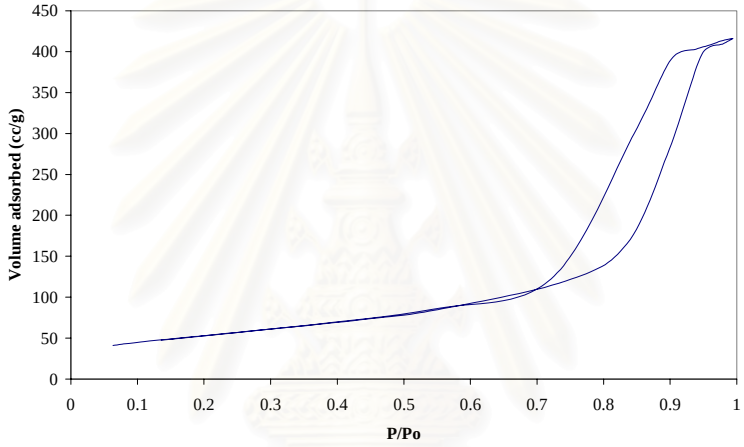
Volume adsorbed (cc/g)
P/Po
0
50
100
150
200
250
300
350
400
450
0
0.1
0.2
0.3
0.4
0.5
0.6
0.7
0.8
0.9
1

(b)

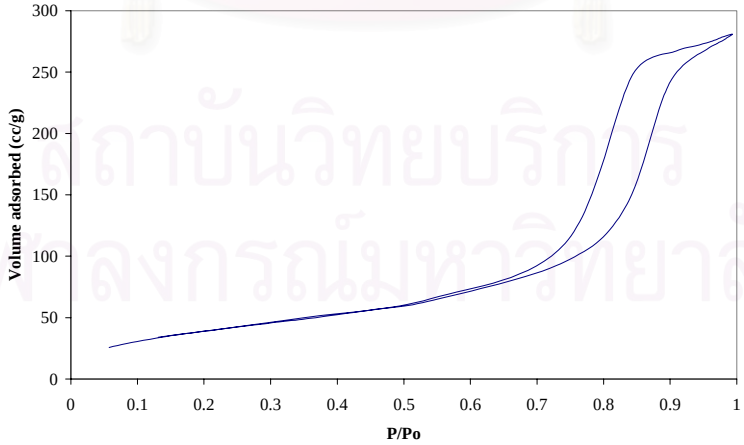
Volume adsorbed (cc/g)
P/Po
0
50
100
150
200
250
300
0
0.1
0.2
0.3
0.4
0.5
0.6
0.7
0.8
0.9
1

(c)

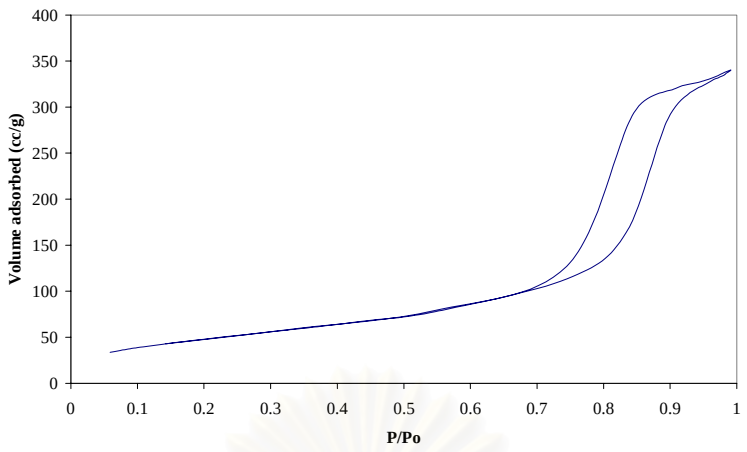

(d)

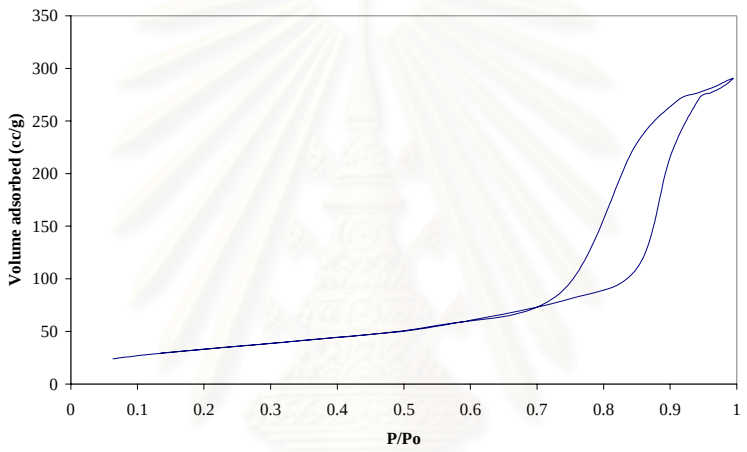

(e)

Figure 5.19: The nitrogen adsorption isotherms of the products prepared by the reaction of AIP in mineral oil under the conditions of: (a) at 250°C for 0 h, (b) at 250°C for 2 h, (c) at 250°C for 6 h, (d) at 270°C for 2 h, (e) at 300°C for 2 h.

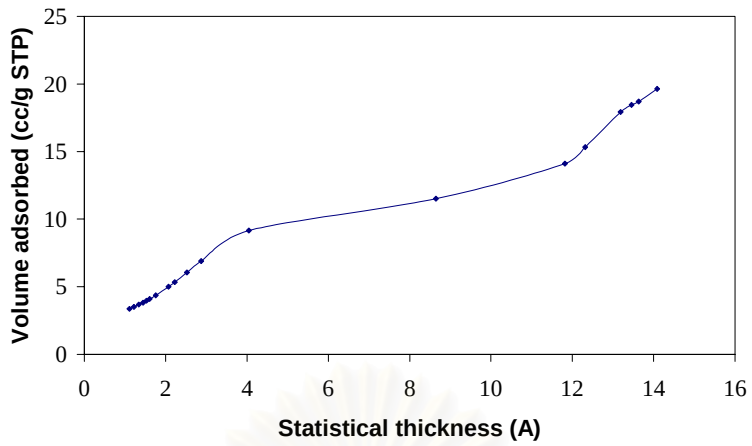
Volume adsorbed (cc/g STP)
0
5
10
15
20
25
0
2
4
6
8
10
12
14
16
Statistical thickness (A)

(a)

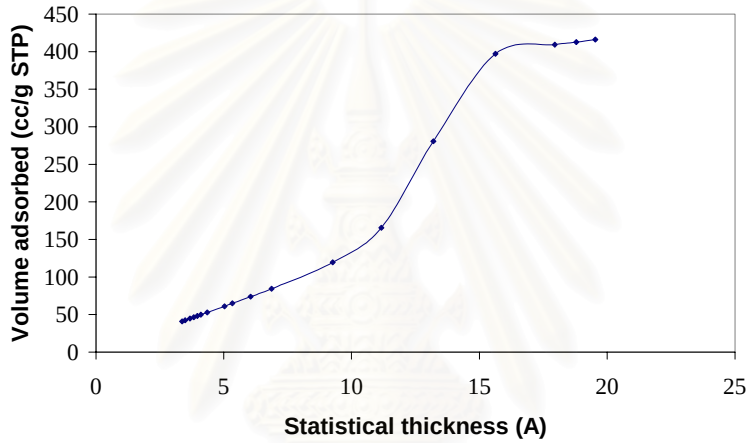
Volume adsorbed (cc/g STP)
0
50
100
150
200
250
300
350
400
450
0
5
10
15
20
25
Statistical thickness (A)

(b)

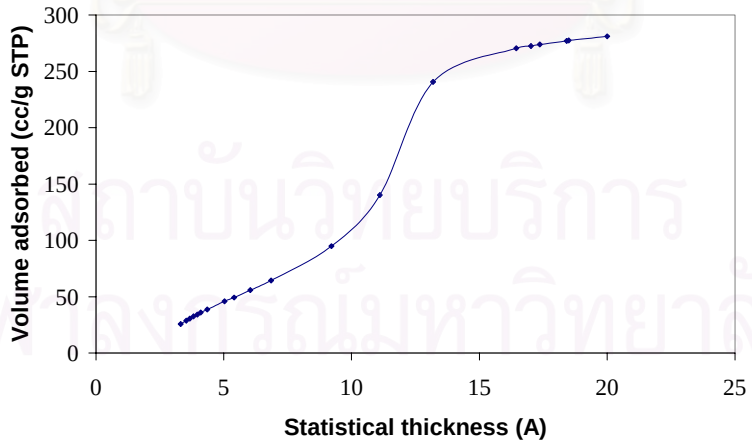
Volume adsorbed (cc/g STP)
0
50
100
150
200
250
300
0
5
10
15
20
25
Statistical thickness (A)

(c)

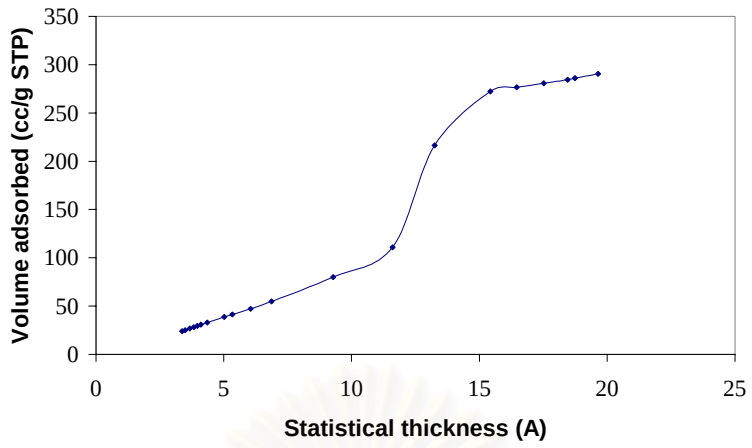

(d)

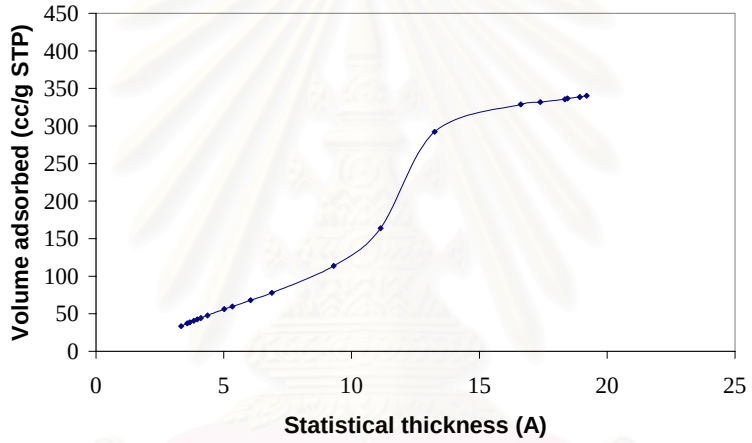

(e)

Figure 5.20: The V-t plot of the products prepared by the reaction of AIP in mineral oil under the conditions of: (a) at 250°C for 0 h, (b) at 250°C for 2 h, (c) at 250°C for 6 h, (d) at 270°C for 2 h, (e) at 300°C for 2 h.

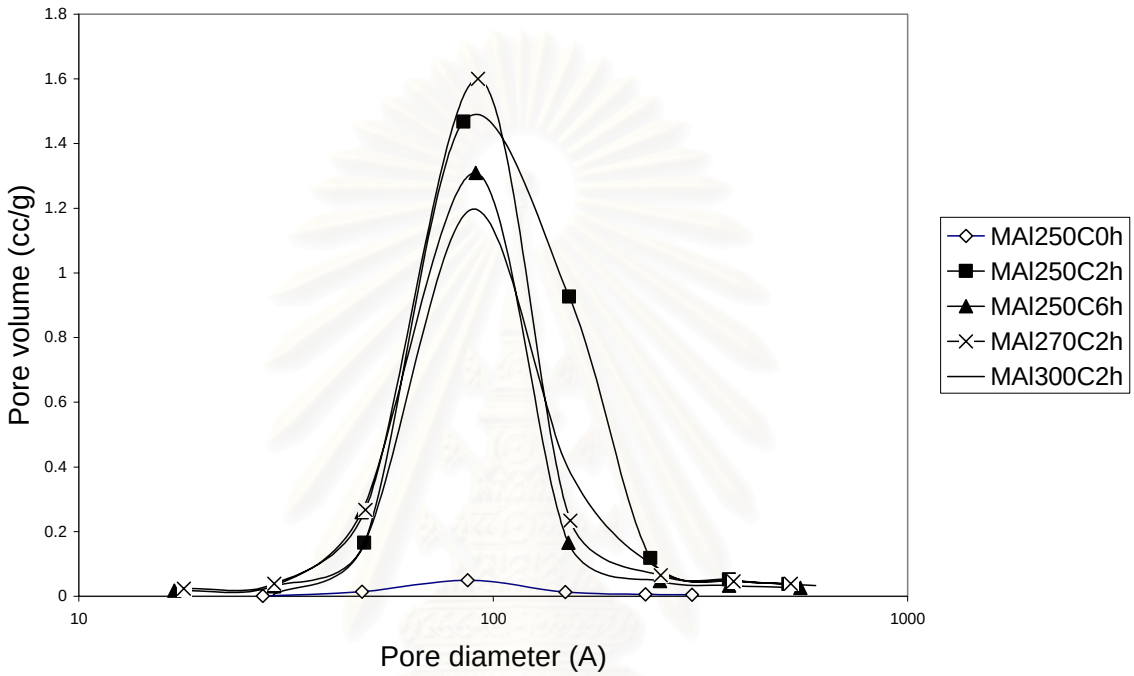

Figure 5.21: Pore size distribution of as-synthesized product prepared by the reaction of AIP in mineral oil under various reaction conditions.

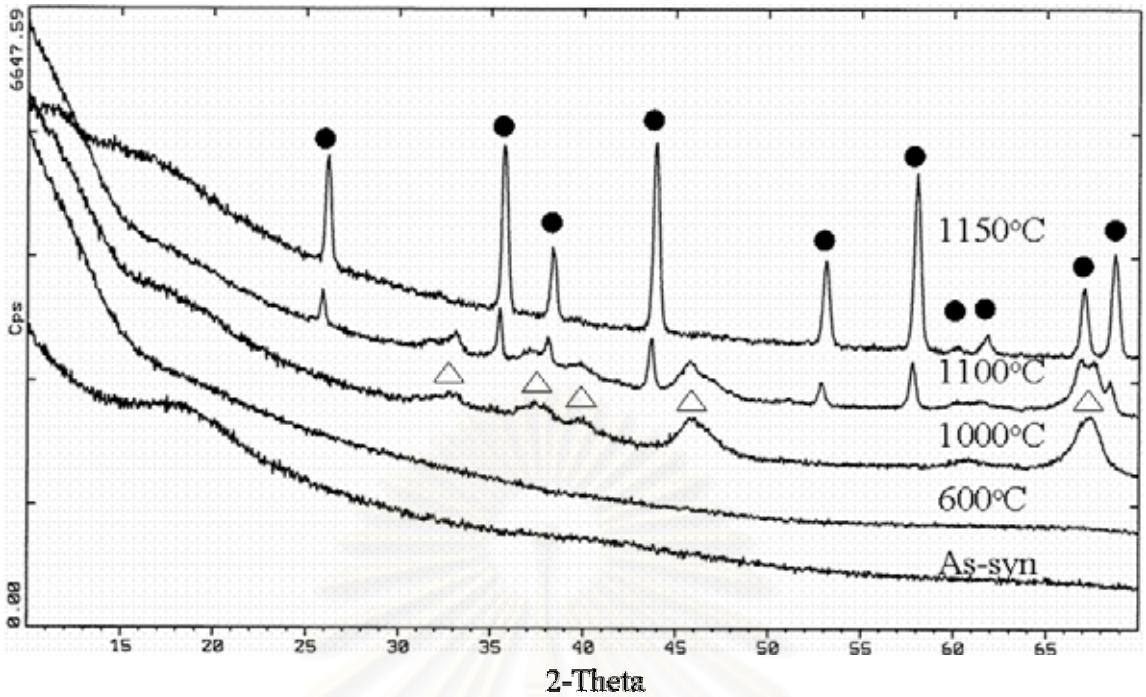

Figure 5.22: The XRD patterns of the product prepared by quenching reaction of AIP in mineral oil after reaction reached 250°C and subsequently calcined at various temperatures; ● (α-alumina) and Δ(γ-alumina).

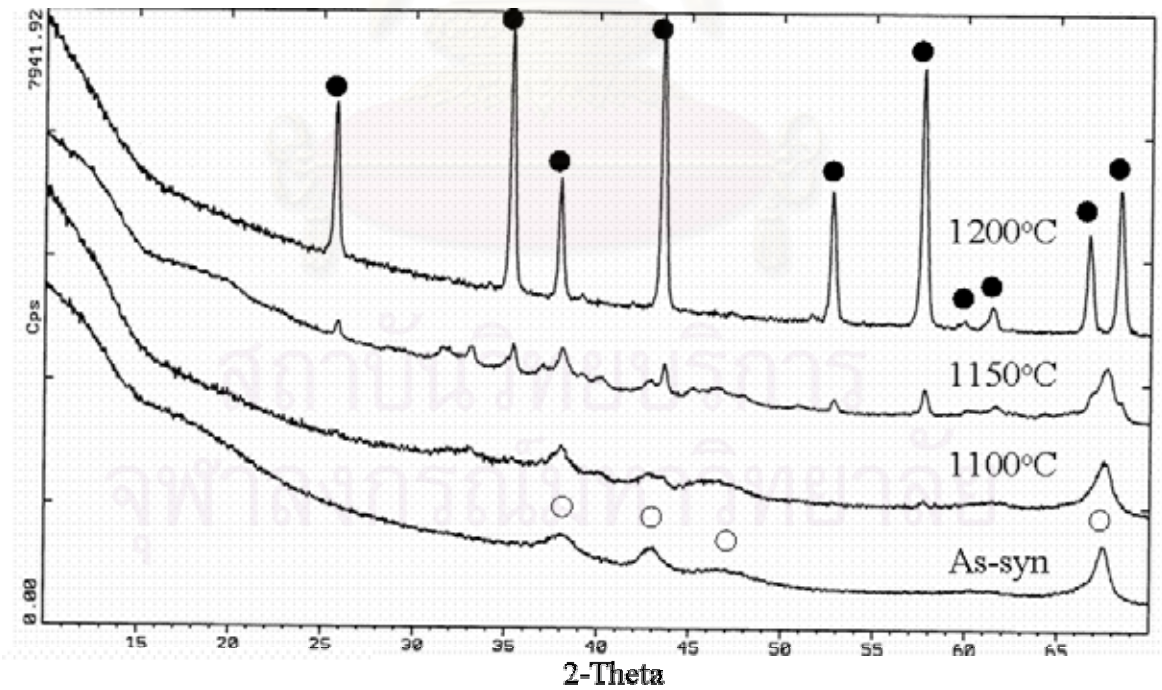

Figure 5.23: The XRD patterns of the product prepared by thermal reaction of AIP in mineral oil at 250°C for 2 h and subsequently calcined at various temperatures; ● (α-alumina) and ○ (χ-alumina).

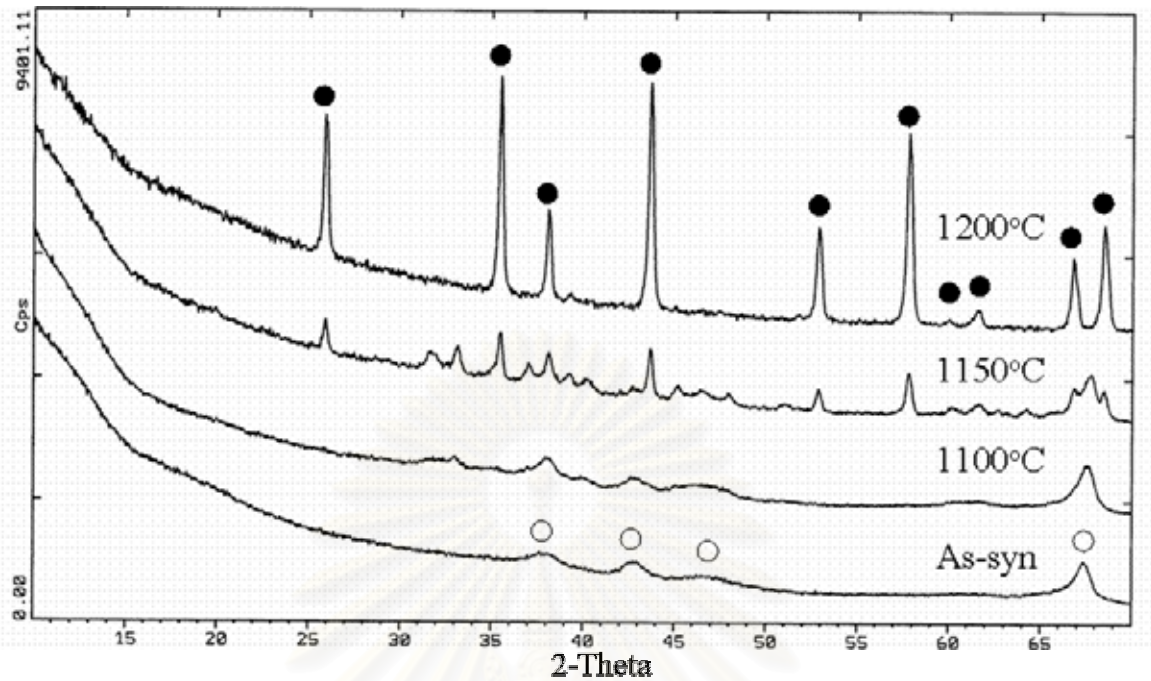

Figure 5.24: The XRD patterns of the product prepared by thermal reaction of AIP in mineral oil at 250°C for 6 h and subsequently calcined at various temperatures; ● (α-alumina) and ○ (χ-alumina).

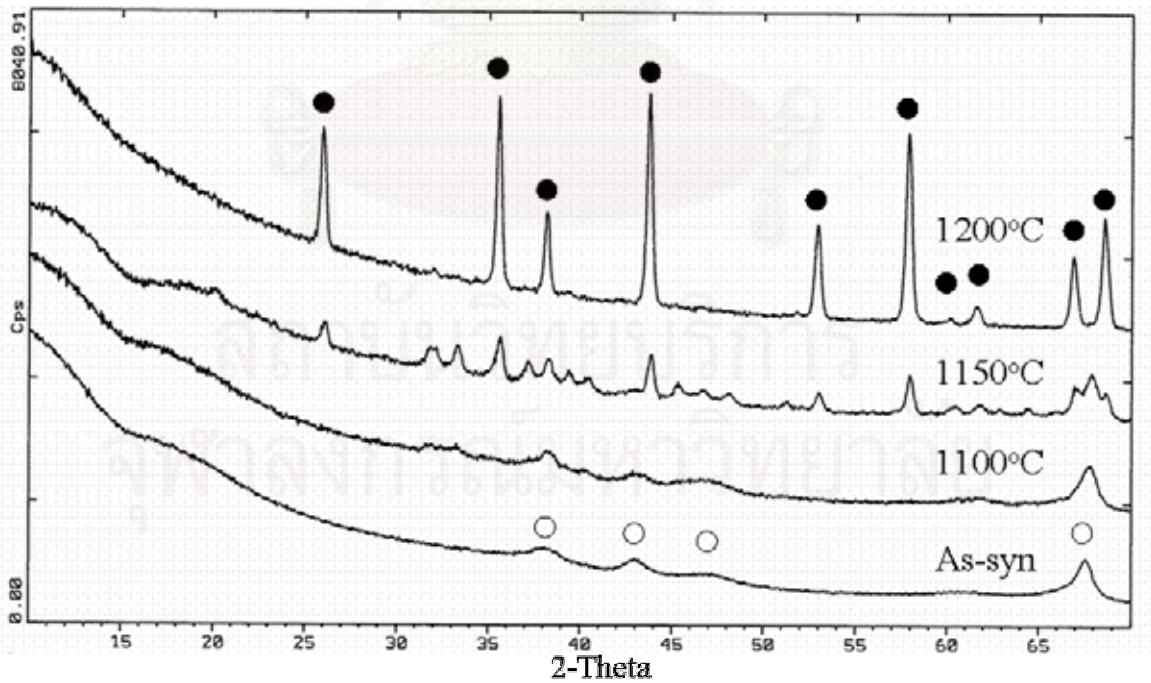

Figure 5.25: The XRD patterns of the product prepared by thermal reaction of AIP in mineral oil at 300°C for 2 h and subsequently calcined at various temperatures; ● (α-alumina) and ○(χ-alumina).

The XRD patterns of the powders obtained by quenching reaction of AIP in mineral oil after reaction temperature reached 250°C and subsequent calcination at various temperatures are shown in Figure 5.22. The product remained amorphous even after calcination at 600°C. After calcination at 1000°C, the amorphous product transformed to γ-alumina, which start direct transformation to α-alumina at 1100°C and complete at 1150°C. Note that the peak at 42.5^{o} is absent indicating that χ-alumina is not formed by calcination of amorphous product. This result suggests that the formation of χ-alumina occurs only in the solvent.

The XRD patterns of the powders obtained by thermal reaction of AIP in mineral oil at various temperatures for 2 and 6 h and subsequent calcination at various temperatures are shown in Figure 5.23-5.25. χ-alumina obtained in every condition transformed to α-alumina by passing the formation of κ-phase, starting at calcination temperature around 1150°C. The transformation is completed at temperature around 1200°C.

Morphologies of as-synthesized and calcined samples observed by SEM are shown in Figure 5.26. The spherical particles with average diameter around 1.8 μm were observed for the amorphous products prepared by quenching the reaction after the temperature reached 250°C. When the holding time was prolonged to 2 h, spherical particle still remained but the average size decreased to1.2 μm (as shown in Figure 5.26); these particles consisted of aggregates of nanocrystalline primary particles of χ-alumina, which were observed by TEM (see in Figure 5.27). Moreover, with increasing in reaction temperature, particle size decreased to 1 μm (see in Figure 5.26). We speculate that AIP decomposes stepwise in the solvent leading to an intermediate complex suspended in mineral oil. We believe that the particles of this complex deposited from the solvent have already a spherical shape. When holding time was prolonged, this complex decomposes giving the nanocrystalline χ-alumina aggregated in a spherical particle. Thus the, decrease of particle size with an increase in holding time and temperature should be due to the loss of the organic moiety in the complex by further decomposition.

(a)

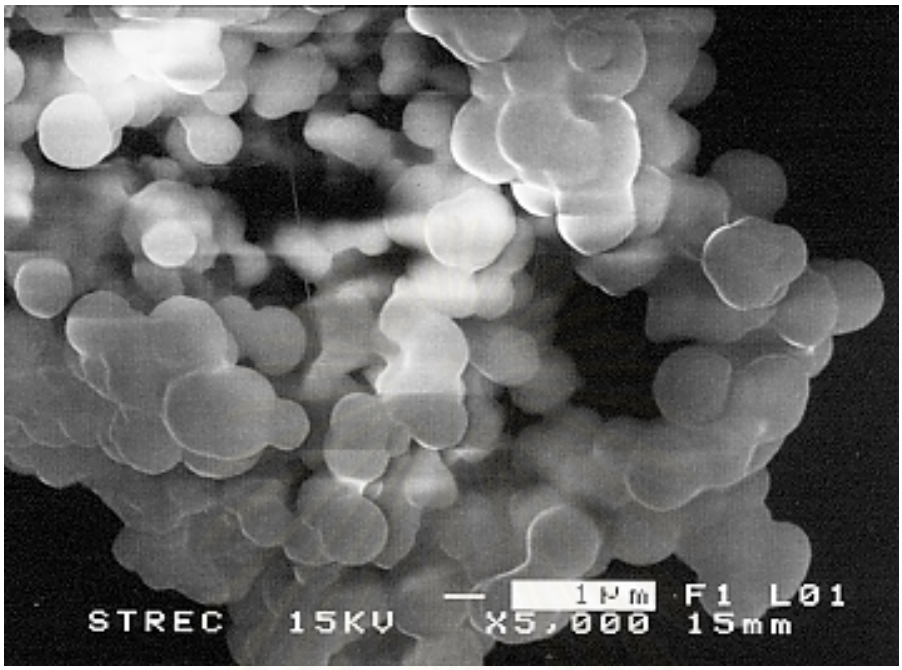
1 µm F1 L01
STREC 15KV X5,000 15mm

(b)

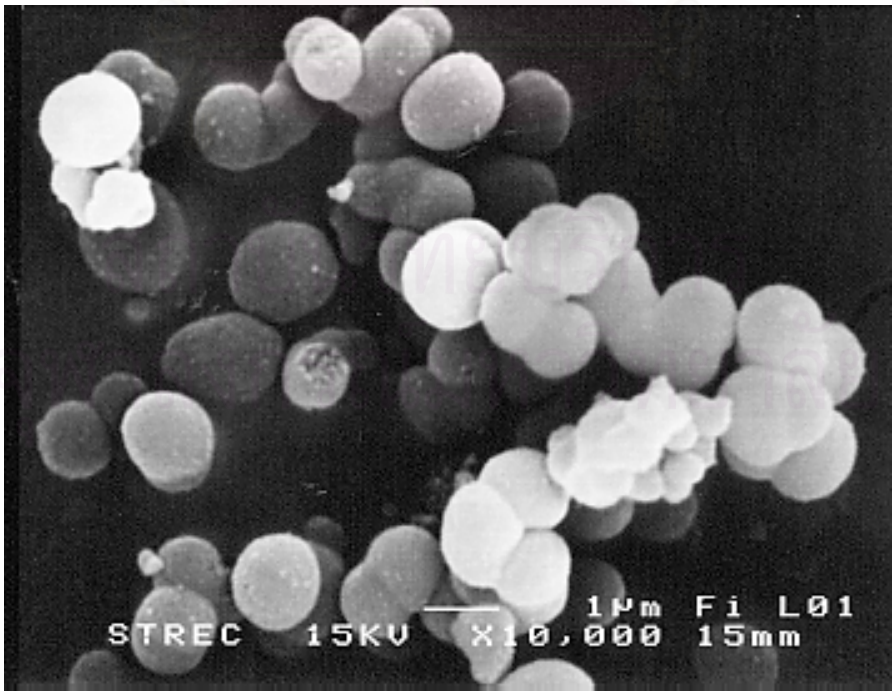
1µm Fi L01
STREC 15KV X10,000 15mm

(c)

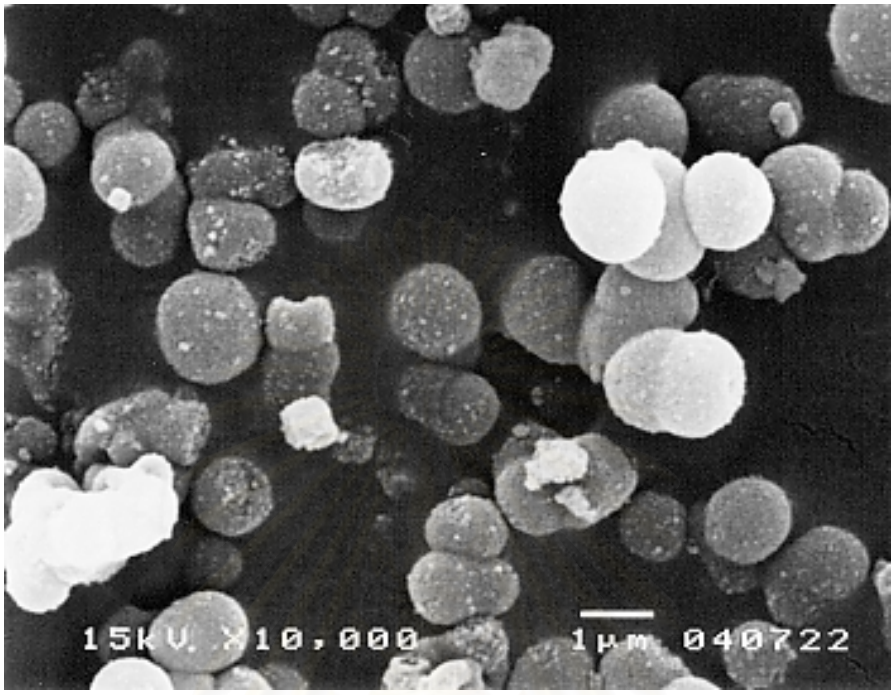

(d)

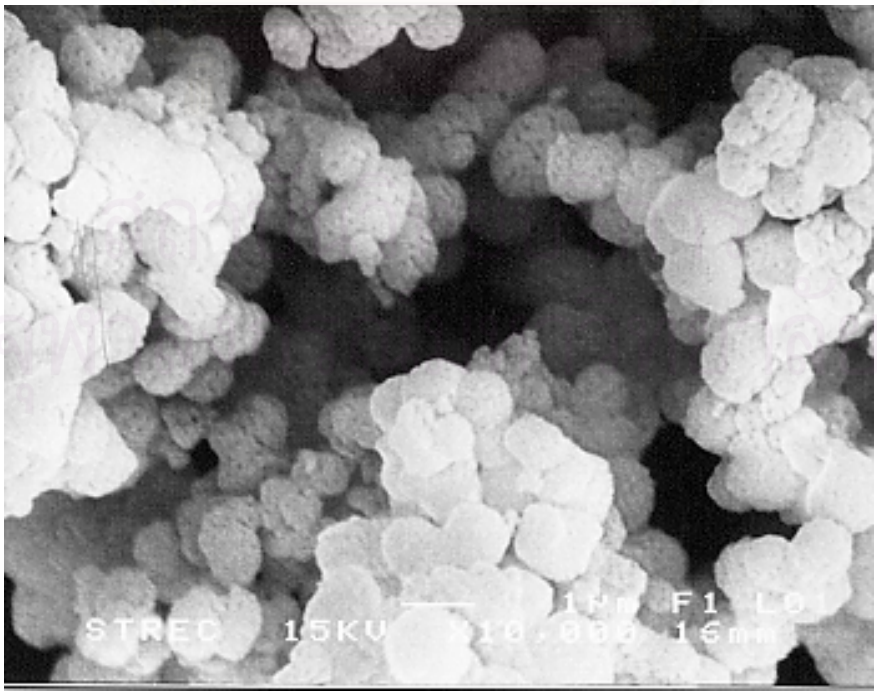

(e)

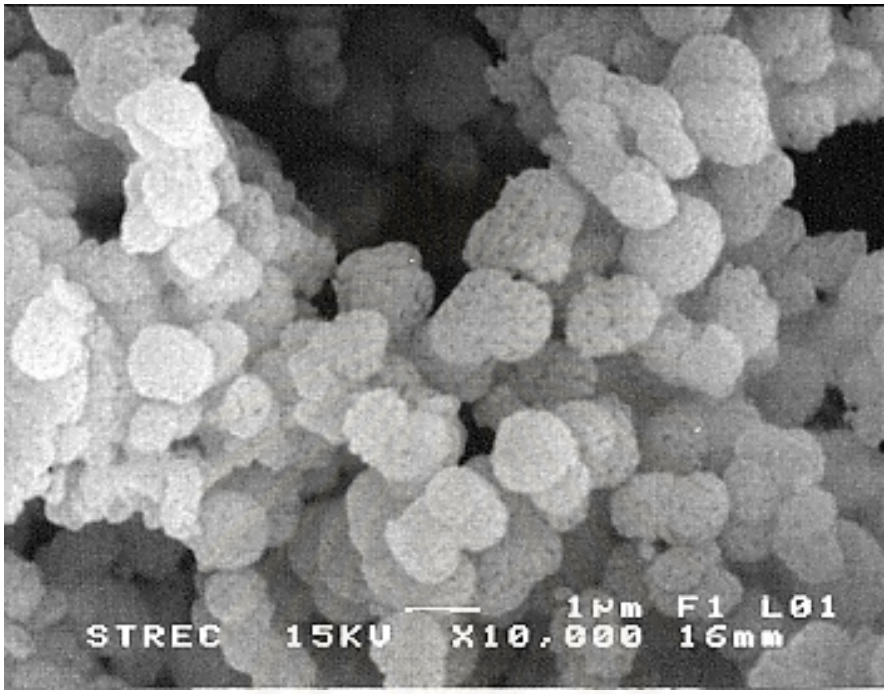

Figure 5.26: SEM images: (a) as-synthesized product prepared by quenching the reaction in mineral oil after temperature reached at 250°C, (b) as-synthesized product prepared in mineral oil at 250°C for 2h, (c) as-synthesized product prepared in mineral oil at 300°C for 2h, (d) product (b) calcined at 1150°C, (e) product (c) calcined at 1150°C.

Transmission electron micrographs of the as-obtained powder and calcined powder are shown in Figure 5.27. The as–synthesized χ-alumina products are spherical of primary particles having average diameter around 10 nm comprised agglomerates. The crystallite size calculated by the Scherrer equation was 9 nm. Good agreement between both values indicates that each primary particle observed by TEM is a single crystal of χ-alumina.

(a)

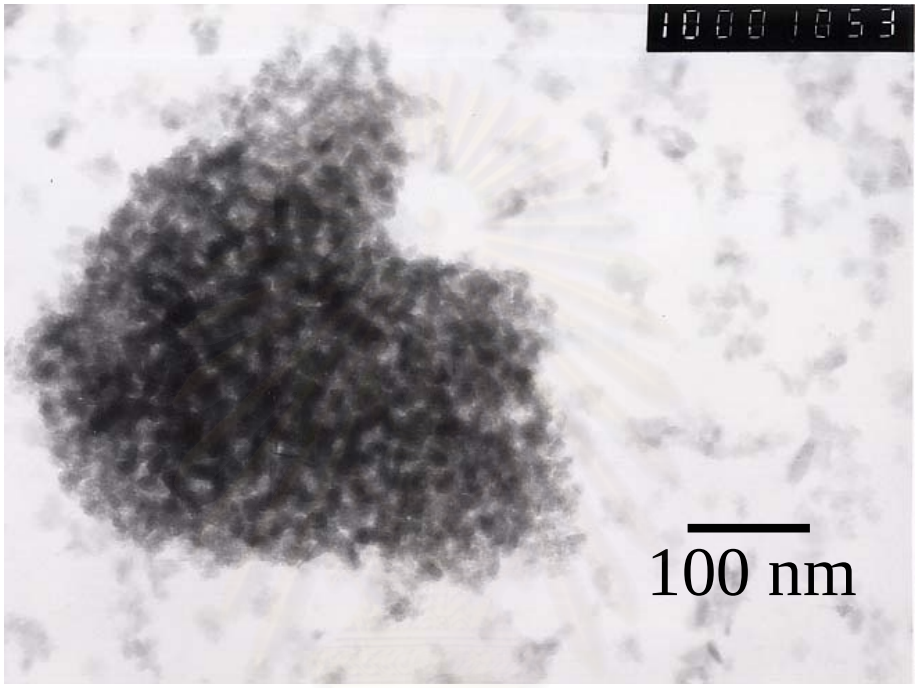

(b)

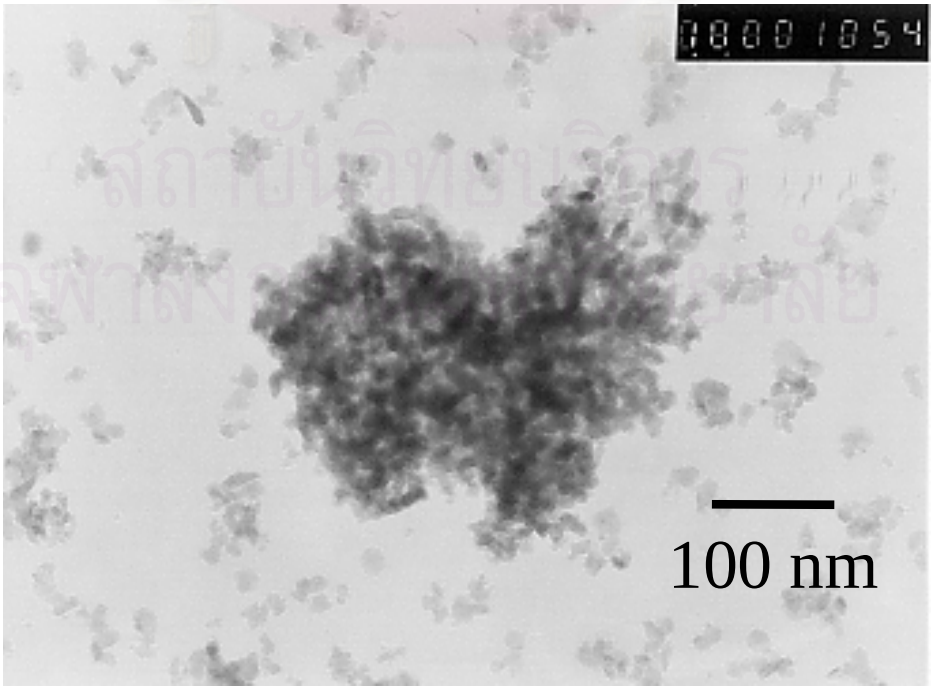

(c)

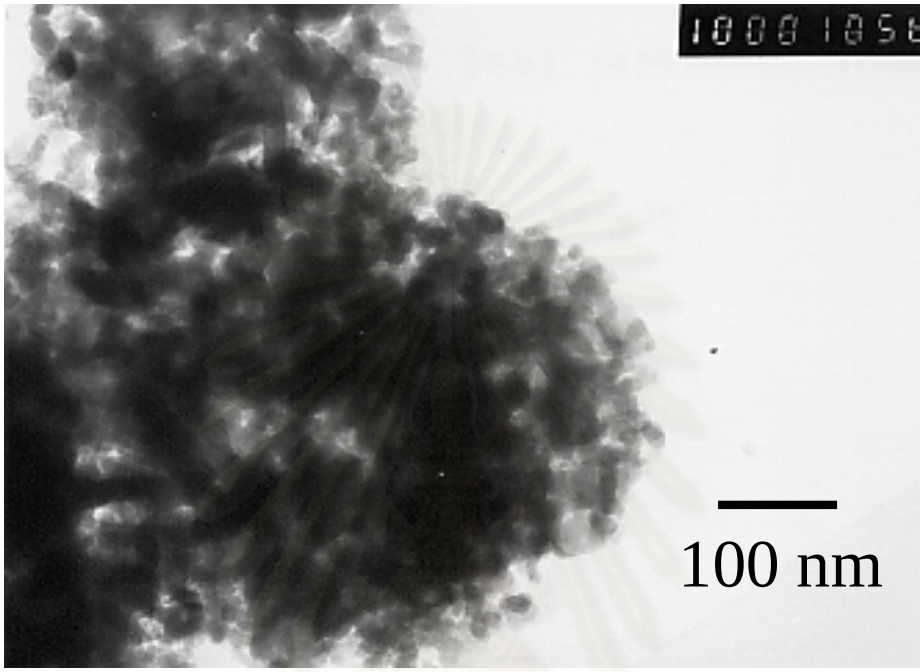

(d)

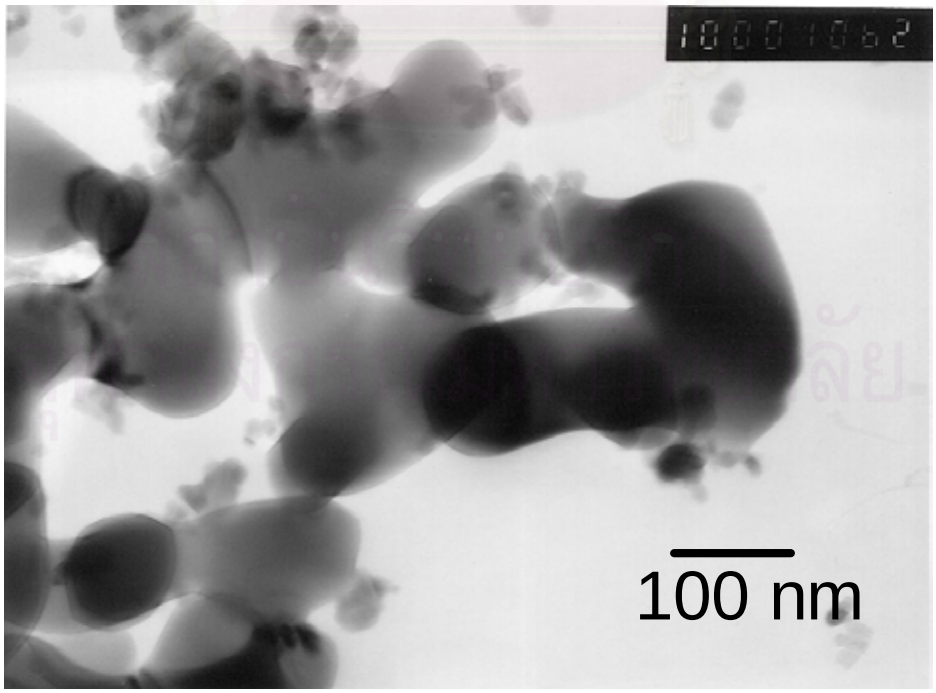

(e)

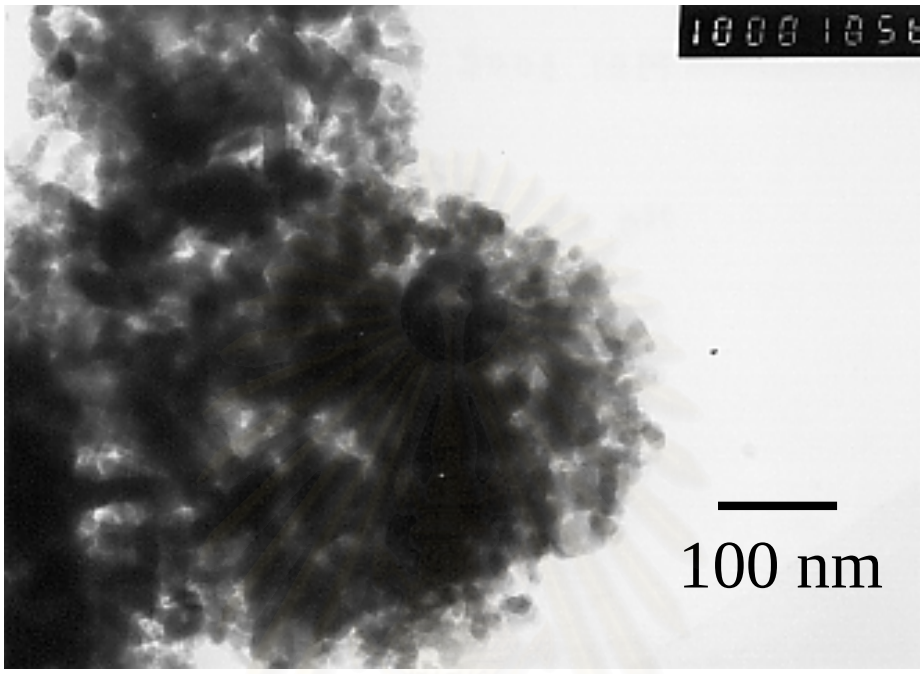

Figure 5.27: TEM images: (a) as-synthesized product prepared in mineral oil at 250°C for 2 h, (b) as-synthesized product prepared in mineral oil at 300°C for 2 h, (c) product (a) calcined at 1150°C, (d) product (a) calcined at 1150°C, (e) product (b) calcined at 1150°C.

When the sample was calcined at high temperature, the spherical shape of secondary particles is still observed with the same average size even after phase transformation (see Figure 5.26). Some finger-like shape of primary particles aggregates on the spherical secondary particles after calcination at 1150°C. TEM micrographs of calcined samples clearly showed that after phase transformation, two types of primary particles are observed. First, the spherical χ-alumina particles, which did not transform to α-alumina, remained in the sample. These particles had crystallite size calculated from the Scherrer equation that was same as particle size observed by using TEM (seen in Figure 5.27c and 5.27e). Second, the finger-like α-alumina (see in Figure 5.27d) obtained from the nucleation and growth mechanism of low-

temperature transition alumina nano-crystals.

The direct phase transformation of χ-alumina to α-alumina is a specific property for the powders prepared by the reaction of AIP in an inert organic solvent. In our previous chapter, we explained this phenomenon by the absence of cation contamination and high crystallinity due to the small amount of water adsorbed on the surface. It is generally known that the contamination of cations and crystallinity of alumina affected on the transformation sequence of transition alumina. For example, traces of sodium favor the formation of θ-alumina in the transformation sequence of boehmite and increase the rate of formation κ-alumina from χ-alumina. While Li and Mg stabilize δ-alumina and prevent the formation of θ-alumina [54]. In the case of crystallinity, when boehmite is less crystalline, the formation of δ-alumina is retarded [54]. Therefore, we prepared our samples by the reaction of AIP in organic solvent which eliminate the contaminations of cations. Moreover, when we compare peaks of χ-alumina in the sample prepared by calcination of gibbsite, the peaks in our sample were more intense which is due to higher crystallinity of the present products.

From data in Table 5.5, the initial crystallite size of χ-alumina obtained is around 9-10 nm and grows to 16 nm after calcination at high temperature. We speculate that χ-alumina grows to the critical size and then abruptly transforms into an α-alumina. This observation is similar to phase transformation from θ- to α-alumina reported by Wen and Yen [48] and Chang et al. [49]. They discovered that phase transformation of θ-alumina nano-crystals resulted in finger-like polycrystalline α-alumina, which was the result from the growth of α-alumina nano-crystals by a sintering process. Moreover, they reported that θ-alumina grew to certain size before transformed into α-alumina, after which the crystallite size increased abruptly [48-49]. This behavior was explained by a nucleation and growth mechanism, in which nucleation was triggered by phase transformation from θ- to α-alumina and followed by crystal growth due to sintering [11-12]. In this work, for χ-alumina, similar behavior was also observed. According to data in Table 5.6, the crystallite size of synthesized χ-alumina was around 9-10 nm and grew up to around 16 nm by the calcination, before phase transformation to α-alumina took place, regardless of the

temperature which the α-phase transformation started. The final product, after phase transformation was complete, was single crystal of α-alumina with much larger crystallite size than the initial crystallite size of χ-alumina. Results from our preliminary results also confirmed this observation. χ-alumina with crystallite size greater than 16 nm has never been observed in our work. This same behavior was found for the χ-alumina prepared by the thermal decomposition of AIP in toluene in next chapter.

5.4 Phase transformation behavior of χ-alumina prepared by thermal reaction of AIP in inert organic solvents.

XRD patterns of the products, prepared in toluene (TA) and mineral oil (MA) followed by calcination at various temperatures, are shown in Figures 5.28a and 5.28b respectively. The XRD pattern of the powder obtained by reaction at 315°C for 2 h. shows a peak at $2\theta = 42.5^{o}$. This peak corresponds to the prohibited (321) diffraction of the spinel structure and it is an indicator of the formation of χ-alumina. With increasing calcination temperature, both samples exhibited the XRD patterns corresponding to χ-alumina together with small amount of α-alumina and θ-alumina, which might be derived from boehmite, a contaminant of our sample. The α-phase transformation was completed at 1180°C. Interestingly, χ-alumina obtained from the thermal decomposition of AIP in both the solvents transformed to stable α-alumina directly, bypassing the formation of κ-alumina. In general, χ-alumina obtained by dehydration of gibbsite (<200 nm) transforms into α-alumina through κ-alumina in the sequence as follows:

gibbsite - χ-alumina - κ-alumina - α-alumina.

(a)

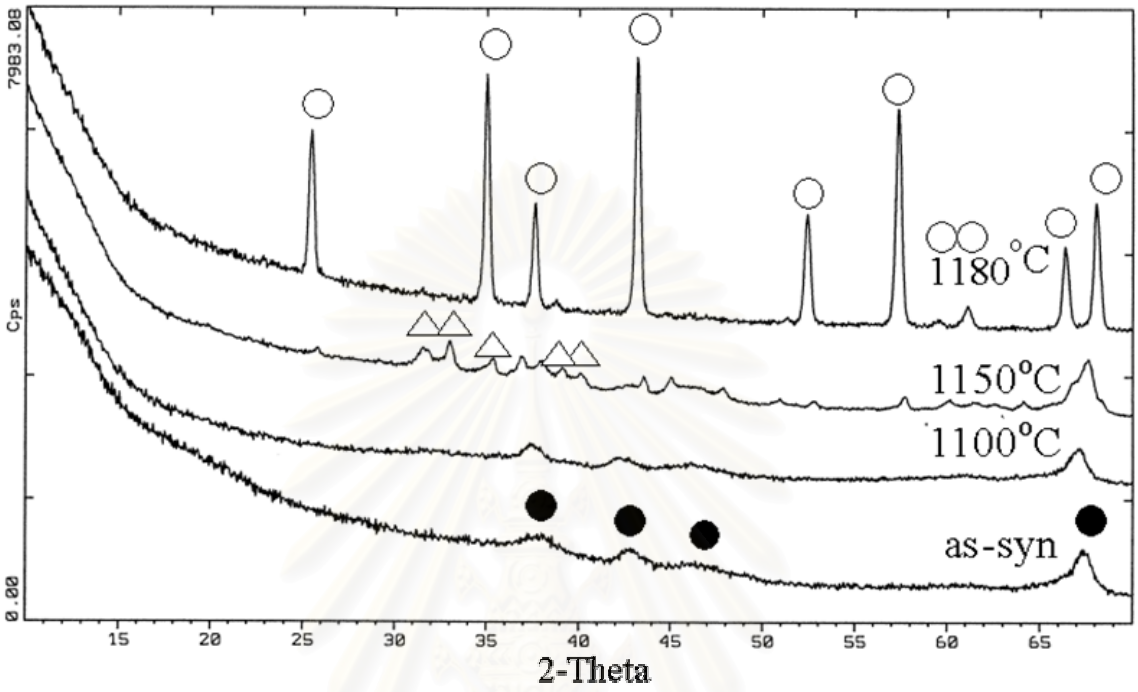

(b)

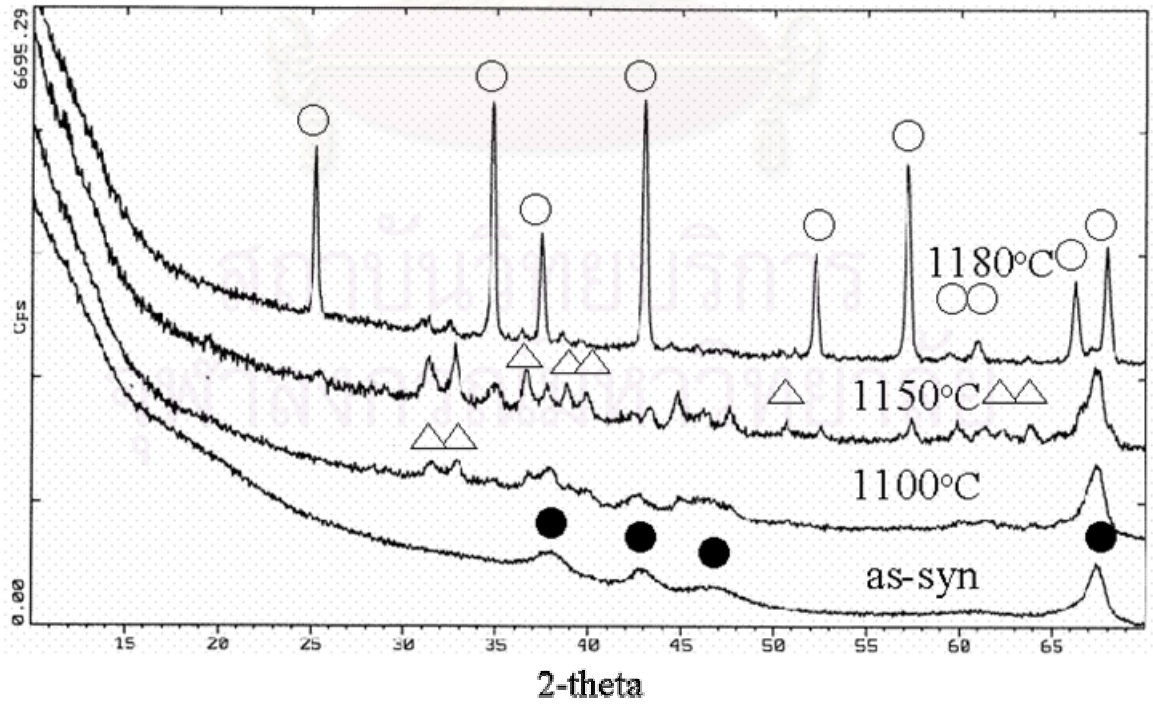

Figure 5.28: The XRD patterns of alumina products calcined at various temperatures:

(a) preparing in toluene and (b) preparing in mineral oil: ● is χ-alumina, ○ is α-alumina and Δ is θ-alumina.

Direct transformation of a low-temperature transition alumina (χ-alumina) into α-alumina is specific property of the alumina formed by thermal decomposition of aluminum alkoxide in inert organic solvents. Gibbsite is always contaminated with a small amount of cations such as Na^+, and thermal dehydration yielding χ-alumina can not eliminate such ions from the matrix. Therefore, it exhibits very broad peaks in its XRD pattern due to low crystallinity and many defects in its structure. Several researchers have reported that addition of cations into the alumina matrix affected the phase transformation behavior [99-102]. Apparently, cations in χ-alumina matrix promote the formation of κ-alumina at high calcination temperature. On the other hand, χ-alumina obtained by the thermal decomposition of AIP in toluene is not contaminated with cations. Moreover, the presence of a small amount of water during the decomposition process increases the crystallinity of the product. This stabilizes the χ-alumina structure and prohibits the formation of κ-alumina. It seems that the direct transformation to α-alumina can be explained by the absence of cations and fewer defects in the crystal structure.

The effect of cations was tested by adding Na^+ ions to the alumina matrix (the atomic ratio of Na/Al = 0.03) by adding sodium tert-butoxide in the reaction system. The XRD patterns of the powder obtained, calcined at various temperatures, are shown in Figure 5.29. It is clearly seen that the χ-alumina did not transform directly to α-alumina at high calcination temperatures.

The physical properties of powders produced are summarized in Table 5.7. The product obtained by the reaction in toluene had higher BET surface area with the same crystallite size due to the more compaction of primary particle.

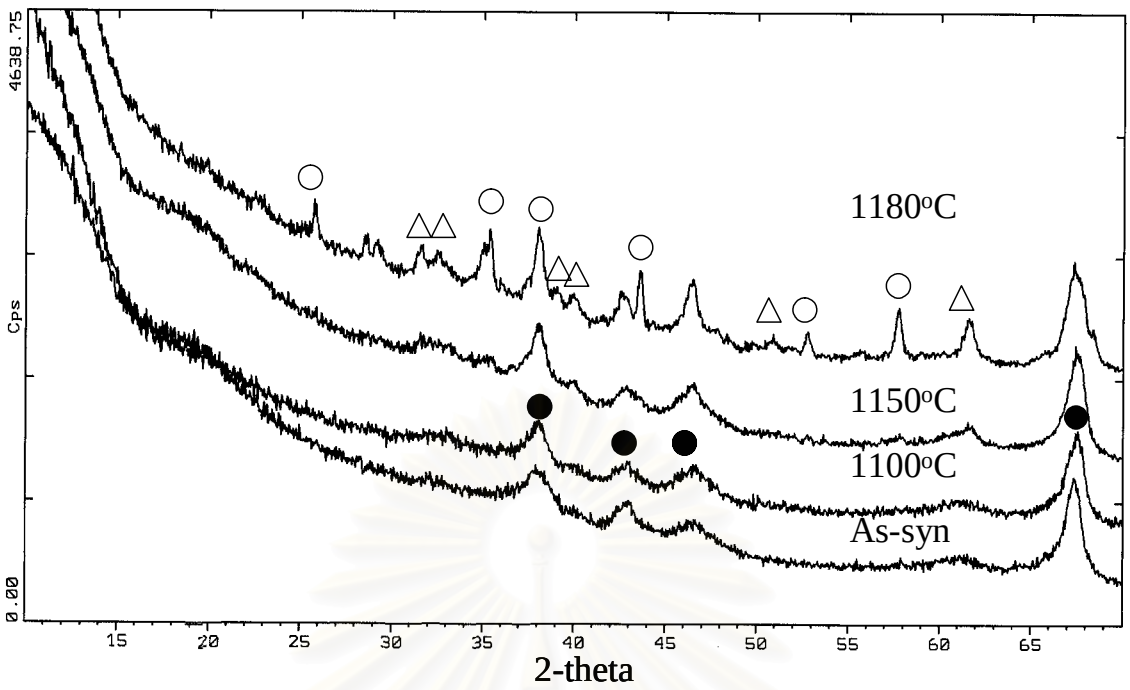

Figure 5.29: The XRD patterns of alumina with sodium contamination (Na/Al atom =0.03) products calcined at various temperatures, ● is χ-alumina, ○ is α-alumina and Δ is θ-alumina.

.

Table 5.7: The physical properties of as-synthesized products

Sample ID	BET surface area (m^2/g)	Crystallite size (nm)	Crystallite size at 1180°C (nm)	Bulk density (g/cm^3)	%Weight loss
Al315C2h	201	10.3	36.5	0.6	14
MAl315C2h	178	10.2	107.5	0.36	12

Thermal analysis results of the as-synthesized products are shown in Figure 5.30. Two weight decrease process were detected, both of which were accompanied by endothermic peaks in DTA. The first step at 80°C is attributed to the desorption of physisorbed water. The second step at 100-500°C is attributed to the dehydration of surface hydroxyl groups.

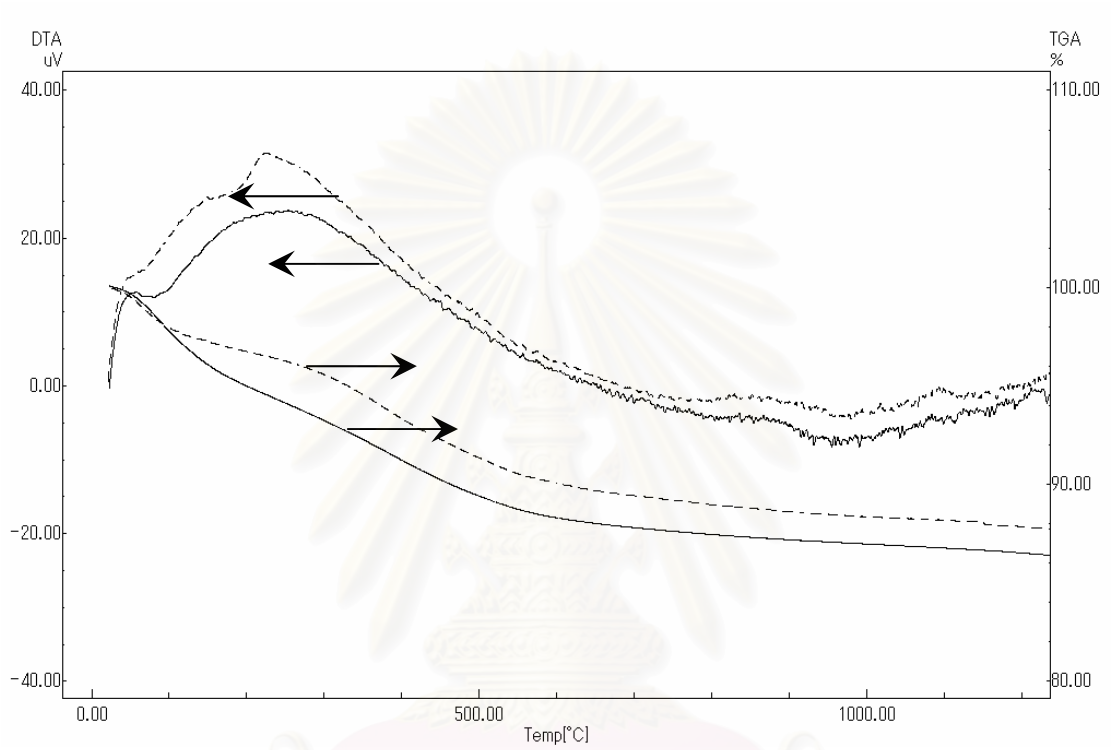

Figure 5.30: TG and DTA data of the as-synthesized products: (—) preparing in toluene and (------) preparing in mineral oil.

Transmission Electron Micrographs of the as-synthesized and calcined samples prepared in both the organic solvents are shown in Figure 5.31. The as–synthesized χ-alumina powders were comprised of agglomerated primary particles having diameter of 6 to 13 nm. The crystallite sizes of the products from the reaction in toluene and mineral oil, calculated by Scherrer equation were 10.4 and 10.2 nm respectively. The particle size calculated from the measured surface area, on the basis of an assumption that the powders consist of uniform spherical particle have a specific gravity of 3 g/cm^3, was 10 nm, which is in good agreement with crystallite size prepared in toluene. On the other hands, the surface area of MA315C2h is 178 m^2/g,

calculated particle size should be slightly smaller than this value. This suggests that each primary particle observed by TEM is a single crystal of χ-alumina. When powders were heated to higher temperature, the size of primary particles increased and α-alumina was detected. Interestingly, the TEM images clearly show two different types of the particles in the α-alumina: vermicular shape (around 100-200 nm) and small spherical particles (around 15-20 nm). We believe the latter are a χ-alumina at a critical size (16 nm). At this size a nucleation process within the particle converts it to nucleated α-alumina sizes, calculated from the Scherrer equation, are summarized in Table 5.8. Generally, the mechanism for the transformation of alumina to α-phase consists of nucleation and growth mechanism. During the phase transformation, α-alumina nuclei occur at contact point of χ-alumina particles by thermal expansion, followed by the growth of nuclei into the surrounding matrix. To confirm this argument, the product synthesized in toluene was calcined in various conditions and the crystallite sizes of χ-alumina and α-alumina were measured. Results are summarized in Table 5.8. The results clearly show that the crystallite size of χ-alumina grows up from 10 to 16 nm then disappears. These results suggests that χ-alumina has a critical size (around 16 nm) beyond which it is unstable and undergoes the phase transformation into the α- form which grows up drastically.

Table 5.8: The crystallite size of the alumina products calcined at various conditions.

Sample ID	Calcination temperature (^{o}C)	Calcination time (h)	Crystallite size of χ-alumina (nm)	Crystallite size of α-alumina (nm)
TAl	1100	1	10.2	-
		4	15.2	31.9
		6	15.4	36
	1150	1	15.9	28
	1180	1	-	36.5
MAl	1100	1	10.2	-
	1150	1	15.7	21.5
	1180	1	-	107.5

From the TEM images, particles having average sizes between 30-100 nm were not detected. This suggests that the growth stage of α-phase direct transformation from χ-alumina occurs rapidly and might be the results from a sintering process between smaller particles occurring in the liquid boundaries of the particles, in which the diffusion is the rate limiting step. Iler [107] proposed that the mechanism of phase transformation involved the intermediate phase having the appearance of a viscous fluid which connected the diminishing to θ crystals to α-alumina. When accretion occurs in the liquid medium, small particles dissolve and larger particles grow by adding the new atom in the interface. Thus, for the grain growth process, the interface structure is very important. For the spherical particles, the interface structure was atomically rough. The arrival atom could get in the crystal lattice without the energy barrier. Therefore, the grain growth process was controlled by diffusion [108].

(a)

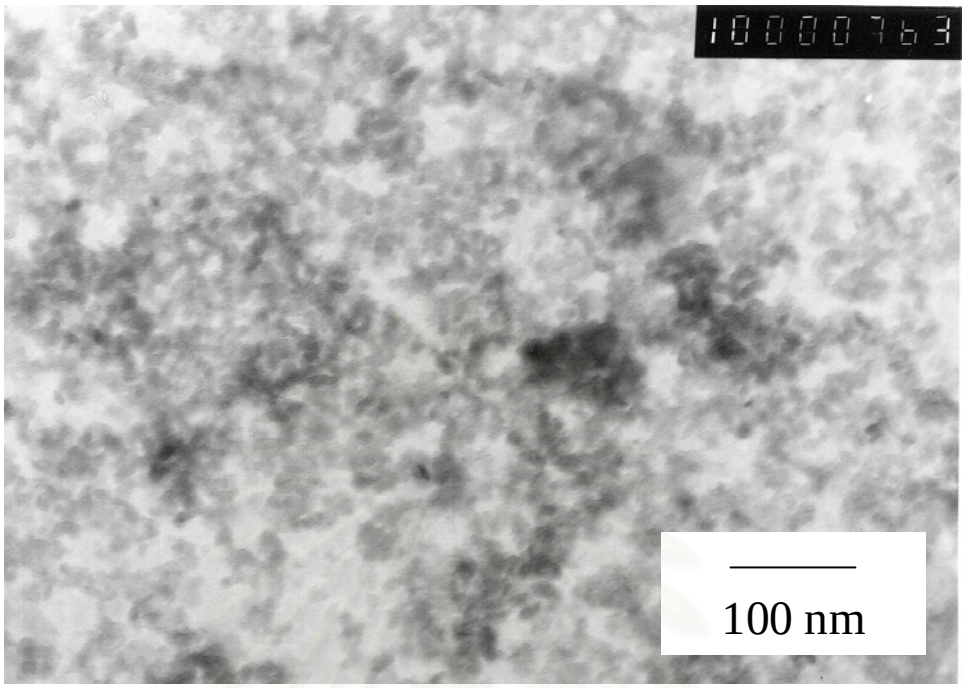

(b)

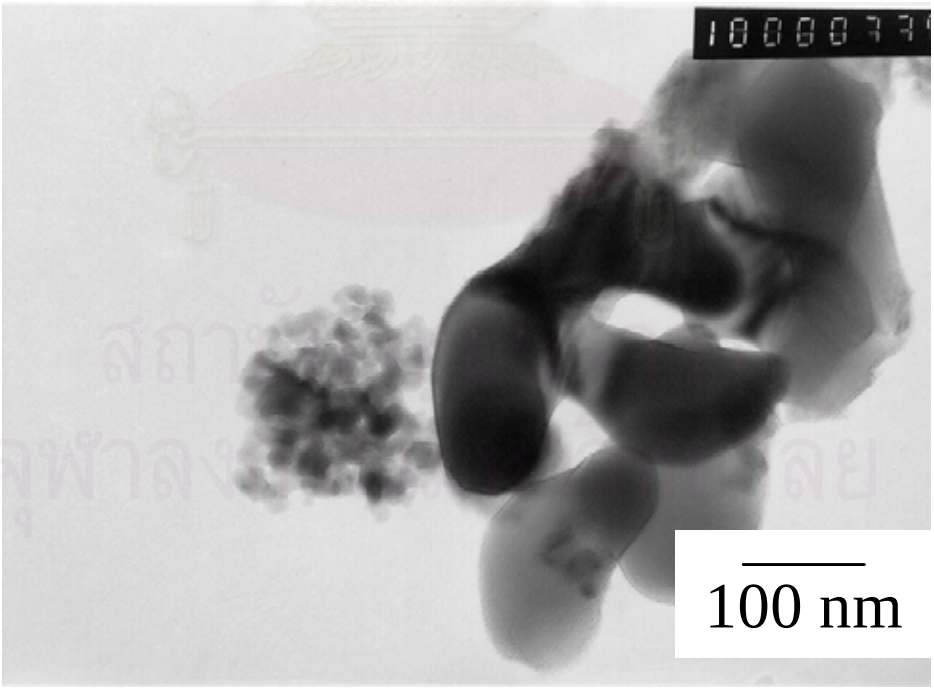

(c)

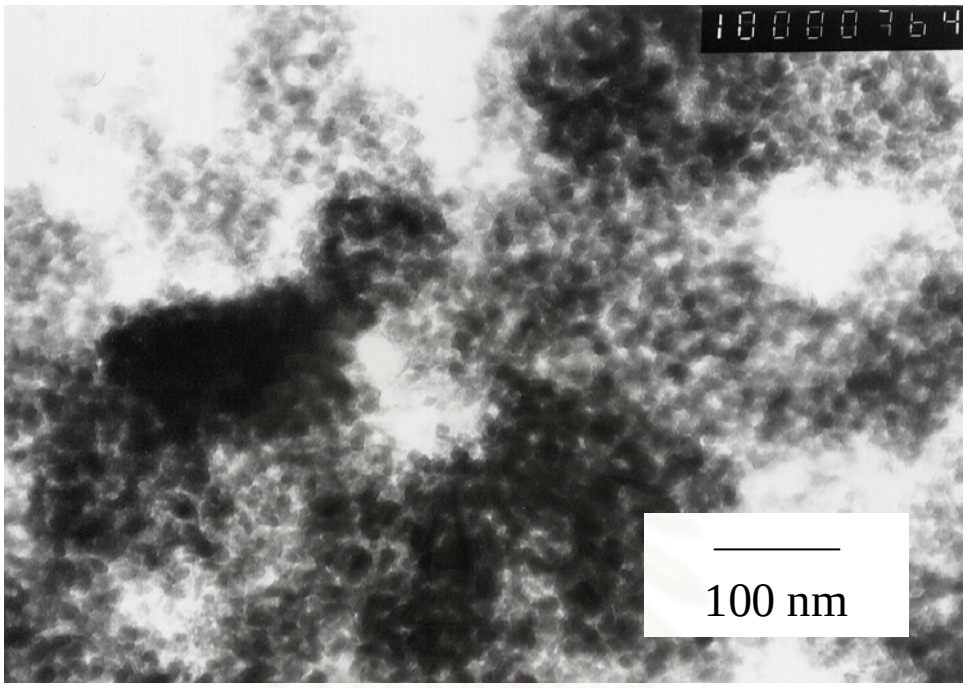

(d)

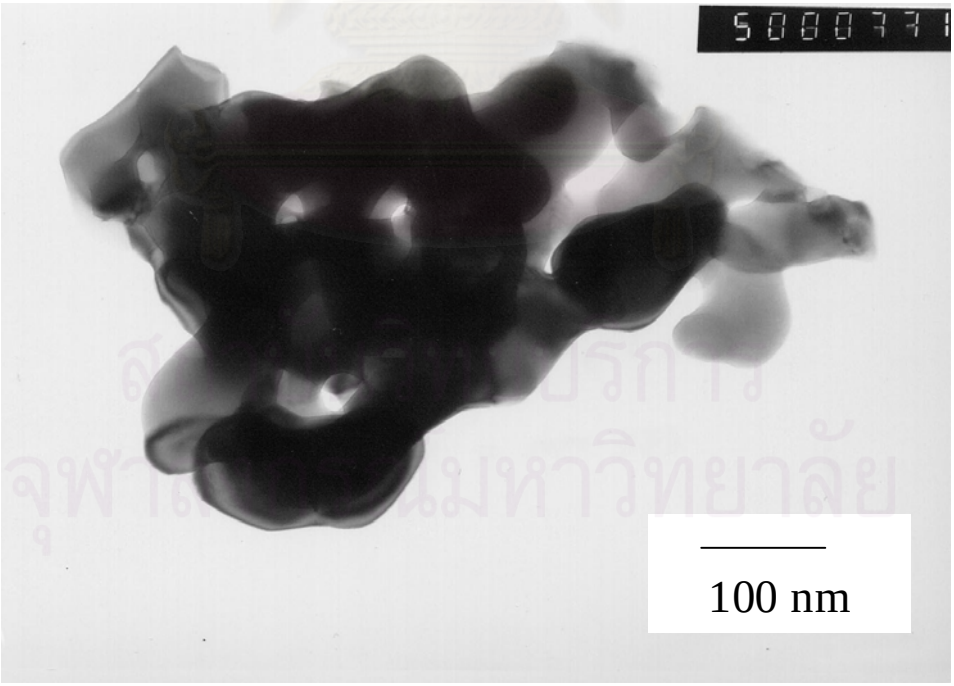

Figure 5.31: TEM images of alumina products: (a) as-synthesized product prepared in toluene, (b) product prepared in toluene calcined at 1180°C, (c) as-synthesized product prepared in mineral oil, (d) product prepared in mineral oil calcined at 1180°C.

Morphologies of as-synthesized and calcined samples observed by SEM are shown in Figure 5.32. It was found that the primary particles of powders obtained in mineral oil agglomerated during heating and formed bigger and more nearly spherical particles. These particles remained spherical even after the α-phase transformation. It appears that the α-phase transformation does not affect the morphologies of particles. On the other hand, in case of reaction in toluene, irregular aggregates made up of nanometer particles were observed (see Fig. 5.32a). When α-phase transformation occurred after the aggregates were heated to high temperature, the nano particles grew significantly and can be identified as individual vermicular particles that are sintered into a large mass.

(a)

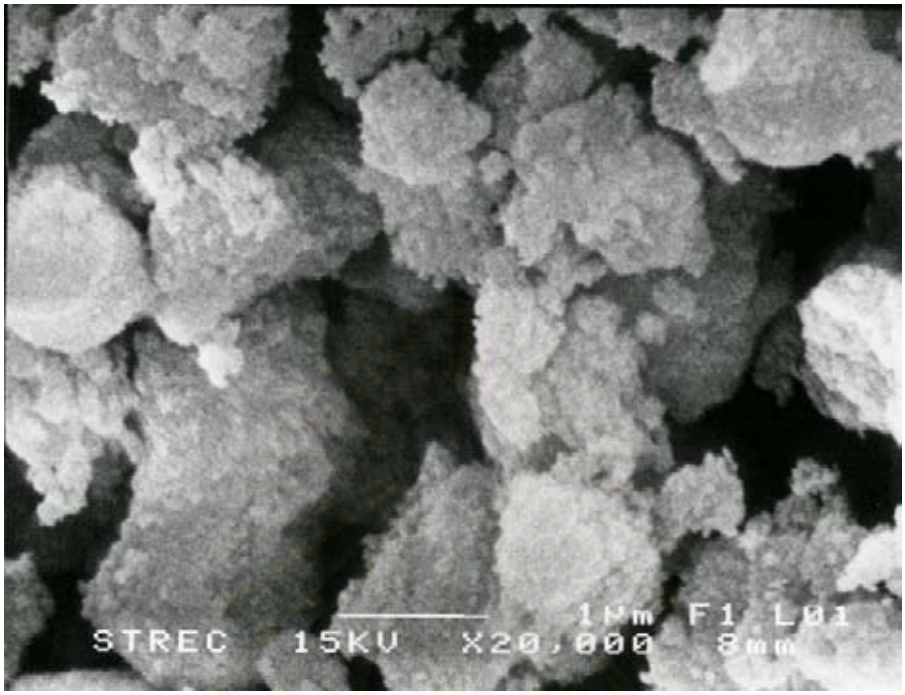
1μm F1 L01
STREC 15KV X20,000 8mm

(b)


1μm F2 L01
STREC 15KV X20,000 8mm

(c)

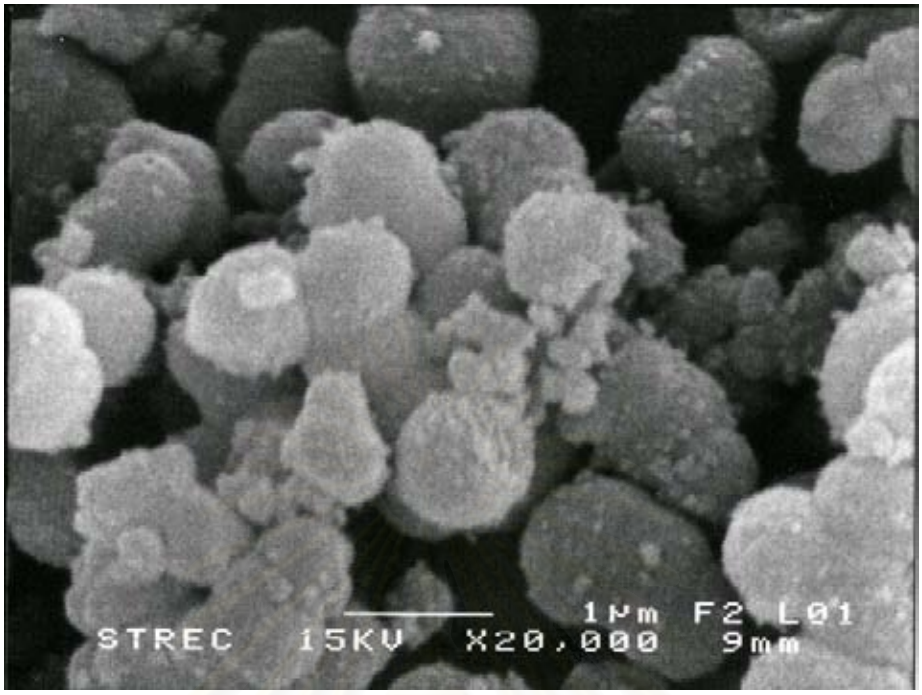

(d)

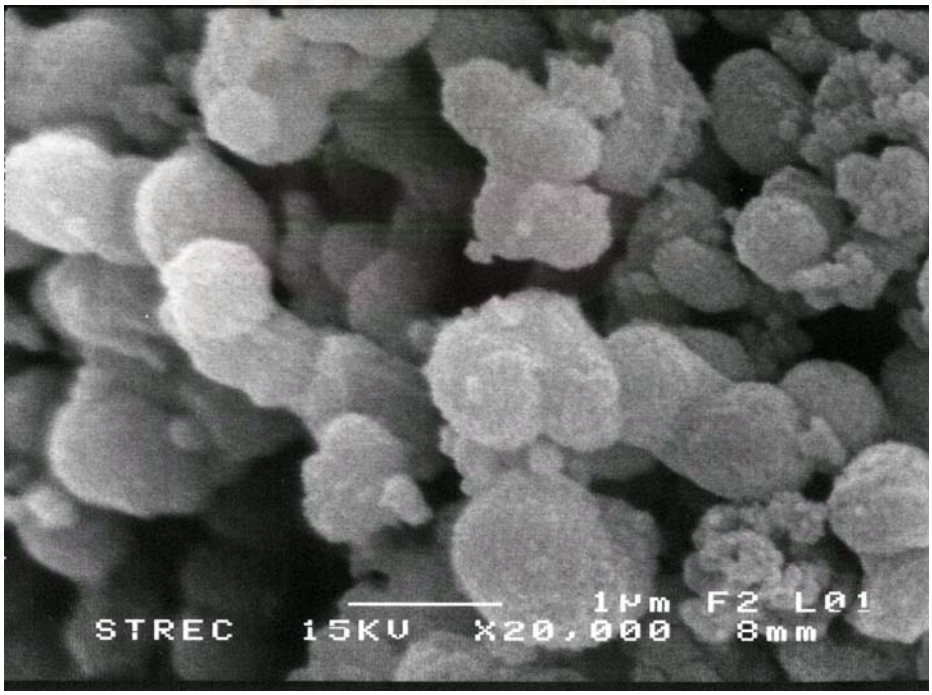

Figure 5.32: SEM images of alumina products: (a) as-synthesized product prepared in toluene, (b) product prepared in toluene calcined at 1180°C, (c) as-synthesized product prepared in mineral oil, (d) product prepared in mineral oil calcined at 1180°C.

CHAPTER VI

CONCLUSIONS AND RECOMENDATION

6.1 Conclusions

In this research, the crystallization and the phase transformation behavior is investigated by using XRD, IR, TG-DTA, SEM and TEM technique. The conclusions of these results are summarized as follow:

1. χ-Alumina was formed by the reaction of AIP in the inert organic solvent at high temperature.

2. The increase of the pore volume and pore size, caused by the preventing of the coagulation of the alumina particles by using the supercritical drying method, contributed to the higher thermal stability of the χ-alumina product.

3. AIP decomposed in mineral yielding amorphous spherical particles through stepwise decomposition in the solvent, these particles shed organic moieties and χ-alumina forms.

4. The direct transformation to α-alumina can be explained by the absence of cations and fewer defects in the crystal structure, whereby disturbing the crystallization of the high-temperature transition alumina (κ-phase).

5. There is a critical size of χ-alumina (around 16 nm) beyond which χ-alumina becomes unstable and undergoes the phase transformation into the α- form which grew up drastically.

6.2 Recommendation

From the previous conclusion, the following recommendation for the future studied can be the following:

1. Because the direct phase transformation to α- alumina is interesting, further investigation is desired.

2. In this work, the critical size of χ-alumina before the a-phase transformation is proposed and it is interesting to prove this assumption.

3. The morphology change affected by the using solvent is interesting, therefore the study of this effect should be done.

REFERENCES

1. Brinker, C. J., and G. W. Scherrer. Sol-Gel Science: The Physics and Chemistry of Sol-Gel Processing San Diego: Academic Press, 1990.
2. Kaya, C., J. Y. He, X. Gu, and E. G. Butler. Nanostructured Ceramic Powders by Hydrothermal Synthesis and Their Applications Micropor. Mesopor. Mat. 54 (2002): 37-49.
3. Deng, S. G., and Y. S. Lin. Microwave Synthesis of Mesoporous and Microporous Alumina Powders. J. Mater. Sci. Lett. 16 (1997): 1291-1294.
4. Sarikaya Y., I. Sevinc, and M. Akinc. The effect of calcination temperature on some of the adsorptive properties of fine alumina powders obtained by emulsion evaporation technique. Powder Technol, 116 (2001): 109-114.
5. Hen, P. -L., and J. -W. Chen. Reactive Cerium(IV) Oxidase Powders by the Homogeneous Precipitation Method. J. Am. Ceram. Soc. 76 (1993): 1577.
6. Inoue, M., Y. Kondo, and T. Inui. Ethylene Glycol Derivative of Boehmite. Inorg. Chem. 27 (1988): 215-221.
7. Inoue, M., H. Kominami, and T. Inui. Thermal Reaction of Aluminum Alkoxide in Glycol. J. Am. Ceram. Soc. 73 (1990): 1100-1102.
8. Inoue, M., H. Kominami, and T. Inui. Thermal Reaction of Aluminum Alkoxide in Various Glycols and the Layer Structure of Their Products. J. Chem. Soc. Dalton Trans. (1991): 3331-3336.
9. Inoue, M., H. Kominami, and T. Inui. Thermal Transformation of χ-Alumina Formed by Thermal Decomposition of Aluminum Alkoxide in Organic Media. J. Am. Ceram. Soc. 75 (1992):2597-98.
10. Inoue, M., H. Kominami, and T. Inui. Novel Synthesis Method for The Catalytic Use of Thermally Stable Zirconia: Thermal Decomposition of Zirconium Alkoxide in Organic Media. Appl. Catal. A 97 (1993): L25-L30.
11. Inoue, M., H. Kominami, and T. Inui**.** Novel Synthesis Method for The Thermally Stable Zirconia: Hydrolysis of Zirconium Alkoxide at High

Temperature With a Limited Amount of Water Dissolved in Inert Organic Solvent from The Gas Phase. Appl. Catal. A 121 (1995): L1-L5.

12. Inoue, M., H. Otsu, H. Kominami, and T. Inui. Synthesis of Thermally Stable, Porous Silica-Modified Alumina via Formation of a Precursor in an Organic Solvent. Ind. Eng. Chem. Res. 35 (1996): 295-306.
13. Inoue, M., H. Kominami, and T. Inui. Thermal decomposition of alkoxides in an inert organic solvent: novel method for the synthesis of homogeneous mullite precursor. J. Am. Ceram. Soc. 75 (1996): 2597-98.
14. Trimm, D. L., and A. Stanislaus. The Control Pore Size in Alumina Catalyst Supports. Appl. Catal. A 21(1986): 215.
15. Rajendran, S. Production of Ultrafine Alpha-Alumina Powders and Fabrication of Fine-Grained Strong Ceramics. J. Mater. Sci. 29 (1994): 5664-5672.
16. Androff, N. W., L. F. Francis, and B. V. Velmakanni. Macroporous Ceramics from Ceramic-Polymer Dispersion Methods. AIChE journal. 43 (1997): 2878.
17. Hellgardt, K. and D. Chadwick. Effect of pH of Precipitation on the Preparation of High Surface Area Aluminas from Nitrate Solutions. Ind. Eng. Chem. Res. 37 (1998): 405.
18. Nagai, H., Y. Oshima, K. Hirano and A. Kato. Synthesis of Aluminium Hydroxide by a Homogeneous Precipitation Method. I Effect of Additives on the Morphology of Aluminium Hydroxide. Br. Ceram. Trans. 90 (1991): 44.
19. Nagai, H., Y. Oshima, K. Hirano and A. Kato. Sintering Behavior of Aluminum-oxide Derived from Aluminum Hydroxides with Various Morphologies. Br. Ceram. Trans. 93 (1993): 114.
20. Tucker, D. S. Gamma-to-Alpha Transformation in Spherical Aluminum Oxide Powder. J. Amer. Ceram. Soc. 68 (1985): C163-164.
21. Johnson, M. F. L. Surface Area Stability of Aluminas. J. Catal. 123 (1990): 245-259.
22. Wefers, K., and C. Misra. Oxides and. Hydroxides of Aluminum. Alcoa Technical Paper No. 19, Alcoa Laboratories, Pittsburgh, PA, 1987.

23. Perego, C., P.L. Villa. The catalytic process from laboratory to the industrial plant. in: D. SanFilippo (Ed.), Proceedings of the 3rd Seminar on Catalysis, Rimini, Italy, June 1994, Italian Chemical Society.

24. Gitzen, W. H. Alumina as a Ceramics Material. Columbus, OH: American Ceramic Society, 1970.

25. Saalfeld, H. Structure Phases of Dehydrated Gibbsite. in Reactivity of Solid. Edited by J.H. de Boer. Elsevier, Amsterdam, Netherlands, 1961.

26. Brindley, G. W., and J. O. Choe. The Reaction Series, Gibbsite to chi-Alumina to kappa-Alumina to Corundum. Am. Mineral. 46 (1961): 771-85.

27. Stiles, A. B. Catalyst Supports and Supported Catalyst. Stoneham: Butterworth Publishers, 1987.

28. Dollimore, D., J. Dollimore, and P. D. Perry. The Thermal Decomposition of Oxalates. Part VIII. Thermalgravimetric and X-ray Analysis Study of the Decomposition of Alumina Oxalate. J. Chem. Soc., A 3 (1967): 448-50.

29. Stumpf, H. C., A. S. Russell, J. W. Newsome, and C. M. Tucker. Thermal Transformations of Aluminas and Alumina Hydrates. Ind. Eng. Chem. 42 (1950): 1398-403.

30. Brindley, G. W., and J. O. Choe. The Reaction Series, Gibbsite to χ-Alumina to κ-Alumina to Corundum. I. Am. Mineral. 46 (1961): 771-85.

31. Kominami, H., J. Kato, Y. Takada, Y. Doushi, B. Ohtani, S. Nishimoto, M. Inoue, T. Inui, and Y. Kera. Novel Synthesis of Microcrystalline Titanium(IV) Oxide Having High Thermal Stability and Ultra-High photocatalytic Activity: Thermal Decomposition of Titanium(IV) Alkoxide in Organic Solvents. J. Catal. Lett. 46 (1997): 235-240.

32. Kominami, H., J. Kato, S. Murakami, Y. Kera, M. Inoue, T. Inui, and B. Ohtani. Synthesis of Titanium(IV) Oxide of Ultra-High Photocatalytic Activity: High-Temperature Hydrolysis of Titanium Alkoxides with Water Liberated Homogeneously from Solvent Alcohols. J. Mol. Catal. A-Chem 144 (1999): 165-171.

33. Fanelli, A. J., and J. V. Burlew. Process for Preparing High Surface Area Alumina. US Patent 4387085, 1983.

34. Armor, J. N., and E. J. Carlson. Palladium on Alumina Aerogel Catalyst

Composition and Process for Making Same. US Patent 4469816, 1984.

35. Armor, J. N., and E. J. Carlson. Variables in Synthesis of Unusually High Pore Volume Aluminas. J. Mater. Sci. 22 (1989), 2549-2556.

36. Praserthdam, P., M. Inoue, O. Mekasuvandumrong, W. Thanakulrangsan, and S. Phatanasri. Effect of Organic Solvents on The Thermal Stability of Porous Silica-modified Alumina Powders Prepared via One Pot Solvothermal Synthesis. Inorg. Chem. Commun. 3 (2000): 671-676.

37. Dynys, F. W., and J. W. Halloran. Alpha alumina Formation in Alum-Derived Gamma Alumina. J. Am. Ceram. Soc. 65 (1982): 442-448.

38. Tjiburg, I. I. M., H. Bruin, P. A. Elberse, and J. W. Geus. Sintering of Pseudoboehmite and γ-Alumina. J. Mater. Sci. 26 (1991): 5945-5949.

39. Dynys, F. W., and J. W. Halloran. Ultrastructure Processing of Ceramics, Glasses and Composites. Hench, L. L., Ulrich, D. R., Eds., New York: John Wiley,1984.

40. Zielinski, P. A., R. Schulz, S. Kaliaguine, A. Neste, and J. Van. Structural Transformation of Alumina by High-Energy Ball-Milling. J. Mater. Res. 8 (1993): 2985-2992.

41. McArdle, J. L., and G. L. Messing, Transformation Microstructure Development and Densification in Alpha-Fe_2O_3-Seeded Boehmite-Derived Alumina. J. Am. Ceram. Soc. 76 (1993): 214-222.

42. Tonejc, A., M. Stubicar, A. M. Tonejc, D. Bagovic, and C. Kosanovic. Transformation of Gamma-AlOOH (Boehmite) and $Al(OH)_3$ (Gibbsite) to Alpha-Al_2O_3 (Corundum) Induced by High-Energy Ball-Milling. Mater. Sci. Eng. 1227 (1994): A181-A182.

43. Yu, Z., Q. Zhao, and Q. Zhang. Effect of Hydrochloric-Acid on The Preparation and Characteristics of Ultrafine Alumina Powder. J. Mater. Sci. Lett. 14 (1995): 531-532.

44. Ding, J., T. Tsuzuki, and P. G. McCormick. Ultrafine Alumina Particles Prepared by Mechanochemical/Thermal Processing. J. Am. Ceram. Soc. 79 (1996): 2956-2958.

45. Kamiya, K., J. Yotani, R. Senba, J. Matsuoka, and H. Nasu. Sol-gel Preparation of Alumina Gels Forming Alpha-Alumina around 500 Degrees C. J. Ceram. Soc. Jpn. 104 (1996): 685-687.

46. Djuricic, B., S. Pickering, P. Claude, D. McGarry, and P. Tambuyser. Thermal

Stability of Transition Phases in Zirconia-Doped Alumina. J. Mater. Sci. 32 (1997): 589-601.

47. Sharma, P. K., M. H. Jilavi, D. Burgard, R. Nass, and H. Schmidt. Hydrothermal Synthesis of Nanosize Alpha-Al_2O_3 from Seeded Aluminum Hydroxide. J. Am. Ceram. Soc. 81 (1998): 2732-2734.
48. Wen, H. L., and F. S. Yen. Growth Characteristics of Boehmite-Derived Ultrafine Theta and Alpha-Alumina Particles during Phase Transformation. J. Cryst. Growth 208 (2000): 696-708.
49. Chang, P. L., F. S. Yen, K. C. Cheng, and H. L. Wen. Examinations on The Critical Sizes during θ- to α- Phase Transformation of Ultrafine Alumina Powders. Nano Letters 1 (2001): 253-261.
50. Simpson, T. W., Q. Z. Wen, N. Yu, and D. R. Clarke. Kinetics of the Amorphous -> γ -> α Transformation in Aluminum oxide: Effect of Crystallographic Orientation. J. Am. Ceram. Soc. 81 (1998):1995.
51. Levin, I., and D. Brandon. Metastable Alumina Polymorph: Crystal Structures and Transition Sequences. J. Am. Ceram. Soc. 81 (1998): 61.
52. Kumagai, M., and G. L. Messing. Enhanced Densification of Boehmite Sol-Gel by α-Alumina Seeding. J. Am. Ceram. Soc. 67 (1984): 230.
53. Shek, C. H., J. K. L. Lai, T. S. Gu, and G. M. Lin. Transformation Evolution and Infrared Absorption Spectra of Amorphous and Crystalline Nano-Al_2O_3 Powders. Nanostructured Materials 8 (1997): 605-10.
54. Lippens, B. C., and J. J. Steggerda. Physical and Chemical Aspects of Adsorbents and Catalysts. New York: Academic Press, 1970.
55. Megaw, H. D. Crystal Structures: A Working Approach. Toronto: Saunders, Philadelphia. London, 1973.
56. Lippens, B. C., and J. H. De Boer. Study of Phase Transformations during Calcination of Aluminum Hydroxides by Selected Area Electron Diffraction. Acta cystallogr.17 (1964): 1312.
57. Zigan, F., W. Joswig, and N. Burger. Die Wasserst off positionen in Bayerit, $Al(OH)_3$. Z Krislallogr. 148 (1978): 255-273.
58. Corbalo, C. E., R. T. Teltenhorst, and G. G. Christoph. Structure Refinement of Deuterated Boehmite. Cloys Clay Miner. 33 (1985): 71-75.
59. Osterhout, V. Acta Crystallogr. 13 (1960): 932.

60. Vamaguchi, H. Yanagida, and S. Ono. New Alumina Hydrate, 'Tohdite' ($5A1_2O_3.H_2O$). Bull. Chem. Soc. Jpn. 37 (1964): 1555-1557.

61. Yamaguchi, G., and M. Okumiya. Refinement of the Structure of Tohdite $5A1_2O_3.H_2O$. Bull. Chem. Soc. Jpn. 42 (1969): 2247-4229.

62. Young, L. Anodic Alumina Films. Academic Press, New York, 1961.

63. El-Mashri, M., R. G. Jones, and A. J. Forty. An Electron-Yield EXAFS Study of Anodic Oxide and Hydrated Oxide Films on Pure Aluminum. Philos. Mog. A 48 (1983): 665.

64. Bourdillon, A. J., S. M. El-Mashri, and A. J. Forty. Application of TEM Extended Electron Energy Loss Fine Structure to the Study of Aluminum Oxide Films. Philos. Mag. A 49 (1984): 341.

65. Bendersky, L. A., A. Roytburd, and W. J. Boettinger. Phase Transformations in the $(Ti,Al)_3Nb$ Section of the Ti-AI-Nb System-1. Microstructural Predictions Based on a Subgroup Relation between Phases. Acta Melall. 42 (1994): 2323.

66. Waseda, Y., K. Sugiyama, and J. M. Toguri. Direct Determination of the Local Structure in Molten Alumina by High-Temperature X-ray Diffraction. Z. Nalulforsch., A: Phys. Sci. 50 (1995): 770-74.

67. Wilson, S J. Phase Transformations and Development of Microstructure in Boehmite-Derived Transition Aluminas. Proc. Br. Ceram. Soc. 28 (1979): 281-94.

68. Hahn, T(Ed.). International Tables of Crystallography, Vol. A. London, U.K.: Kluwer, 1995.

69. Shirasuka, K., H. Yanagida, and G. Yamaguchi. The Preparation of η-Alumina and Its Structure. Yogyo Kyokai-shi 84 [12] (1976): 610-13.

70. John, C. S., V. C. M. Alma, and G. R. Hays. Characterization of Transition Alumina by Solid-State Magic Angle Spinning Aluminum NMR. Appl. Catal. A (1983): 6341-46.

71. Zhou, R. S., and R. L. Snyder. Structures and Transformation Mechanisms of the η, γ and θ Transition Aluminas. Acta Crystallogr., Sect. B: Struct. Sci. 47 (1991): 617-30.

72. Ernst, F., P. Pirouz, and A. H. Heuer. HRTEM Study of a $Cu-Al_2O_3$, Interface. Philos. Mag. A 63 [2] (1991): 259-77.

73. Blonski, S., and S. H. Garofalini. Molecular Dynamics Simulations of α-Alumina and γ-Alumina Surfaces. Surf. Sci. 295 (1993): 263-74.

74. Yamaguchi, G., and H. Yanagida. Thermal Effects on the Lattices of η and γ-Aluminum Oxide. Bull. Chem. Soc. Jpn. 37 (1964): 1229-31.

75. Doychak, J., J.L. Smialek, and T.E. Mitchell. Transient Oxidation of Single-Crystal Nickel-Aluminum (β-NiAl). Metall. Trans. A 20 (1989): 499.

76. Prussner, K., J. Bruley, U. Salzberger, H. Zweygart. E. Schumann, and M. Rilhic. SEM and TEM Observations on the Development of the Oxide Scale on Y-implanted Single Crystalline β-NiAl under Low Oxygen Partial Pressure. 435 in Microscopy of Oxidation-2, Proceedings of 2nd International Conference, Edited by S. Newcomb and M. Bennett. Cambridge University Press, Cambridge, U. K., 1993.

77. Rooksby, H. P., and C. J. M. Rooymans. The Formation and Structure of Delta Alumina. Clay Miner. Bull. 4 (1961): 234.

78. Dauger, A., D. Fargeot, and J. P. Laval. Metastable Phases of Alumina. Mater. Res. Soc. Symp. Proc. 21 (1984): 207.

79. Bonevich, J. E., and L. D. Marks. The Sintering Behavior of Ultrafine Alumina Particles. J. Mater. Res. 7 [6] (1992): 1489-500.

80. Jayaram, V., and C. G. Levi. The Structure of δ-Alumina Evolved from the Melt and the γ–δ Transformation. Acta Metall. 37 [2] (1989): 569-78.

81. Kohn, A., G. Katz, and J. D. Broder. Characterization of β-Ga,O, and its Alumina Isomorph, θ-Al_2O_3. Am. Mineral. 42 (1957): 398-407.

82. Levin, I., and D. Brandon. Metastable Alumina Polymorph: Crystal Structures and Transition Sequences. J. Am. Ceram. Soc. 81 (1998): 61.

83. Okumiya, M., G. Yamaguchi, O. Yamada, and S. Ono. The Formation of κ- and κ'- Al_2O_3 from the Dehydration of Tohdite $5Al_2O_3.nH_2O$. Bull. Chem. Soc. Jpn. 44 (1971): 418-23.

84. Liu, P., and J. Skogsmo. Space-Group Determination and Structure Model for κ-Al_2O_3 by Convergent-Beam Electron Diffraction (CBED). Acta Crystallogr., Sect. B: Struct. Sci. 47 (1991): 425-33.

85. Kronberg, M. L. Plastic Deformation of Single Crystals of Sapphire-Basal Slip and Twinning. Acta Metall. 5 (1957): 507-24.

86. Bilde-Sorensen, J. B., B. F. Lawlor, T. Geipel, P. Pirouz, A. H. Heuer, and K.

P. D. Lageribf. On Basal Slip and Basal Twinning in Sapphire (α-Al_2O_3)-I. Basal Slip Revisited. Acta Metall. Mater. 44 [5] (1996): 2145-52.

87. Kaplan, W. D., P. R. Kenway, and D. G. Brandon. Polymorphic Basal Twin Boundaries and Anisotropic Growth in α- Al_2O_3. Acta Metall. Mater. 43 (1995): 35-48.

88. Pirouz, P., B. F. Lawlor, T. Geipel, J. B. Bilde-Sorensen, A. H. Heuer, and K. P. D. Lagerlof. On Basal Slip and Basal Twinning in Sapphire ((α-Al_2O_3)-II. A New Model of Basal Twinning. Acta Metall. Mater. 44 [5] (1996): 2153-64.

89. Aegerter, M. A., M. Jafelicci Jr., D. F. Souza, and E. D. Zanatto. Sol-Gel Science and Technology. Proceedings of the Winter School on Glasses and Ceramics from Gels, Brazil 1989.

90. West, A. R. Solid State Chemistry and Its Applications, John Wiley & Sons 1997.

91. Kingery, W. D., H. K. Bownen, and D. R. Uhlmann. Introduction to Ceramics, 2d ed., John Wiley, New York.

92. Cobel, R. L., and J. E. Burke, Progress in Ceramic Science, Vol. 3, New York : Pergamon Press., 1963.

93. Yan, M. F. Advances in Powder Technology, G. Y. Chin, Am. Soc. Metals 1982.

94. Kingery, W. D., and B. Francois, Sintering and Related Phenomena, New York: Gordon Breach, 1967.

95. Chou, T. C., and T.G. Nieh. Nucleation and Concurrent Anomalous Grain Growth of α-Al_2O_3 during γ–α Phase Transformation. J. Am. Ceram. Soc. 74 (1991): 2270.

96. Johnson, G. P., R. Muenchausen, D. M. Smith, W. Fahrenholtz, and S. Foltyn. Reactive Laser Ablation Synthesis of Nanosized Alumina Powder. J. Am. Ceram. Soc. 75 [12] (1992): 3293-98.

97. Ogihara, T., H. Nakagawa, T. Yanagawa, N. Ogata, and K. Yoshida. Preparation of Monodisperse, Spherical Alumina Powders from Alkoxides. J. Am. Ceram. Soc. 74 [9] (1991): 2263-69.

98. Johnson D. W., and F. J. Schnettler. Characterization of Freeze-Dried Al_2O_3

and Fe_2O_3. J. Am. Ceram. Soc 53 [8] (1970): 440-44.

99. Kato, E., K. Daimon, and M. Nanbu. Decomposition of Two Aluminum Sulfates and Characterization of the Resultant Aluminas. J. Am. Ceram. Soc. 64 [8] (1981): 436-45.

100. Sacks, M. D., T.-Y. Tseng, and S. Y. Lee. Thermal Decomposition of Spherical Hydrated Basic Aluminum Sulfate. Ceram. Bull. 63 [2] (1984): 301-10.

101. Morrissey, K. J., K. K. Czanderna, C. B. Carter, and R. P. Merrill. Growth of α-Alumina within a Transition Alumina Matrix. J. Am. Ceram. Soc. 67 [5] (1984): C-88-90.

102. Bagwell, R. B., G. L. Messing, and P. R. Howell. The Formation of α-Alumina from θ-Alumina: The Relevance of a "Critical Size" and: Diffusional Nucleation or "Synchro-Shear". J. Mater. Sci. 36 [7] (2001): 1833-41.

103. Imamura, S., T. Kitao, H. Sasaki, and K. Utani. Properties of χ-Alumina as Related to Catalysis. React. Kinet. Catal. Lett. 55 [1] (1995): 19-24.

104. de Boer, J. H. The Structure and Properties of Porous Materials. London: Butterworth, 1958.

105. Lippens B. C., and J. H. de Boer. Studies on Pore Systems in Catalysts. I. The Adsorption of Nitrogen; Apparatus and Calculation J. Catal. 3 [1] (1964): 32-37

106. Lippens B. C. and J. H. de Boer. Studies on Pore Systems in Catalysts. V. The *t* Metod. J. Catal. 4 [3] (1965): 319-23.

107. Ishikawa, T., R. Ohashi, H. Nakabayashi, U. Kakuta, A. Ueno, and A. Furuta. Thermally Stabilized Transitional Alumina Prepared by Frame Pyrolysis of Boehmite Sols. J. Catal. 134 [1] (1992): 87-97.

108. Skoog, D. A., and J. J. Leary. Principles of Instrumental Analysis. Philadelphia, San Diego: Saundres College Publishing, 1992.

109. Bahlawane, N., and T. Watanabe. New Sol-Gel Route for the Preparation of Pure α-Alumina at 950°C. J. Am. Ceram. Soc. 83 [9] (2000): 2324-26.

110. Saito, T., S. Takei, A. Hayashi, A. Yasumari, K. Okada. Effect of Crystalline and Amorphous SiO_2 Additives on the γ-Alumina to the α-Alumina Phase Transition. J. Am. Ceram. Soc. 81 (1998): 2197.

111. Johnson D. W., and F. J. Schnettler. Characterization of Freeze-Dried Al_2O_3 and Fe_2O_3. J. Am. Ceram. Soc. 53 [8] (1970): 440-44.

112.Kato, E., K. Daimon, and M. Nanbu. Decomposition of Two Aluminum Sulfates and Characterization of the Resultant Aluminas. J. Am. Ceram. Soc. 64 [8] (1981): 436-45.

113. Sacks, M. D., T.-Y. Tseng, and S. Y. Lee. Thermal Decomposition of Spherical Hydrated Basic Aluminum Sulfate. Ceram. Bull. 63 [2] (1984): 301-10.

114.Okada, K., A. Hattori, Y. Kamechima, and A. Yasumori. Concentration Effect of Cs^+ to the γ-Alumina to the α-Alumina Phase Transition Mater. Lett. 42 (2000): 175.

115. Okada, K., A. Hattori, Y. Kamechima, A. Nukui, and R. Das. Effect of Divalent Cation Additives on the γ-Alumina to the α-Alumina Phase Transition. J. Am. Ceram. Soc. 83 (2000): 928-932.

116. Wu, Y., Y. Zhang, G. Pezzotti, and J. Guo. Influence AlF_3 and ZnF_2 on the Phase Transformation of γ-Alumina to the α-Alumina. Mater. Lett. 52 (2002): 366.

117. Iler, R. K. Fabrillar Colloidal Boehmite; Progressive Conversion to Gamma, Theta, and Alpha-Alumina. J. Am. Ceram. Soc. 44 (1961): 618.

118. Sunggi, B. in Proceeding of 10th International Ceramics Congress & 3rd Forum on New Materials, Florence Italy, July 14-18 2002.

APPENDICES

APPENDIX A

PROCEDURE OF *t*-PLOT ANALYSIS

The statistical thickness can be transformed from N_2 isotherm measured at 77 K by converting relative pressure (P/P_o) in to t value by equation A1: [109]

$$t = [13.99/(\log(P_o/P) + 0.034)]^{0.5} \quad \text{(A1)}$$

Example A.1: Find *t*-plot of MA300C2h

Relative pressure (P/P_o)	Volume adsorbed (cc/g STP)	Statistical thickness (Å)
0.0633	24.012	3.36898
0.0764	25.1316	3.486493
0.0994	26.8888	3.673672
0.1194	28.269	3.823436
0.1394	29.5495	3.965318
0.1594	30.7813	4.101802
0.1982	33.0294	4.357182
0.3011	38.7258	5.01937
0.3487	41.4167	5.334895
0.4488	47.1971	6.052116
0.5472	54.6618	6.876544
0.7439	79.9481	9.27901
0.8512	110.8366	11.60001
0.9001	216.5871	13.24813
0.9446	272.2581	15.43112
0.9602	276.5346	16.45974
0.9737	280.7408	17.52049
0.9838	284.5514	18.45117
0.9867	285.973	18.74503

Relative pressure (P/P_o)	Volume adsorbed (cc/g STP)	Statistical thickness (Å)
0.9948	290.5125	19.64127
0.9832	287.528	
0.9739	284.5702	
0.9622	281.3668	
0.9409	276.4117	
0.9098	268.7211	
0.8461	225.048	
0.7368	87.7062	
0.5466	55.333	
0.3499	41.6731	
0.1352	29.4659	

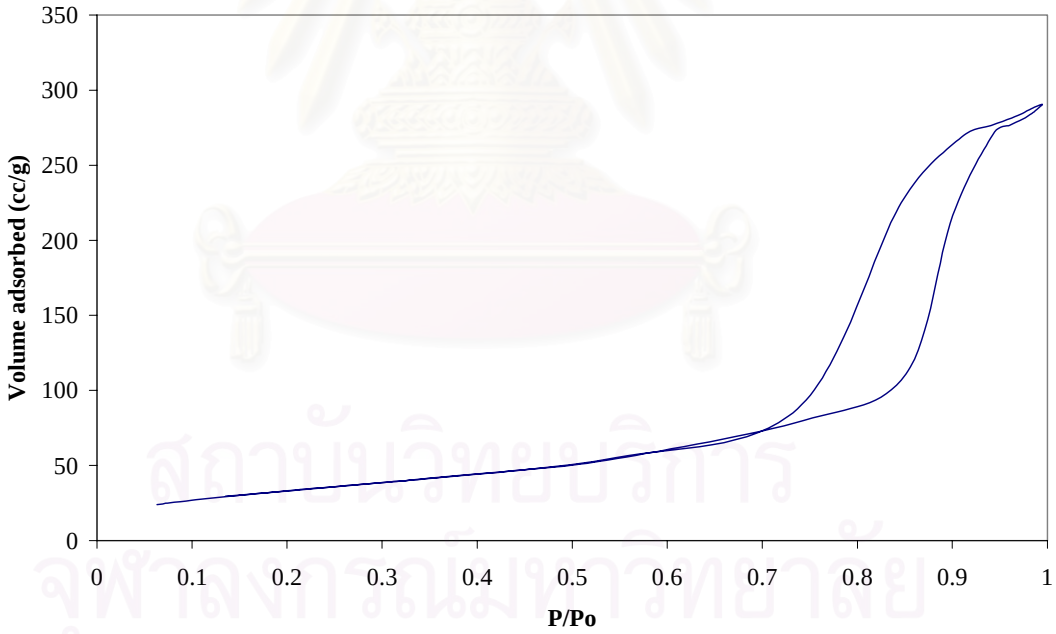

Figure A.1 Isotherm plot of MA300C2h

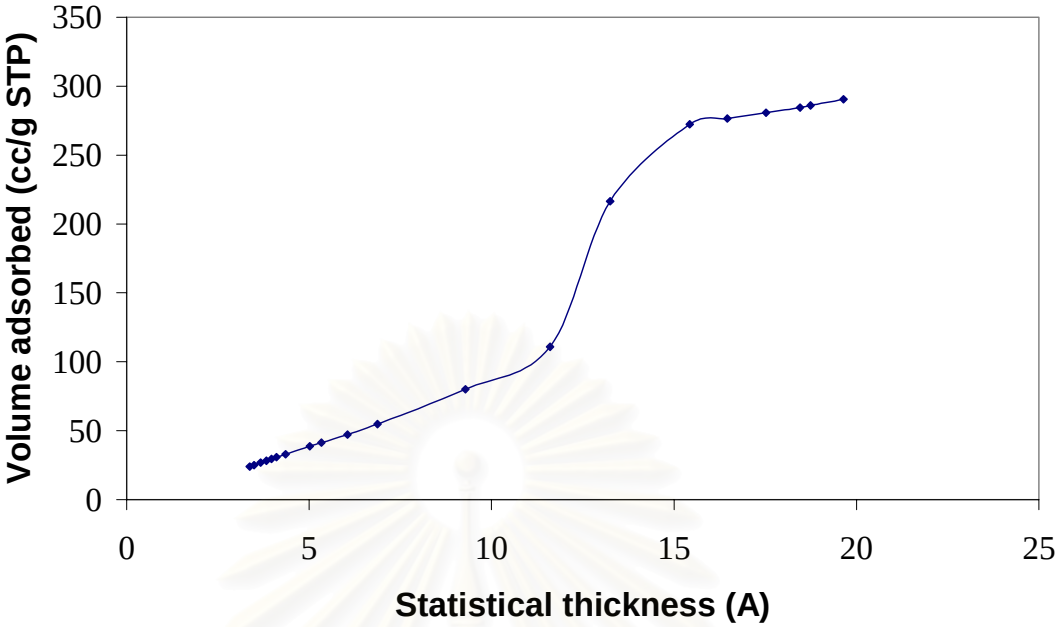

Figure A.2 *t*-plot of MA300C2h

The external surface area can be calculated by equation A2: [89]

$$S_t = 15.47 V_a/t \qquad \text{(A2)}$$

$$S_t = 15.47 * 8.9118$$

$$S_t \text{ (MA300C2h)} = 139 \text{ m}^2/\text{g}$$

APPENDIX B

TEM EXPERIMENTAL

B.1 Procedure of specimen preparation

Appropriate amounts of powder were diffused on ethanol in a test tube, which was then place in the sonic baht for 15 minute. The obtained solution was dropped on the specimen film and dried with air.

B.2 Measurement of particle sizes by TEM image

Particle sizes measured from TEM photograph of the as-synthesized products and calcined products of the metal oxides were estimated as follows,

Example B.1: The measurement of crystallite size from TEM photograph

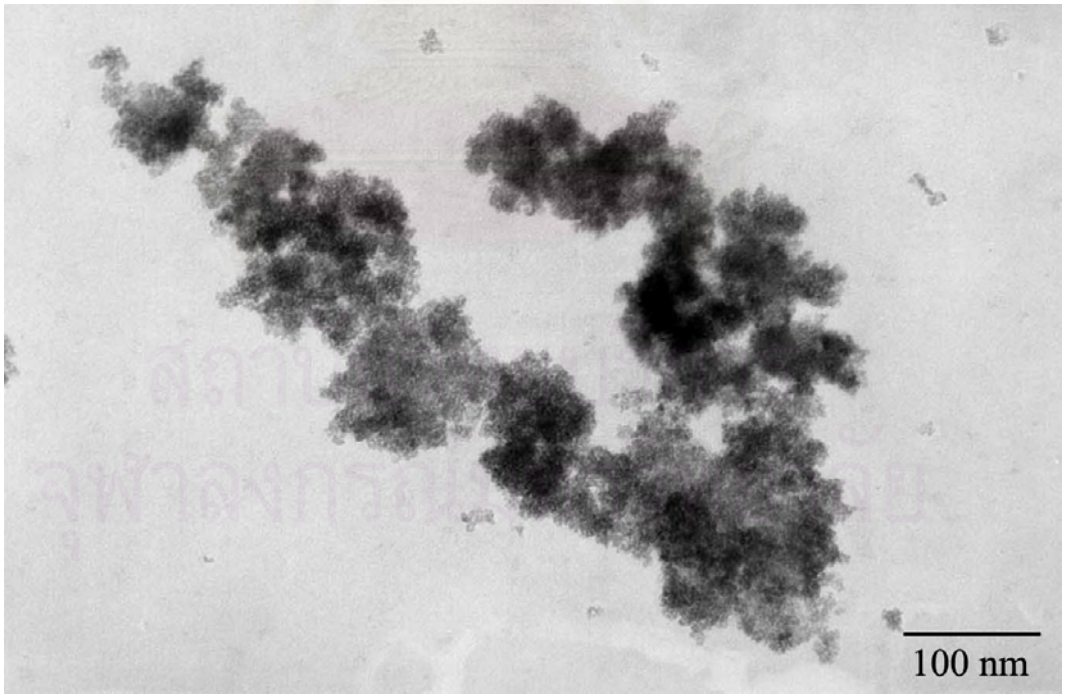

Figure B.1 TEM photograph of as-synthesized metal oxide (x150000)

At X150000 magnification, the scale is

150 mm = 1 μm

= 1000 nm

From TEM photograph, it was found that the crystallite size of the particles closed to each other and that was 0.8 mm. Therefore, the crystallite size observed by TEM is

$$\text{Crystallite size} = \frac{1000\ \text{nm}}{150\ \text{mm}} \times 0.8\ \text{mm}$$

Crystallite size = 5.33 nm

APPENDIX C

EXPERIMENTAL DETAILS OF SUPER CRITICAL DRYING METHOD

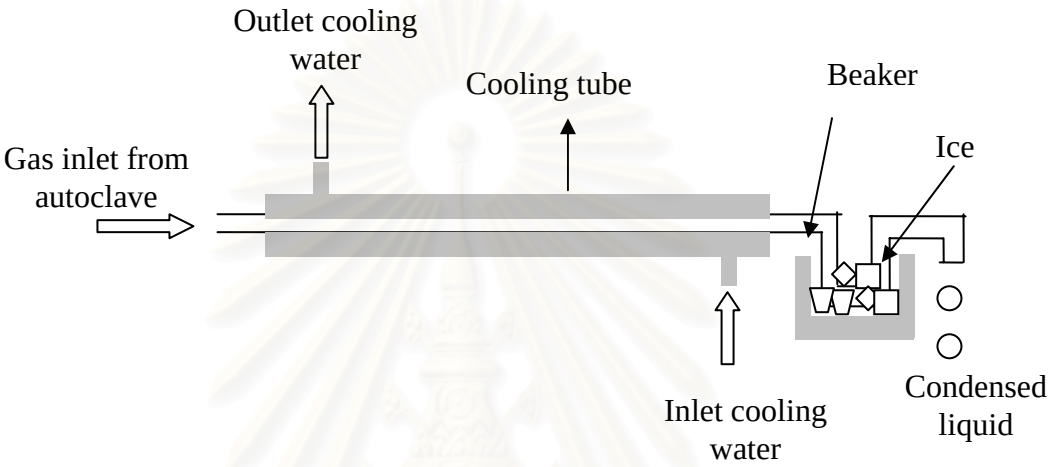

Figure C.1 Diagram of the cooling line for the supercritical drying

First, the cooling line was connected with the autoclave. The cooling water was feed in the cooling tube and the cooling coin was merged in a glass of ice.

After the reaction finished, the valve of autoclave was slightly opened to release the organic solvent from the autoclave by flash evaporation while keeping at the reaction temperature. The valve was opened until the pressure inside the autoclave was decreased to atmospheric level. The organic solvent was condensed and kept in a beaker. The dry products were obtained directly after the assembly was cooled down without the step of washing.

APPENDIX D

LISTS OF PUBLICATIONS

1. Okorn Mekasuwandumrong, Peter L. Silveston, Piyasan Praserthdam, Masashi Inoue, Varong Pavarajarn and Waraporn Tanakulrungsank, Synthesis of thermally stable micro spherical χ-alumina by thermal decomposition of aluminum isopropoxide in mineral oil, Inorganic Chemistry Communications, Volume 6, Issue 7, July 2003, Pages 930-934

2. Okorn Mekasuwandumrong, Piyasan Praserthdam, Masashi Inoue, Varong Pavarajarn and Waraporn Tanakulrungsank, Phase Transformation Behavior of Nanocrystalline χ-alumina Powder Obtained by Thermal Decomposition of AIP in Inert Organic Solvent, Journal of Material Science, (Accepted)

VITA

Mr. Okorn Mekasuwandumrong was born in Bangkok, Thailand, on May 29, 1977. He received the degree of Bachelor of Engineering (Chemical Engineering) from Chulalongkorn University on May 1997 and the degree of Master of Engineering (Chemical Engineering) from Chulalongkorn University on May 1999.